AD NUMBER

AD240961

NEW LIMITATION CHANGE

TO

Approved for public release, distribution unlimited

FROM

Distribution authorized to U.S. Gov't. agencies and their contractors; Administrative/Operational Use; Apr 1960. Other requests shall be referred to Air Force Research Div., ARDC, Bedford, MA.

AUTHORITY

AFCRL ltr, 3 Nov 1971

VOLTAGE BREAKDOWN OF ANTENNAS AT HIGH ALTITUDES

By: W. E. Scharfman and T. Morita

Prepared for:

AIR FORCE RESEARCH DIVISION
LAURENCE G. HANSCOM FIELD

AIR RESEARCH AND DEVELOPMENT COMMAND
BEDFORD, MASSACHUSETTS

SOUTHERN CALIFORNIA LABORATORIES
OF STANFORD RESEARCH INSTITUTE

SOUTH PASADENA, CALIFORNIA

SRI

STANFORD RESEARCH INSTITUTE
MENLO PARK, CALIFORNIA

SRI

April 1960

Technical Report 69

VOLTAGE BREAKDOWN OF ANTENNAS AT HIGH ALTITUDES

By: W. E. Scharfman and T. Morita

S R I Project 2494

Prepared for:
AIR FORCE RESEARCH DIVISION
LAURENCE G. HANSCOM FIELD
AIR RESEARCH AND DEVELOPMENT COMMAND
BEDFORD, MASSACHUSETTS
Contract AF 19(604)-3458

Approved:

for R. C. Tanner
S. B. COHN, MANAGER, ELECTROMAGNETICS LABORATORY

J. E. Scheuch
J. E. SCHEUCH, ASSISTANT DIRECTOR OF ENGINEERING RESEARCH

Copy No.

ABSTRACT

The signal received from electronic systems on various missiles has contained evidence of voltage breakdown on antennas at altitudes from 50,000 to 300,000 feet at VHF, UHF, and microwave frequencies. Since continuous telemetry and tracking information is often necessary to determine impact position and system performance, an experimental investigation has been made of the power-handling capabilities of antennas at high altitude. The principal aims of the study are (1) to determine the physical mechanisms involved, (2) to measure and tabulate experimental data on breakdown field strength for various antenna types, and (3) to study methods for improving the power-handling capabilities of antennas.

The various physical mechanisms which may be important in the breakdown process, and how these mechanisms determine the breakdown field strength for various transmission systems, are discussed. Both pulse and CW conditions are considered. Breakdown data are presented for parallel-plate, rectangular waveguide and coaxial-line transmission lines. With this material as background, the discussion of the breakdown of monopole antennas is presented. Data from measurements on a wide variety of monopoles is presented. It is shown that a single curve of $(E_s/p)_n$ as a function of pr is sufficient to describe the breakdown condition.

The relation between rectangular waveguide and aperture breakdown is discussed. Breakdown data for aperture antennas are presented and it is shown that for narrow slot antennas a single curve of $(E_s/p)_n$ as a function of pd is sufficient to describe the breakdown condition.

An ionized medium near the antenna may severely affect its power-handling capability. Data from measurements made with a plasma caused by a DC discharge over a 380-Mc slot antenna are presented, illustrating this effect.

Ways to improve the power-handling capability of antennas are considered. Quantitative data are presented which show how DC bias can increase in the power-handling capability of monopoles.

CONTENTS

ABSTRACT ii

LIST OF ILLUSTRATIONS v

I INTRODUCTION 1
- A. Background 1
- B. Breakdown Mechanism 1
  - 1. Diffusion-Controlled Breakdown Curve 3
  - 2. Free and Ambipolar Diffusion 5

II LOW-PRESSURE VOLTAGE BREAKDOWN IN TRANSMISSION LINES 7
- A. Background 7
- B. CW Breakdown of Parallel-Plate Systems 7
- C. Pulsed Breakdown of Parallel-Plate Systems 11
  - 1. Single Pulse Breakdown 11
  - 2. Multiple Pulse Breakdown 13
- D. CW Breakdown of Rectangular Waveguide 15
- E. Pulsed Breakdown of Rectangular Waveguide 15
- F. CW Breakdown of Coaxial Lines 21

III CYLINDRICAL MONOPOLE BREAKDOWN 27
- A. Comparison Between Coaxial Line and Cylindrical Monopole Breakdown . . 27
- B. Effects of Monopole Diameter and Height on CW Breakdown 31
- C. Effects of Tip Shape on CW Breakdown 41
- D. Pulsed Breakdown of Monopole Antennas 41

IV BREAKDOWN OF APERTURE ANTENNAS 48
- A. Background 48
- B. CW Breakdown of Open Slot Antenna 48
- C. CW Breakdown of Covered Slot Antenna 51
- D. Pulsed Breakdown of Covered Slot Antenna 53

V ANTENNA OPERATION IN A WEAKLY IONIZED MEDIUM 61
- A. Background 61
- B. Antenna Operation in the Presence of a DC Discharge 61

VI METHODS FOR INCREASING THE POWER HANDLING CAPABILITY OF ANTENNAS 67
- A. Background 67
- B. Increasing the Loss Rate 67
  - 1. Monopole Breakdown with DC Fields 68
  - 2. Aperture Breakdown with DC Fields 70
- C. Decreasing the Ionization Rate 72

VII CONCLUSION 74

CONTENTS

APPENDIX A DETERMINATION OF THE ELECTRIC FIELD AT THE TIP OF A MONOPOLE . . . 76

APPENDIX B CALCULATION OF THE ELECTRIC FIELD IN A NARROW SLOT ANTENNA UP TO $\lambda/2$ LONG 80

APPENDIX C CALCULATION OF THE FIELD IN THE APERTURE OF A LARGE HORN ANTENNA . 83

APPENDIX D CALCULATION OF E_{max} IN A WAVEGUIDE THAT IS NOT MATCHED 85

ACKNOWLEDGMENT 88

REFERENCES 89

LIST OF REPORTS IN THIS SERIES 90

ILLUSTRATIONS

Fig. 1 Illustration of Diffusion- and Attachment-Controlled Breakdown 3

Fig. 2 Solution for Parallel Plate CW Breakdown (from Gould and Roberts) 9

Fig. 3 Normalized Solution for Parallel Plate CW Breakdown (from Gould and Roberts) . . 10

Fig. 4 Normalization Factor, Δ, as a Function of $p\lambda$ (from Gould and Roberts) 11

Fig. 5 Solution for Parallel Plate Pulsed Power Breakdown (from Gould and Roberts) . . 12

Fig. 6 Results of the Effect of PRF on Breakdown (from Gould and Roberts) 14

Fig. 7 Results of CW Breakdown in Rectangular Waveguide (from Gould and Roberts) . . . 16

Fig. 8 Block Diagram of Experimental Set-Up Used in X-Band Pulsed Power Breakdown Measurements on Rectangular Waveguide 18

Fig. 9 Peak Power as a Function of Pressure to Initiate Breakdown in a Rectangular Waveguide at X-Band 19

Fig. 10 $(E_c/p)_N$ as a Function of pr for Different Values of pb for a Rectangular Waveguide with $a/b = 2.25$ 20

Fig. 11 Normalized Curves Showing Effect of PRF on Peak Power to Initiate Breakdown . . 22

Fig. 12 Peak Power as a Function of Pressure to Initiate and Maintain Breakdown in a Rectangular X-Band Waveguide with a Pulse Width of 1 Microsecond 22

Fig. 13 Coaxial Line CW Breakdown Data (from Gould) 24

Fig. 14 Coaxial Line CW Breakdown Data for $p\lambda = \infty$ (from Herlin and Brown) 25

Fig. 15 Coaxial Line CW Breakdown Data from Herlin and Brown, Gould, and Paska in Gould's Notation 26

Fig. 16 Monopole Configuration Used for CW Breakdown Studies 28

Fig. 17 Computed Values of $(E_c/p)_N$ as a Function of pr, for CW Breakdown Between Coaxial Cylinders when $r_2/r_1 = \infty$ 29

Fig. 18 Block Diagram of Measurement Set-Up for CW Breakdown Studies of Monopole Antennas 29

Fig. 19 CW Power to Initiate and Maintain Breakdown on a Monopole 0.24λ-Long 30

Fig. 20 Computed Values of $(E_c/p)_N$ as a Function of pr, for CW Breakdown Between Coaxial Cylinders when $r_2/r_1 = \infty$, and Average of Measured Values for 0.24λ-Long Monopole Antennas 31

Fig. 21 Measured Values of $(E_c/p)_N$ as a Function of pr, for Three Different Monopole Diameters 32

Fig. 22 Measured Values of Power to Initiate Breakdown as a Function of Pressure for Three Different Monopole Diameters 33

Fig. 23 Measured Values of Power to Initiate Breakdown as a Function of Pressure for Monopoles 0.08λ, 0.16λ, 0.24λ, and 0.32λ 34

Fig. 24 Normalized Values of Breakdown Parameters for CW Breakdown of Monopoles, for Monopole Length of 0.08λ to 0.32λ 35

Fig. 25 Normalized Value of Breakdown Parameters for CW Breakdown, for 0.24λ Monopoles at 240 and 399.9 Mc 36

ILLUSTRATIONS

Fig. 26 Average Value of Normalized Breakdown Parameters for CW Breakdown of Monopole Antennas . . . 37

Fig. 27 CW Power to Initiate and Maintain Breakdown of a 0.40λ-Long Monopole Antenna as a Function of Pressure . . . 38

Fig. 28 $(E_e/p)_N$ as a Function of pr for Feed and Tip Breakdown . . . 39

Fig. 29 CW Power to Initiate Breakdown on a Monopole Antenna as a Function of Antenna Length . . . 40

Fig. 30 CW Power to Initiate Breakdown on a Monopole Antenna 0.24λ Long as a Function of Pressure for Different Tip Angles . . . 42

Fig. 31 Configuration Used for Measuring Pulsed Monopole Breakdown Characteristics at *X*-Band . . . 43

Fig. 32 Pulse Power Breakdown of a 0.24λ-Long Monopole at *X*-Band with a Pulse Width of 0.60 Microsecond . . . 44

Fig. 33 Pulse Power Breakdown of a 0.24λ-Long Monopole at *X*-Band with a Pulse Width of 1.04 Microsecond . . . 45

Fig. 34 Pulse Power Breakdown of a 0.24λ-Long Monopole at *X*-Band with a Pulse Width of 2.25 Microseconds . . . 46

Fig. 35 Normalized Results of Breakdown Measurements on a 0.24λ-Long Monopole Subjected to *X*-band Pulse Power . . . 47

Fig. 36 Sketch of Worth's Cavity-Fed Slot . . . 49

Fig. 37 Normalized Data on Worth's Slot Compared to Parallel Plate Breakdown . . . 50

Fig. 38 Sketch of 1- by 17-Inch Slot Antenna . . . 52

Fig. 39 Power to Initiate and Maintain Breakdown as a Function of Pressure for 1- by 17-Inch and 0.5- by 17-Inch Slot Antennas . . . 52

Fig. 40 Normalized Data on CW Breakdown of Slot Antennas and Rectangular Waveguide . . . 53

Fig. 41 Power to Initiate Pulsed Breakdown of *X*-Band Aperture for Three Pulse Widths. . . . 54

Fig. 42 Normalized Data for Breakdown of Pulsed Apertures and Waveguides . . . 55

Fig. 43 Power to Initiate Pulsed Breakdown for Various Slot Widths . . . 56

Fig. 44 Normalized Data for Pulsed Breakdown of Slot Antennas . . . 56

Fig. 45 Field Fall-Off for Different Antennas . . . 58

Fig. 46 Power to Initiate Pulsed Breakdown of a Sectoral and Pyramidal Horn . . . 59

Fig. 47 Normalized Data for Pulsed Breakdown of Different Height Antennas . . . 60

Fig. 48 Configuration Used in Producing a DC Plasma . . . 62

Fig. 49 Propagation Characteristics of a 373-Mc Slot Antenna in the Presence of a DC Plasma Pressure = 0.2 mm Hg, 500 Volts DC . . . 63

Fig. 50 Propagation Characteristics of a 373-Mc Slot Antenna in the Presence of a DC Plasma Pressure = 0.2 mm Hg, 670 Volts DC . . . 64

Fig. 51 Propagation Characteristics of a 373-Mc Slot Antenna in the Presence of a DC Plasma Pressure = 1.0 mm Hg, 560 Volts DC . . . 65

Fig. 52 CW Power to Initiate Voltage Breakdown as a Function of Applied DC Biasing Voltage for a 0.24-Wavelength Monopole . . . 69

Fig. 53 Pulsed Power to Initiate Voltage Breakdown as a Function of Applied DC Biasing Voltage for a 0.24-Wavelength Monopole . . . 70

Fig. 54 CW Power to Initiate Voltage Breakdown as a Function of Applied DC Biasing Voltage for a 380-Mc Slot Antenna . . . 71

Fig. 55 Sketch of Top-Loaded Folded Monopole 0.10 Wavelengths High . . . 72

VOLTAGE BREAKDOWN OF ANTENNAS AT HIGH ALTITUDES

I INTRODUCTION

A. BACKGROUND

Examination of the received signal from electronic systems on various missiles have indicated the presence of voltage breakdown at the antennas in the altitude range of 50,000 to 300,000 feet at VHF, UHF and microwave frequencies. The presence of voltage breakdown is manifested by a decrease in transmitted signal intensity, change in the input impedance and the radiation pattern of the missile antenna, modification of the pulse shape, and noise radiation on the signal.[1*] Since it is important in many cases to obtain continuous telemetry and tracking information to determine impact position and system performance data, an experimental investigation has been carried out to study the power-handling capabilities of antennas at high altitude. The principal aims of this study are (1) to determine the physical mechanism involved, (2) to measure and tabulate experimental data on breakdown field for various antenna types, and (3) to study methods for improving the power-handling capability of antennas.

B. BREAKDOWN MECHANISM

The high-frequency breakdown mechanism has been thoroughly investigated in the past for circuit elements such as transmission lines and cavities.[2,3] The source of primary ionization is due to electron motion, and breakdown occurs when the gain in electron density becomes equal to the loss of electrons by diffusion and attachment. This relationship is expressed as:

$$\frac{\partial n}{\partial t} = (\nu_i - \nu_a)n + S + \nabla^2(Dn) \qquad (1)$$

* References are listed at the end of the report.

where

n is the electron density

ν_i is the ionization rate

ν_a is the attachment rate

S is the ionization produced by an external source

D is the diffusion coefficient for electrons.

The measurements reported here confirm that the processes that are important for microwave circuit elements also determine the minimum power-handling capability of antennas in air at low pressure.

For a parallel plate configuration, the solution of the electron continuity equation (1) gives for the breakdown condition:

$$\nu_i - \nu_a = \frac{D}{\Lambda^2} \tag{2}$$

where Λ is the characteristic diffusion length and describes the gas container shape in a typical diffusion problem. For spacing L between parallel plates

$$\Lambda = \frac{L}{\pi} \tag{3}$$

The diffusion coefficient is

$$D = \frac{lv}{3} \tag{4}$$

where l is the mean free path and v the velocity of the electron. For a given configuration at a fixed pressure, D is a constant. If the parallel plate spacing is decreased, then Λ decreases while D/Λ^2 will increase. Thus the net ionization rate, $\nu_i - \nu_a$, must be increased to initiate breakdown. Since the net ionization rate increases with increasing electric field, one obtains the interesting result that by decreasing the spacing between parallel plates, one increases the field strength required to initiate breakdown.

1. Diffusion-Controlled Breakdown Curve

A plot of the typical variation of the breakdown field with pressure is shown in Figure 1. If the breakdown field is controlled only by attachment, the field strength required to initiate breakdown is shown by the solid line and is given approximately by $E_e = 30p$. Here p is the pressure in mm Hg; E_e is the effective field which would produce the same energy transfer to the electron as a DC field and is given by

$$E_e = \frac{E\nu_c}{[\nu_c^2 + \omega^2]^{1/2}} \tag{5}$$

where E is the rms field

ν_c is the collision frequency in collisions per second

$\omega = 2\pi f$ = angular frequency.

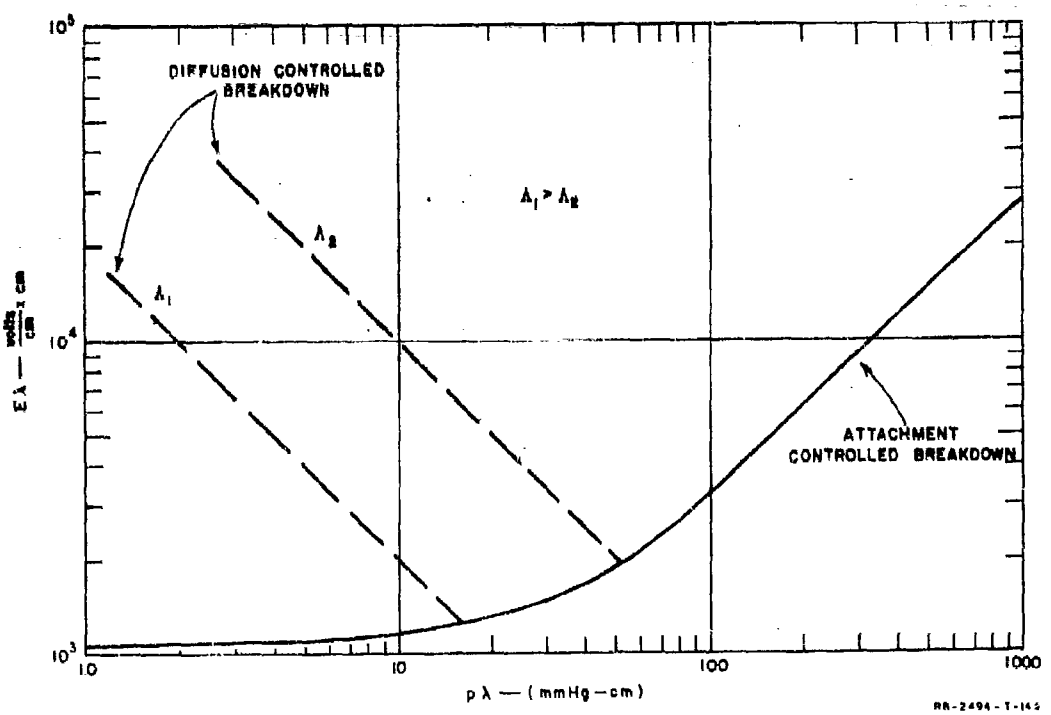

FIG. 1

ILLUSTRATION OF DIFFUSION- AND ATTACHMENT-CONTROLLED BREAKDOWN

At high pressures, the mean free time of the electron is small compared to the RF period, and the energy gained by the electron per collision is small. Since the electron must gain energy corresponding to the ionization potential more electric field strength is required as the pressure is increased. Thus, in this region the value of E to initiate breakdown varies directly with the pressure, since for air

$$\nu_e = 5.3 \times 10^9 p \qquad (6)$$

where p is the pressure in mm mercury.

At very low pressures the electrons make many oscillations per collision. Since the electrons gain energy only through collision, the energy transfer is poor and the curve flattens out at low pressure. The knee of the curve in Fig. 1 represents the pressure at which the collision frequency is equal to the RF frequency. Since the attachment and ionization rates do not depend on geometry, the breakdown field will be independent of geometry.

If diffusion becomes an important loss parameter, the curve begins to rise at low pressure. In fact, the field strength varies inversely as the pressure and diffusion length. In Fig. 1 two curves are shown for the diffusion-controlled case, where $\Lambda_1 > \Lambda_2$. Here, Λ_2 corresponds to increased diffusion loss, and in the case of a parallel plate this corresponds to a narrower spacing. This figure illustrates the fact that associated with a given frequency of operation, there is *no* single pressure at which a minimum field strength is required for breakdown. The pressure at which maximum power transfer to the electron occurs, serves as an estimate for the pressure at which minimum breakdown occurs. At this frequency the collision frequency ν_e is equal to the angular RF frequency—i.e.,

$$f = \frac{5.3 \times 10^9 p}{2\pi} = 8.45 \times 10^8 p \qquad . \qquad (7)$$

As diffusion loss becomes important the minimum occurs at higher and higher pressure, as shown in Fig. 1.

In pulsed breakdown, the pulse is normally on for such a short time that breakdown is less dependent on geometry and, hence, on diffusion.

In this case breakdown will occur when the difference between ionization and attachment rate is large enough so that within the time the pulse is on, the electron density will build up to the breakdown density.

At pressures so low that the mean free path is of the order of or greater than the characteristic dimension, the breakdown process is no longer diffusion-controlled and Eq. (1) no longer applies.

A study of the factors making up Eq. (1) shows that for geometrically similar antennas, frequency scaling is applicable[4] for the type of discharge under consideration. Aside from the usual electromagnetic similitude principle, it is required that

$$p\lambda = \text{constant}$$

where

p is the pressure in mm Hg

λ is the wavelength.

Also if the form of the near-zone field remains the same with some varying dimension (as with parallel plate transmission lines with varying spacing, narrow slot antennas with varying width, and monopoles with varying diameter) the value of the ratio of effective field required for breakdown, E_e, to pressure, p, is a function of pressure times the characteristic dimension.

If the near-zone field region about an antenna does not vary with varying characteristic dimension, E_e/p is no longer simply a function of pressure times the characteristic dimension. This occurs, for example, with slot antennas when the slot width becomes appreciable compared to a wavelength.

2. Free and Ambipolar Diffusion

For breakdown in air the diffusion coefficient D_f is due to diffusion of free electrons and is given by

$$D_f = \mu_e \frac{kT_{ef}}{e} \tag{8}$$

where

μ_e = electron mobility = $\dfrac{e}{m\sqrt{\nu_c^2 + \omega^2}}$

k = Boltzmann's constant

T_{ef} = electronic temperature with free diffusion.

The free diffusion condition exists at low pressure (high altitude) and can be simulated in a vacuum chamber.

A phenomenon which is unique to high altitude missile operation is the transmission of signal through the ionized medium associated with re-entry into the earth's atmosphere. The effect of the ionized medium is to change the electron loss mechanism from free diffusion to ambipolar diffusion.[5] The diffusion of electrons from a neutral plasma brings about the increased mobility of the heavy positive ions since the plasma tends to charge neutrality. A positive space charge is developed as a sheath around the antenna which retards the high velocity electrons and accelerates the positive ions. In the plasma to be considered in this report, the electron temperature is large compared to the positive ion temperature and the ambipolar diffusion coefficient is then given by

$$D_a \approx \mu_+ \frac{kT_{ea}}{e} \tag{9}$$

where

μ_+ = positive ion mobility

T_{ea} = electronic temperature with ambipolar diffusion.

Therefore

$$\frac{D_a}{D_f} \approx \frac{\mu_+ T_{ea}}{\mu_e T_{ef}} \tag{10}$$

The net result is to decrease the diffusion loss of electrons, thus decreasing the power-handling capability in an ionized medium.

II LOW-PRESSURE VOLTAGE BREAKDOWN IN TRANSMISSION LINES

A. BACKGROUND

Most of the investigations that have been conducted in the past have been concerned with breakdown in transmission lines. Breakdown in transmission lines differs from antenna breakdown principally in two ways. First, in transmission lines one is usually concerned only with the two-dimensional electric field variations. In antennas, the three-dimensional field variations must be considered. In unmatched transmission lines, where standing waves are present, the longitudinal distribution of field may be of importance, but in most cases it varies more slowly than the transverse fields. Secondly, in most transmission systems the fields are contained by conductors in such a way that there are surfaces to which electrons can diffuse. In antennas, the electrons may drift away from the vicinity of the aperture without being lost to a surface.

Nevertheless, because data and theoretical approaches are available from researches into transmission line breakdown, they will be used as a starting point.

B. CW BREAKDOWN OF PARALLEL-PLATE SYSTEMS

Consider a transmission line system composed of two infinite parallel plates separated by a distance, d, with a uniform electric field, E, between the plates. Both Brown[2] and Gould and Roberts[3] have analyzed this configuration, and the following discussion will review their results.

For CW breakdown to occur, the rate of change of electron density with time, $\partial n/\partial t$, must be slightly greater than zero. Under these conditions the electron density will increase exponentially with time at a rate determined by the value of $\partial n/\partial t$. The rate of change of electron density is determined by the difference between the rate of increase of electron density and the rate of loss of electron density. This relationship is expressed as

$$\frac{\partial n}{\partial t} = \nu_i n - \nu_a n + \nabla^2 (Dn) \quad . \tag{11}$$

Here, ν_i is the frequency of ionization per electron, so that $\nu_i n$ is the number of ionizations produced per second; and ν_a is the frequency of attachment per electron, so that $\nu_a n$ is the number of electrons lost by attachment per second. The loss of electrons per second due to diffusion to the plates is given by $\nabla^2 (Dn)$. This equation may be written in integral form as

$$ln \left(\frac{n}{n_0}\right) = \int_0^\tau \left[(\nu_i - \nu_a) + \frac{\nabla^2 (Dn)}{n}\right] dt \qquad (12)$$

when n_0 ambient electron density before the electric field is applied.

Brown has solved for the electron density distribution for this case and shown that it is of the form sin $(\pi x/d)$, where x is distance measured from one plate. For a uniform field distribution, D is a constant, and $\nabla^2 (Dn)$ may be written as $D\nabla^2 n$. Since n is of the form sin $(\pi x/d)$

$$\nabla^2 (Dn) = \left(\frac{\pi}{d}\right)^2 Dn \qquad (13)$$

Substituting this expression into Eq. (12), and integrating, we obtain

$$\frac{ln\left[\frac{n}{n_0}\right]}{\tau} = \langle\nu_{net}\rangle + D\left(\frac{\pi}{d}\right)^2 \qquad (14)$$

where $\langle\nu_{net}\rangle$ is the average net value of $\nu_i - \nu_a$ over the time τ. Normalizing with respect to pressure [Eq. (14)] becomes

$$\frac{ln\left[\frac{n}{n_0}\right]}{p\tau} = \frac{\langle\nu_{net}\rangle}{p} + \frac{Dp\pi^2}{(pd)^2} \qquad (15)$$

For CW breakdown τ can be made indefinitely large, so the breakdown is defined by setting the left side of Eq. (15) equal to zero:

$$0 = \frac{\langle\nu_{net}\rangle}{p} - \frac{Dp\pi^2}{(pd)^2} \qquad (16)$$

Gould and Roberts show that $\langle \nu_{net} \rangle / p$ is a function only of E_e/p and $p\lambda$, while MacDonald[6] has shown that Dp is a function E_e/p. Therefore, the value of E_e/p required for breakdown is a function of pd and $p\lambda$. Equation (16) has been solved and the results of Gould and Roberts[3] are plotted in Fig. 2 for the CW case. These curves have been verified by a number of measurements, including Herlin and Brown's[7] at 3000 Mc and Pim's[8] at 200 Mc.

The fact that the curve flattens out for pd greater than about 25 mm Hg-cm indicates that for these values of pd electron loss by diffusion to the walls is negligible and the predominant loss is by attachment. That is, the walls no longer play a part in removing electrons and so any value of pd requires the same value of E_e/p for breakdown. The equation for breakdown under this condition is then

$$0 = \frac{\langle \nu_{net} \rangle}{p}$$

and the value of E_e/p for breakdown is approximately 30.

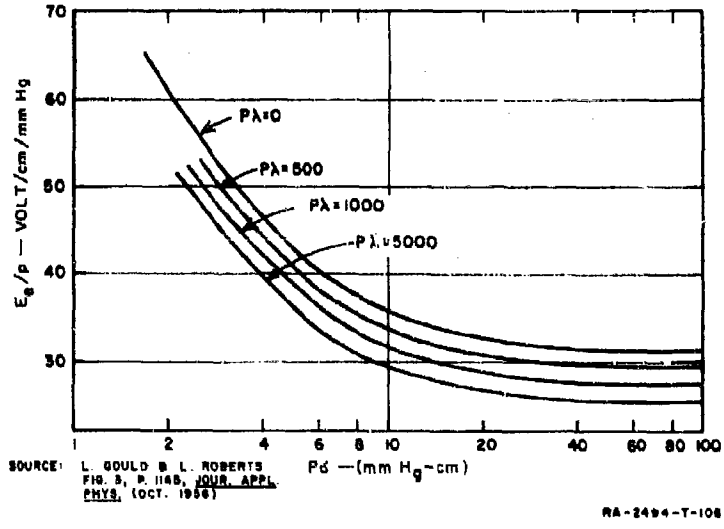

FIG. 2

SOLUTION FOR PARALLEL PLATE CW BREAKDOWN
From Gould and Roberts

For values of pd less than 25 mm Hg-cm, electrons are lost to the plates by diffusion, and higher values of E_e/p are required to make up for the increased loss.

Since the value of E_e/p for a given pd varies only slightly over the range of $0 \leq p\lambda \leq 5000$, where λ is the wavelength in cm, a normalized curve of E_e/p as a function of pd has been plotted in which the parameter $p\lambda$ has been eliminated by plotting only the values of E_e/p for $p\lambda = 0$. This curve, shown in Fig. 3, with the aid of the correction shown in Fig. 4, contains all the information necessary to determine the value of E_e/p for any $p\lambda$ and pd. The relation between the value of E_e/p at a given $p\lambda$ and for $p\lambda = 0$ is

$$\left(\frac{E_e}{p}\right)_{p\lambda} + \Delta = \left(\frac{E_e}{p}\right)_{p\lambda=0}$$

where Δ is given in Fig. 4 and $(E_e/p)_{p\lambda=0}$ shall be called $(E_e/p)_n$.

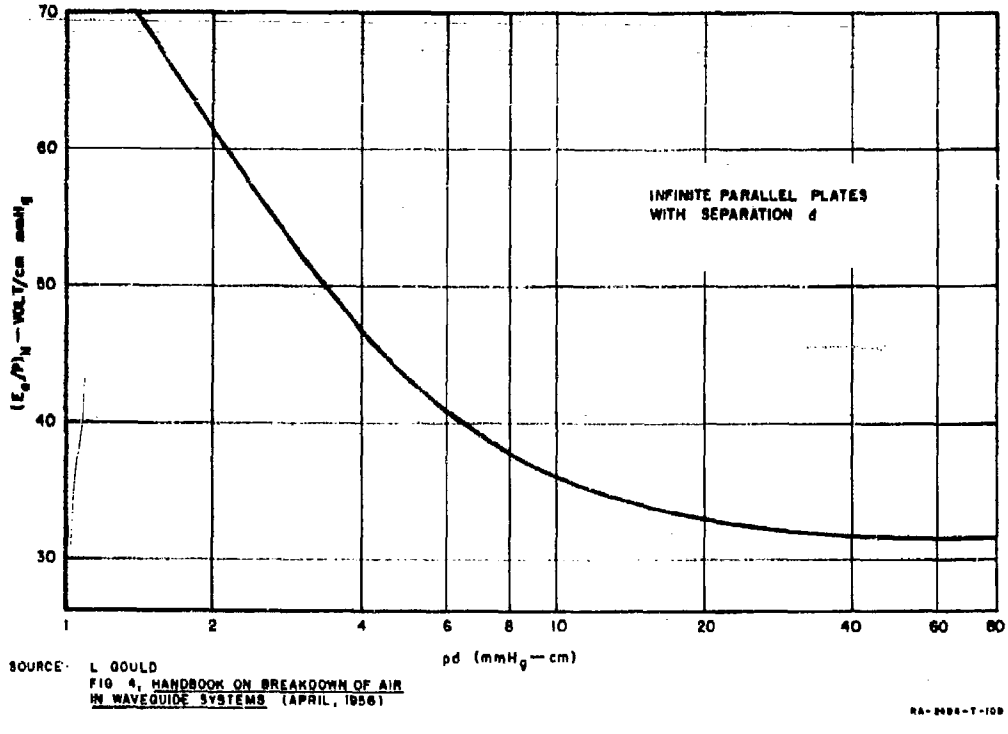

FIG. 3

NORMALIZED SOLUTION FOR PARALLEL PLATE CW BREAKDOWN
From Gould and Roberts

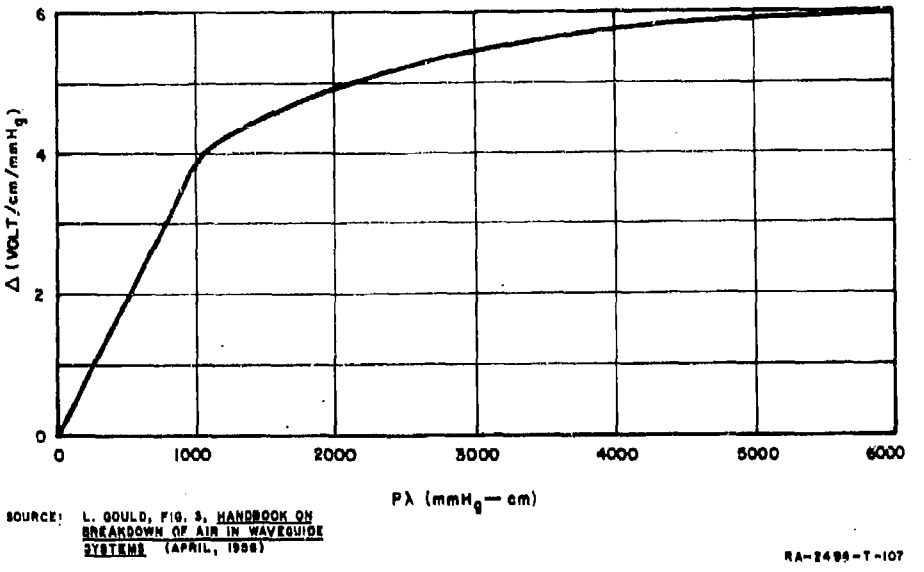

FIG. 4

NORMALIZATION FACTOR, Δ, AS A FUNCTION OF pλ
From Gould and Roberts

Also shown in Fig. 3 are the results of a series of measurements by Herlin and Brown[9] at a wavelength of 9.6 cm. Their data, which were presented as curves of E as a function of p for three different values of d, has been converted into the notation of E_e/p, $p\lambda$, and pd. These data extend Gould and Roberts data 2 orders of magnitude.

C. PULSED BREAKDOWN OF PARALLEL-PLATE SYSTEMS

1. Single Pulse

For breakdown to occur within a single pulse width, τ, it is necessary for the electron density to build up to some breakdown value, n_b, in a finite time. Referring to Eq. (15), the left hand side of the equation is no longer zero but some finite value. Gould and Roberts[3] have solved Eq. (15) and obtained a solution in the form of

$$\frac{E_e}{p} = f[pd,\ p\tau,\ p\lambda] \quad .$$

A ratio of 10^8 was assumed, since n_b and n_0 are somewhat indeterminate, and since 10^8 produced the closest check with experimental results. Their data are shown in Fig. 5.

Once again there is a region over which the curve flattens out. As $p\tau$ is increased for a given pd, the breakdown approaches the character of a CW breakdown. When there is no longer any decrease of E_e/p with increasing $p\tau$, the breakdown is precisely the same as in the CW case. The shorter the value of τ, the more rapidly must the electron density build up to reach n_b. This can be done if the ionization rate (and hence E_e/p) is increased while the attachment and diffusion losses remain the same or become smaller. The attachment loss is constant as a function of τ, but the diffusion loss decreases as τ decreases, since there is less time for the electrons to diffuse to the walls. However, in general

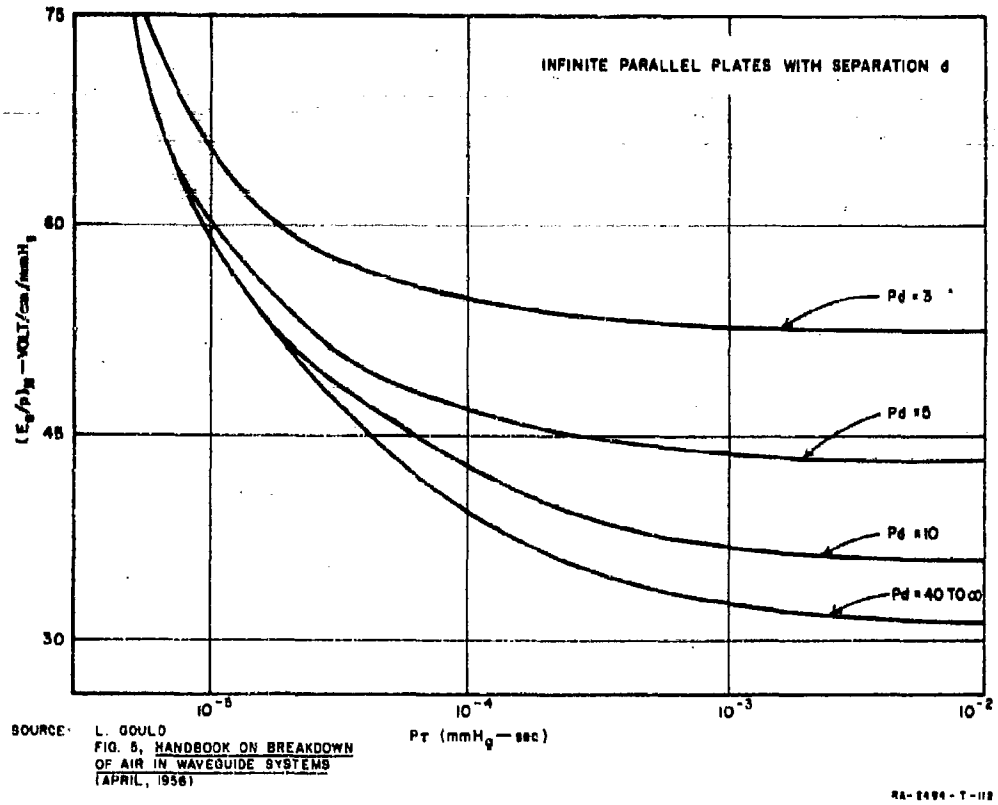

FIG. 5

SOLUTION FOR PARALLEL PLATE PULSED POWER BREAKDOWN
From Gould and Roberts

the decrease in diffusion loss is more than offset by the reduced time available for the electron density to reach n_b. Thus as $p\tau$ decreases, for a given pd, E_e/p increases.

In addition, since at lower values of $p\tau$ the diffusion loss becomes less important than the attachment loss, the curves for different values of pd tend to merge as $p\tau$ decreases. That is, the spacing between the plates no longer is important when the breakdown process is attachment-controlled.

2. Multiple Pulse

If the pulse repetition frequency (PRF) is sufficiently high, breakdown may occur at lower values of E_e/p than for single pulse breakdown. This may be explained as follows:

Consider a pulse of amplitude slightly below the value necessary to produce single pulse breakdown. Even though breakdown does not occur, a significant electron density is produced while the pulse is on. When the pulse is off, the electron density decreases due to recombination, diffusion and attachment. However, these processes require a finite time. Therefore, when the next pulse occurs, the initial electron density, n_0, for this pulse will be greater than for the first pulse, so that the electron density at the end of the second pulse will be greater than at the end of the first pulse. After a sufficient number of such pulses, breakdown will occur. The shorter the time between pulses (higher PRF) the larger will be the residual electron density from the previous pulse, and therefore a lower value of E_e/p will be required for breakdown.

Measurements of this phenomenon have been made by Gould and Roberts and by Allen and Keenan.[10] Gould and Roberts' results are shown in Fig. 6. As can be seen from the figure, over the usual range of pulse repetition frequencies used in radars, the variation of E_e/p with PRF is a relatively small factor. Over the entire range of parameters described by Allen and Keenan the value of E_e/p varies only by a factor of two at the most.

One further point illustrated by the measured results is that the PRF at which E_e/p begins to depart from the single pulse values, increases with increasing pressure. That is, the time between pulses must decrease as the pressure increases in order for there to be a significant increase in electron density from pulse to pulse. This is reasonable when it is realized that the recombination rates increase as the pressure increases.

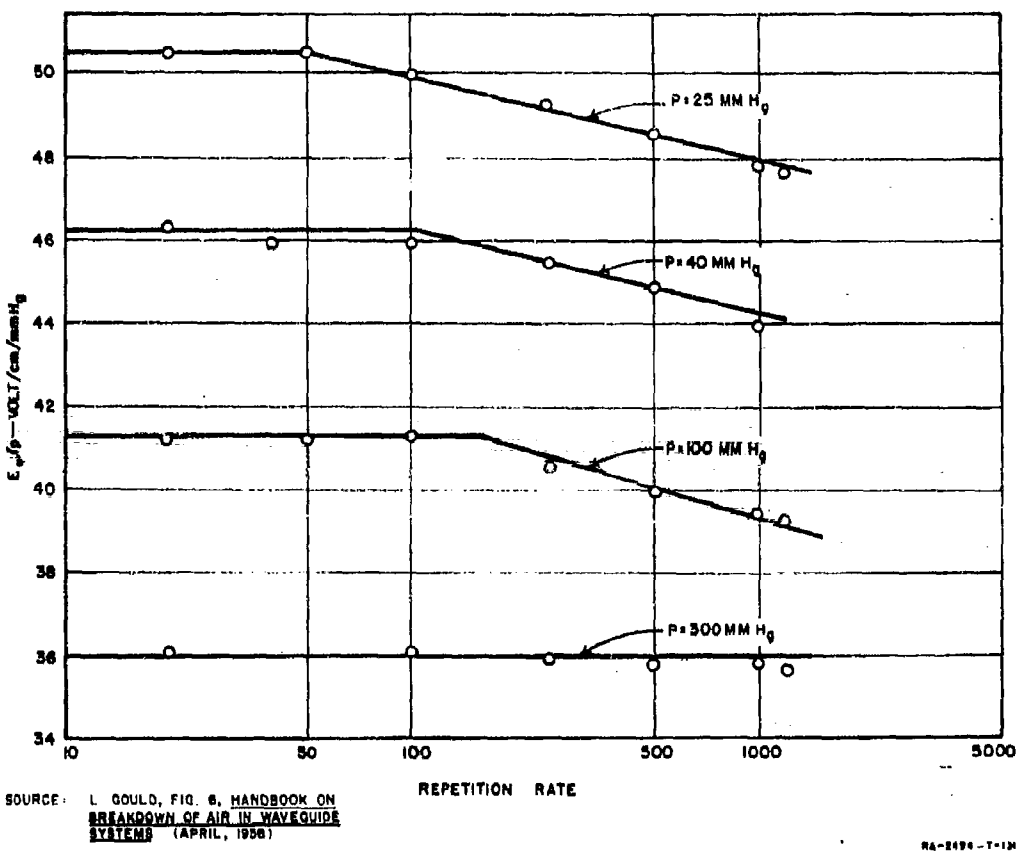

SOURCE: L. GOULD, FIG. 6, HANDBOOK ON BREAKDOWN OF AIR IN WAVEGUIDE SYSTEMS (APRIL, 1956)

FIG. 6

RESULTS OF THE EFFECT OF PRF ON BREAKDOWN
From Gould and Roberts

D. CW BREAKDOWN OF RECTANGULAR WAVEGUIDE

When side walls are added to a parallel plate structure, a rectangular waveguide is formed. This discussion shall be limited to the TE_{10} mode of excitation of such a waveguide. The main effect of adding side walls is to alter the field configuration between the parallel plates. The transverse field distribution from the bottom to the top plate is still uniform, but this field now has a sinusoidal variation of the form $\sin(\pi y/2a)$ across the waveguide, where y is measured from one side wall and a is the guide width. Since the field is no longer uniform across the waveguide, transverse diffusion as well as diffusion to the top and bottom walls may be an important mechanism for the removal of electrons. That is, electrons produced near the center of the waveguide will diffuse into field regions where they no longer can obtain ionizing energy and hence are not effective in producing breakdown. Since the electron loss mechanism has been increased, it would be expected that higher values of E_e/p would be required for waveguide breakdown than for parallel plate breakdown. That this is actually the case is illustrated in Fig. 7, taken from Gould's report.[11] In this figure the value of CW E_e/p for breakdown as a function of pb (b is the height of the waveguide) is plotted for several values of the ratio a/b. For a given value of b, the larger the ratio a/b, the more slowly the transverse field varies and hence the more closely waveguide breakdown appears like parallel plate breakdown. Thus, for each value of pb the larger the ratio a/b, the smaller is the required E_e/p for breakdown. The curve for $a/b > 8$ is almost identical with the parallel plate breakdown data.

For the larger values of pb, where attachment is the dominant loss mechanism, the transverse diffusion of electrons in rectangular waveguide is unimportant for all values of a/b considered. Therefore, at these values of pb the ratio of a/b makes little difference and all the curves merge to the value for attachment controlled parallel plate breakdown.

E. PULSED BREAKDOWN OF RECTANGULAR WAVEGUIDE

As may be gathered from the numerous references to the work of Gould and Roberts, that source has been used as a starting point for much of the work that the authors of this report have carried out. Valuable as their work is, however, their data are limited to values of E_e/p less than about

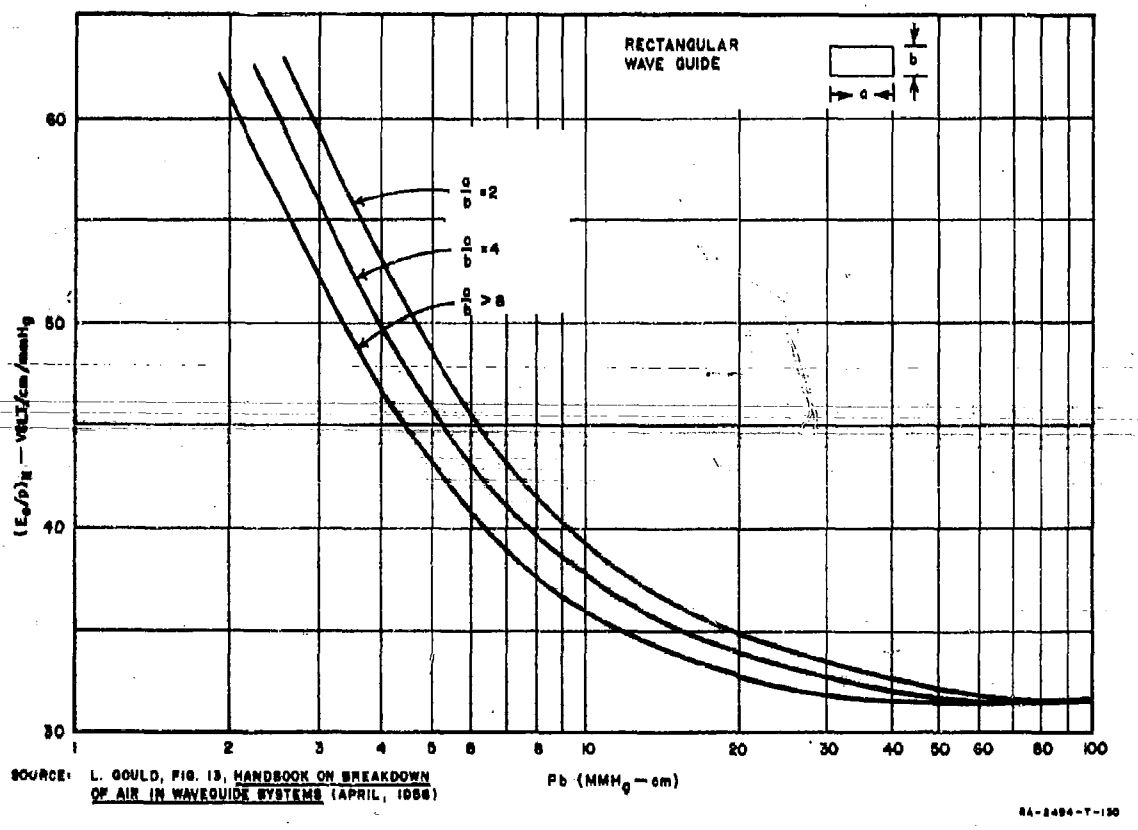

FIG. 7

RESULTS OF CW BREAKDOWN IN RECTANGULAR WAVEGUIDE
From Gould and Roberts

80 volts/cm/mm Hg. Therefore, in order to check our experimental technique against previously measured results, and also to extend the data beyond the presently available range, measurements of breakdown inside a rectangular waveguide were made.

Measurements were made on a standard size X-band rectangular waveguide (inside dimensions a = 0.9 inches, b = 0.4 inches) radiating into free space. Under these conditions the input VSWR was 1.7 with the maximum voltage point not in the aperture. This ensured that the breakdown would occur inside the guide and not in the aperture. At the same time the VSWR was low enough that longitudinal variations in the field should have only a small effect on the results. A waveguide many wavelengths long was used so that the aperture was far from the point of breakdown, and so that higher order modes were not present near the breakdown point.

A block diagram of the experimental set-up is illustrated in Fig. 8. Note the use of a strip of polonium, an alpha particle source, taped to the inside side wall of the waveguide. To initiate the breakdown process a free electron is required. Using this source, measurements were quite repeatable without waiting for long periods of time.

Power was measured through a calibrated directional coupler, a calibrated variable attenuator, and a bridge type of power meter. A ferrite isolator in the line directly out of the magnetron prevented the occurrence of appreciable power variations or frequency-pulling under breakdown conditions.

The reflected pulse was monitored on an oscilloscope and breakdown was determined by any alteration in either the amplitude or shape of the reflected pulse. Since the breakdown was occurring inside the waveguide it was more certain to determine breakdown by the change in the reflected pulse than by visual observations. In general, even when visual observation is possible, as on an antenna aperture, for weak breakdowns the reflected pulse method is more sensitive than visual observations of the aperture. Further, since the effect of breakdown on a system is of concern, measured electromagnetic effects are more important than visual effects.

Three pulse widths (approximately 0.5, 1.0, and 2.3 microseconds) were available, and data at each pressure were taken with all three.

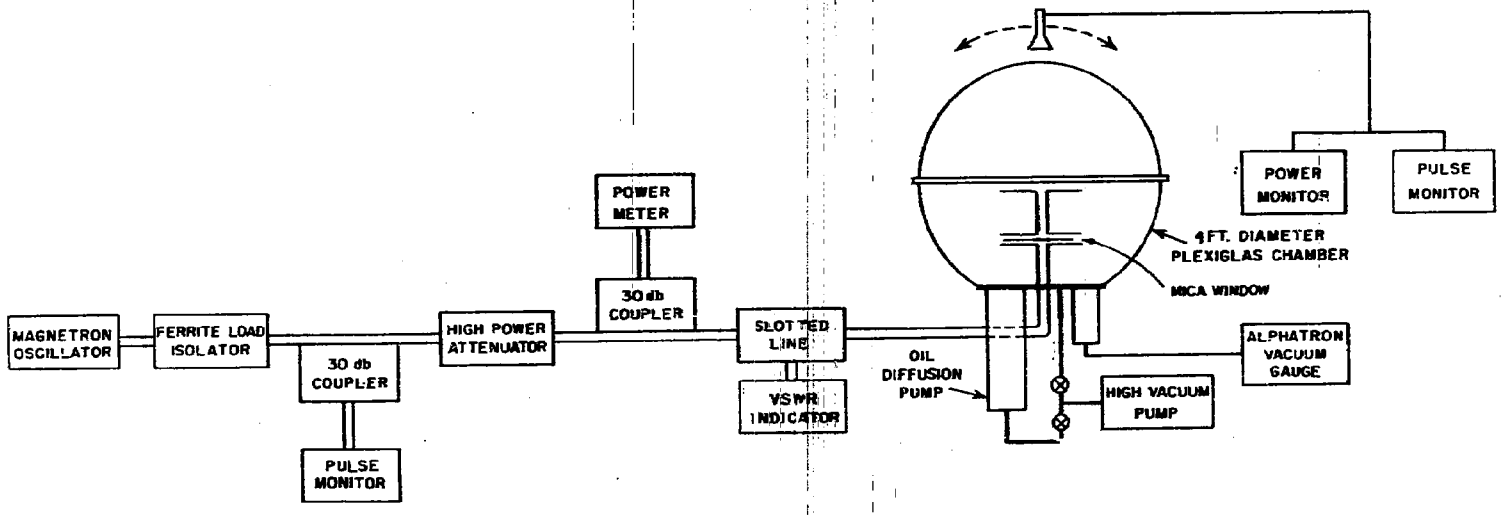

FIG. 8

BLOCK DIAGRAM OF EXPERIMENTAL SET-UP USED IN X-BAND PULSED POWER BREAKDOWN MEASUREMENTS ON RECTANGULAR WAVEGUIDE

Since the breakdown fields are not greatly affected by PRF, a value of 200 pps was chosen rather arbitrarily for these measurements. A plot of the directly measured parameters, peak power and pressure, is shown in Fig. 9. These curves exhibit the usual pattern for breakdown, with a minimum power for breakdown required at approximately the pressure at which the collision frequency equals the angular frequency. In this case the measured minimum occurs at a pressure of about 5 mm Hg while the pressure at which $\nu_c = \omega$ is about 11 mm Hg.

The data on power have been transformed into electric field values (see Appendix D), and the data normalized into terms of $(E_g/p)_n$, $p\tau$, and pb. The results are plotted in Fig. 10. Also shown for comparison is

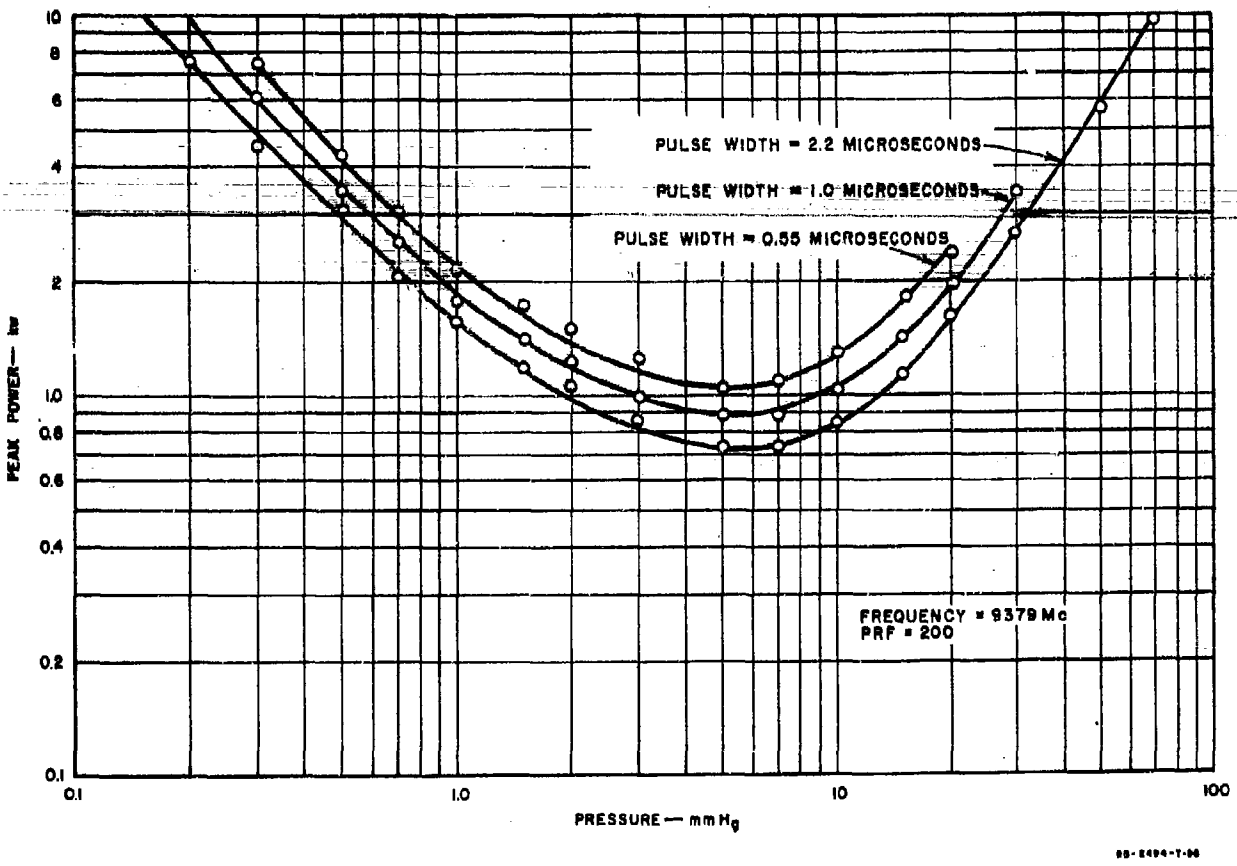

FIG. 9

PEAK POWER AS A FUNCTION OF PRESSURE TO INITIATE BREAKDOWN IN A RECTANGULAR WAVEGUIDE AT X-BAND

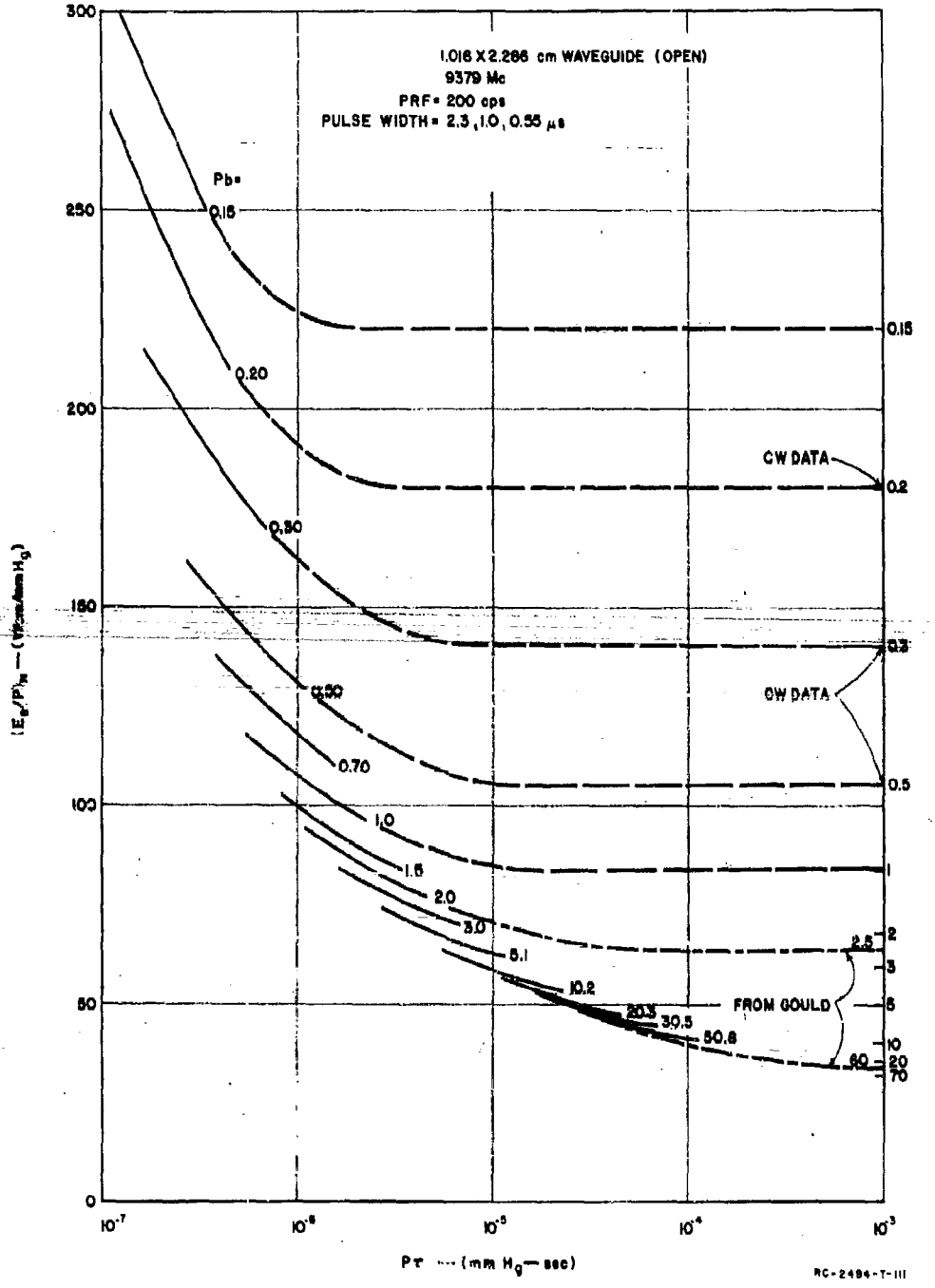

FIG. 10

$(E_e/p)_N$ AS A FUNCTION OF pτ FOR DIFFERENT VALUES OF pb FOR A RECTANGULAR WAVEGUIDE WITH a/b = 2.25

the entire range of data available from Gould's report.[11] The agreement between their data and the measured data over the range where these two sets of data overlap is quite good.

The CW breakdown values of $(E_e/p)_n$ taken from Herlin and Brown's[9] data on parallel plates are indicated at the highest value of $p\tau$ plotted ($p\tau \approx 10^{-3}$ mm Hg-sec). These values are taken as asymptotes which should be reached as $p\tau$ increases indefinitely. The dashed lines connecting the measured pulse data with the CW data are estimated values and are drawn to conform with the pattern characteristic of the variation of $(E_e/p)_n$ as a function of $p\tau$ for $2.5 \leq pb \leq \infty$. The close agreement between the two sets of data over the range $2.5 \leq pb \leq \infty$ suggests that some degree of confidence may be placed in the estimated curves.

In order to verify the effect of PRF on breakdown power, a series of measurements were made in which the peak power for breakdown as a function of PRF was measured for pressures above, at, and below the minimum. The results are shown in Fig. 11. At each pressure the data have been normalized to the peak power for breakdown at one pulse per second. The results are similar to those of previous workers, described in an earlier section.

The variation in peak power for breakdown for the range of PRF's from 1 to 200 is less than 5% over the pressure range from 0.7 to greater than 30 mm Hg. Therefore, the results shown in Fig. 10 should be applicable with only a small error for PRF's other than 200.

In Fig. 12 the curves of power required to initiate and to maintain breakdown for a matched waveguide as a function of pressure are plotted for a pulse width of 1.0 microseconds. Throughout the whole pressure range over which measurements were made there is only a small difference between the initiating and the maintaining power. This is so because the breakdown is essentially a single pulse breakdown and therefore extinguishes itself at the end of every pulse. Even under ambi-polar diffusion, when the pulse is off, the electron density decreases rapidly compared to the period between the pulses.

F. CW BREAKDOWN OF COAXIAL LINES

Radio frequency breakdown within coaxial lines has been studied by Gould[11] and Herlin and Brown.[12] In coaxial lines the radial field varies

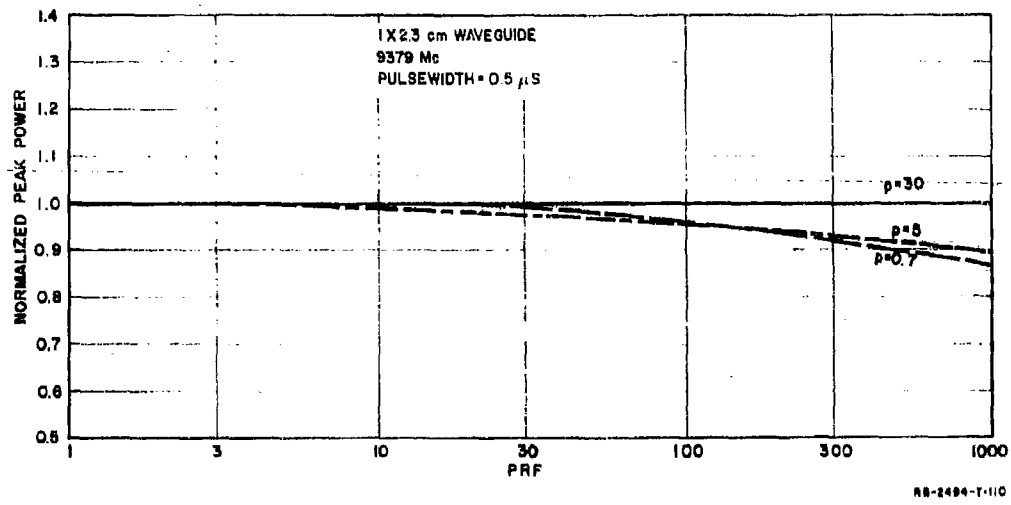

FIG. 11

NORMALIZED CURVES SHOWING EFFECT OF PRF ON PEAK POWER TO INITIATE BREAKDOWN

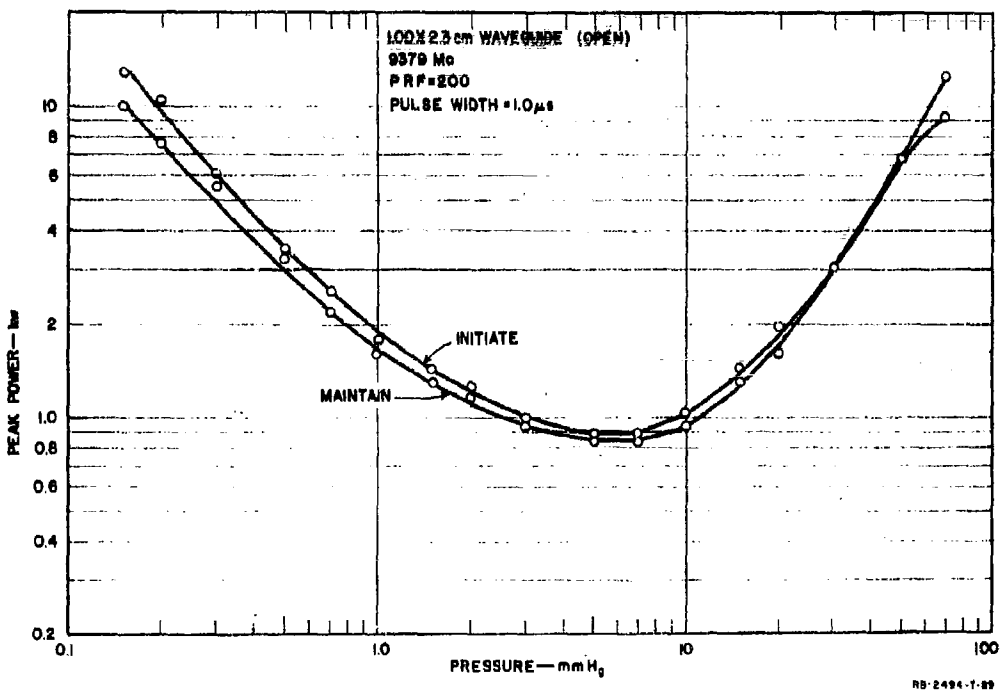

FIG. 12

PEAK POWER AS A FUNCTION OF PRESSURE TO INITIATE AND MAINTAIN BREAKDOWN IN A RECTANGULAR X-BAND WAVEGUIDE WITH A PULSE WIDTH OF 1 MICROSECOND

as r_1/r (r_1 is the inner conductor radius and r is the radial distance measured from the center of the inner conductor) with the maximum field at the surface of the inner conductor so that radial diffusion is important. As electrons are formed in the high fields near the inner conductor they diffuse radially outward and enter lower field regions where they cannot gain ionizing energy. At the higher pressures where the mean free path is small the breakdown tends to form about the inner conductor. At lower pressures the mean free path increases so that the random velocity of the electrons may carry them away from the inner conductor before they collide with a gas molecule. Therefore, at lower pressures the breakdown occurs at some distance from the inner conductor moving outwards as the pressure decreases.

The theoretical analysis of coaxial line breakdown is complicated by the fact that the ionization frequency, the attachment frequency and the diffusion coefficient are all functions of the radial distance r.

Gould[11] has given the results of his solution of the breakdown equation for a value of $r_2/r_1 = 2.3$ (r_2 is the outer conductor radius) which corresponds to a characteristic impedance of 50 ohms. Unfortunately, the method of solution is not given, so that data for other values of r_2/r_1 cannot be calculated. Also, his data only extend to values of $(E_s/p)_n$ of about 85. Gould's calculated data are presented in Fig. 13.

Herlin and Brown[12] have used an approximate analysis and described the details of their solution. Using curves of ζ (ionization/volt^2) as a function of E/p which have been determined from parallel plate data, they approximate the actual variation of ζ as a function of E/p by a straight line (on log-log paper) which is tangent to the actual curve at the value of E/p which corresponds to the field at the surface of the inner conductor. With this approximation a solution of the diffusion equation in terms of Bessel functions is obtained. Introducing the boundary conditions for the electron density at r_1 and r_2 (n=0) a complete solution is obtained. However, since there is a different curve of ζ as a function of E/p for every value of $p\lambda$, a different solution is obtained for each value of $p\lambda$. The solution for $p\lambda = \infty$ has been worked out by Herlin and Brown[12] and should be useful down to values of $p\lambda$ greater than 100 mm Hg-cm. Fig. 14 presents the results in graphical form. These data check quite well with Herlin and Brown's experimental results as well as with the measured results of Paska[13] on a variety of coaxial lines. These data can be converted into Gould's notation with the results shown in Fig. 15.

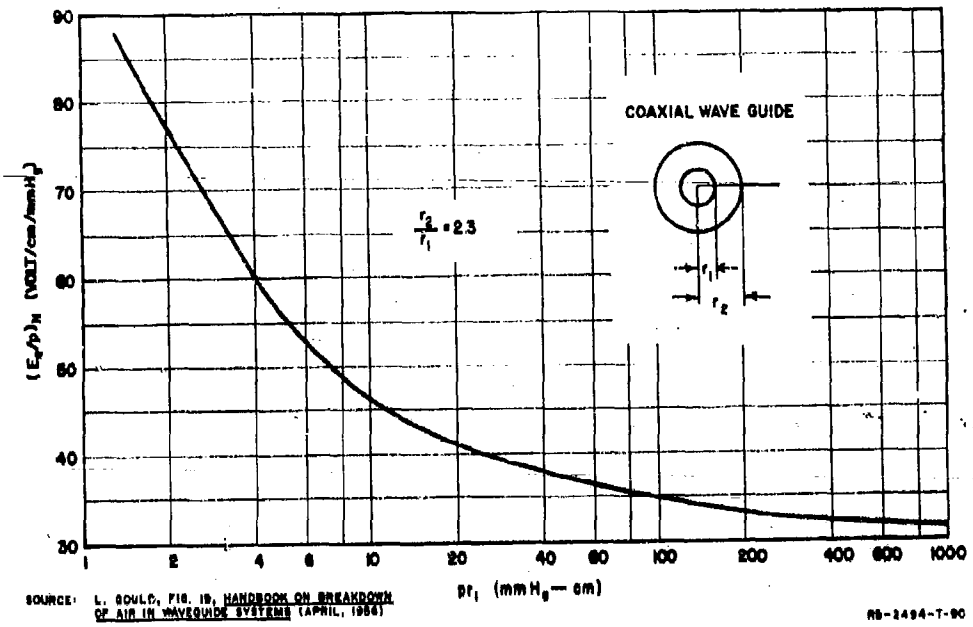

FIG. 13

COAXIAL LINE CW BREAKDOWN DATA
From Gould

Just as in the parallel plate case, at high values of pressure or large values of r_1 the curve flattens out. In fact it flattens out to approximately the same value of $(E_e/p)_n$ as for parallel plates. The reason for the flattening is that the major loss mechanism for large p is attachment. For large values of r_1 and p, the field is slowly varying with radial distance near the inner conductor. Because of the high pressure the electrons can collide often in this high field region, thus producing ionization near the inner conductor. Increasing r_1 beyond this point will not decrease $(E_e/p)_n$ since the radial field is already almost uniform within the range of electron motion. As r_1 is made smaller, the field within the electrons range of motion becomes less uniform and high energy electrons can move into low field regions without gaining ionizing energy. Thus $(E_e/p)_n$ increases as pr_1 decreases. In this case electrons are "lost" by diffusion to the low field regions while in parallel plate breakdown they are "lost" by diffusion to the walls.

The extension of coaxial line breakdown to monopole antenna breakdown is discussed in Sec. III.

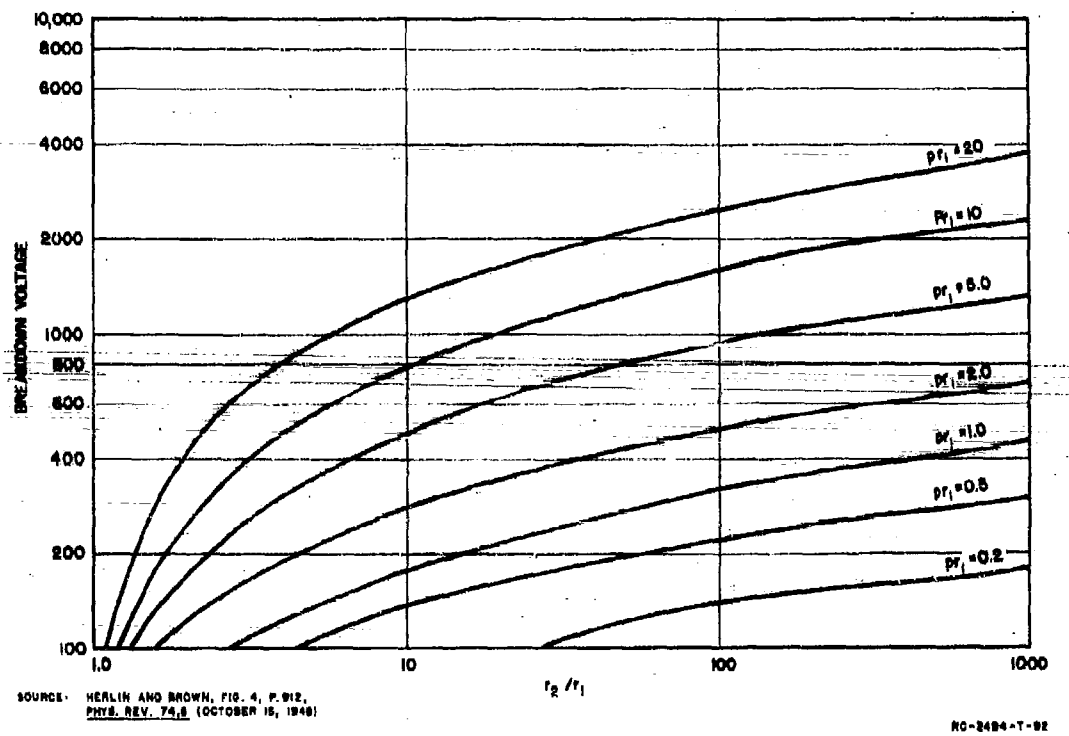

FIG. 14

COAXIAL LINE CW BREAKDOWN DATA FOR $p\lambda = \infty$
From Herlin and Brown

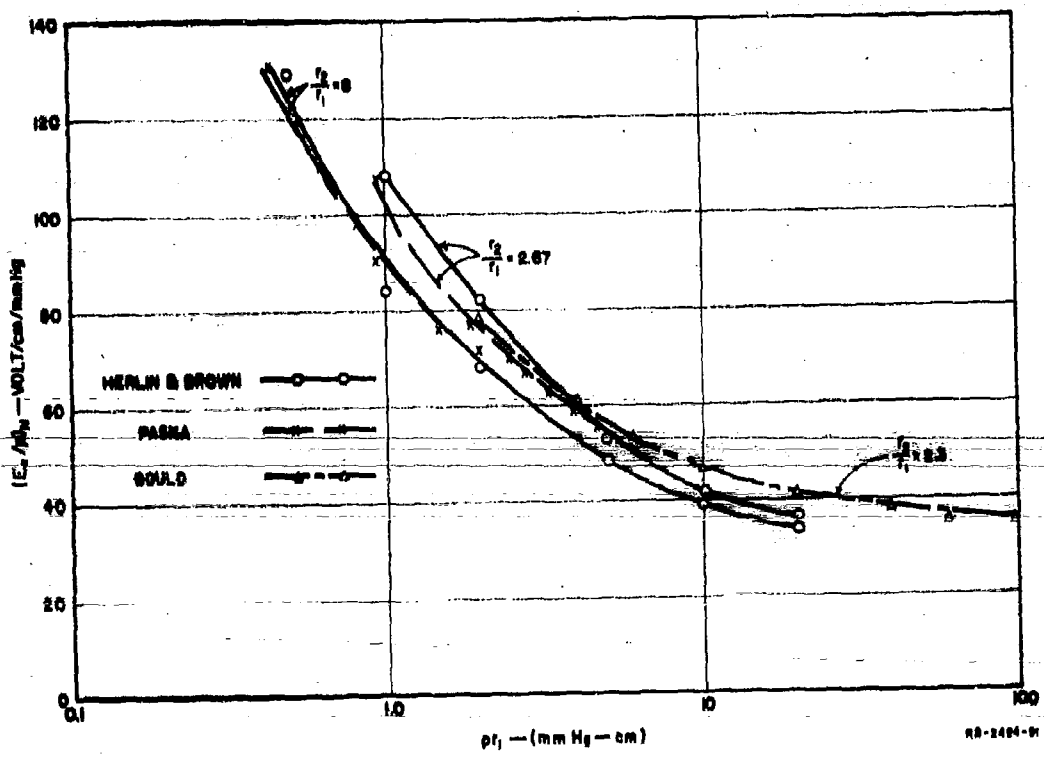

FIG. 15

COAXIAL LINE CW BREAKDOWN DATA FROM HERLIN AND BROWN, GOULD, AND PASKA IN GOULD'S NOTATION

III CYLINDRICAL MONOPOLE BREAKDOWN

A. COMPARISON BETWEEN COAXIAL LINE AND CYLINDRICAL MONOPOLE BREAKDOWN

With the background material on coaxial line breakdown presented in Sec. III the process of CW voltage breakdown on circularly cylindrical monopole antennas may be understood. The discussion is presented in terms of monopole antennas, although the results should be applicable to dipole breakdown when the breakdown is near the tips of the dipole. The monopole is referred to because all the measurements were made on this antenna rather than on a dipole. Accurate measurements on monopoles are simpler to carry out than on a dipole. The configuration to be discussed is illustrated in Fig. 16.

There are two types of breakdown on monopoles. The first occurs when the length of the monopole is such that the maximum field strength is at the tip of the monopole (tip breakdown), such as when the monopole is about $\lambda/4$ long. The second type occurs when the maximum field strength is at the feed point (feed breakdown), such as when the monopole is about $\lambda/2$ long. Which type of breakdown will occur can usually be predicted from a knowledge of the voltage distribution along the monopole, although in cases where the tip and feed point fields are approximately the same it may be difficult to say where the breakdown will occur because of the different geometry and hence different diffusion rate in the two cases.

The radial field variation near the tip of a monopole is a complex function of position, but may be approximated by a r_1/r fall-off, where r_1 is the radius of the monopole. This field configuration near the tip is the same as for a coaxial line with $r_2/r_1 = \infty$, where r_2 and r_1 are the outer and inner radius of the coaxial line. It is true, however, that the monopole ends, while the coaxial line is assumed to be infinitely long. But in these cases where the distribution along the length of the monopole is slowly varying (slow with respect to the range of the electrons and the radial field fall-off), the breakdown conditions a small distance from the tip (see point z in Fig. 16) will look quite similar to the conditions for coaxial line breakdown. Here again, the dominant electron loss mechanisms will be attachment and diffusion out of the high field region.

With a coaxial line feeding the monopole, the radial field variation at the feed point is approximately r_1/r also. Breakdown at the feed point is more complicated due to the presence of the dielectric insulator as well as a ground plane near the breakdown point. This plane provides a surface to which electrons may diffuse in addition to any radial diffusion losses that may be present. Thus, for the same pressure and field strength at the tip and at the feed point, it would be expected that the tip would break down first. Once the tip has broken down, the distribution along the monopole will be radically changed. The field distribution near the feed point is further complicated by the presence of non-propagating, higher order modes set up by the discontinuity in the transition from coaxial line to monopole.

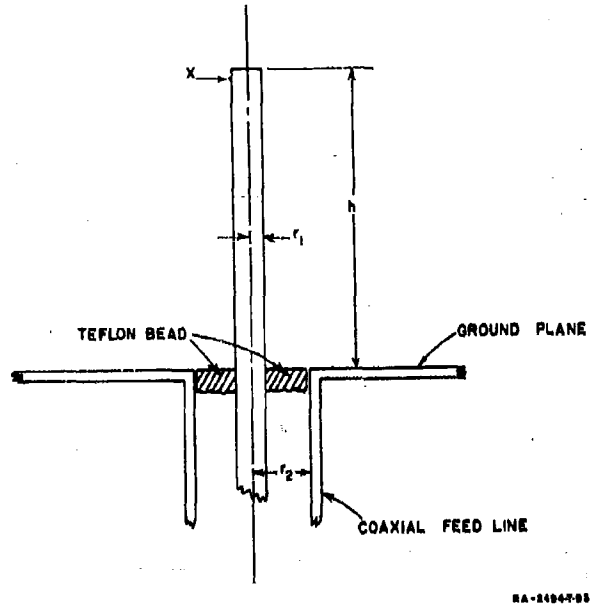

FIG. 16
MONOPOLE CONFIGURATION USED FOR CW BREAKDOWN STUDIES

In order to confirm that monopole breakdown near the tip may be considered as an extreme case of coaxial line breakdown, a computation of the breakdown fields at the surface of a coaxial line with $r_2/r_1 = \infty$ was carried out along the lines suggested by the work of Herlin and Brown.[12] The results are necessarily rough because of the limited data available for the graphical portion of the analysis. The results have been put into terms of $(E_e/p)_n$ and pr_1 and are shown in Fig. 17. Next, a measurement was made of the power required to produce CW breakdown at the tip of a monopole approximately a quarter-wavelength long as a function of pressure. The measurement was made on a ⅛ inch diameter brass rod at 240 Mc. A block diagram of the measurement set-up is shown in Fig. 18. Breakdown was determined by a change in the incident power and/or visual observation of a glow at the tip. The measured results are shown in Fig. 19. Both power to initiate breakdown and power to maintain breakdown are shown.

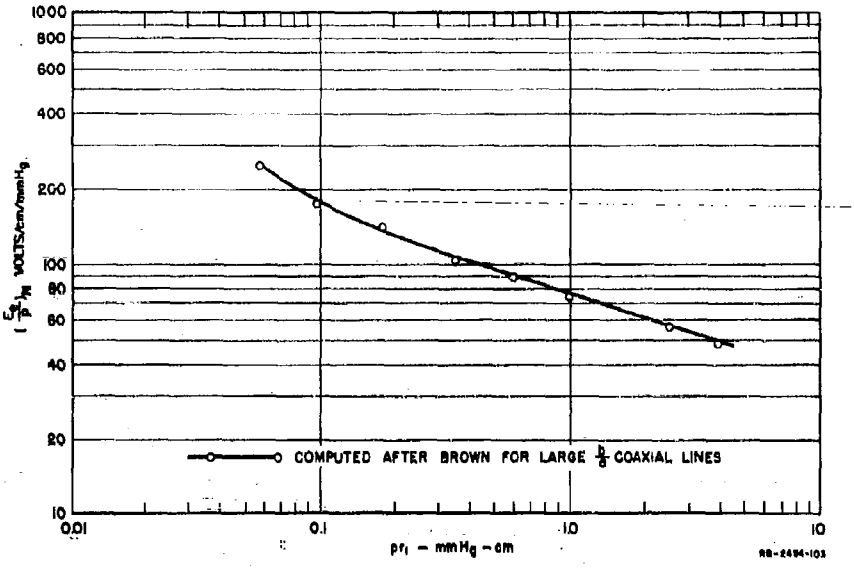

FIG. 17

COMPUTED VALUES OF $(E_e/p)_N$ AS A FUNCTION OF pr, FOR CW BREAKDOWN BETWEEN COAXIAL CYLINDERS WHEN $r_2/r_1 = \infty$

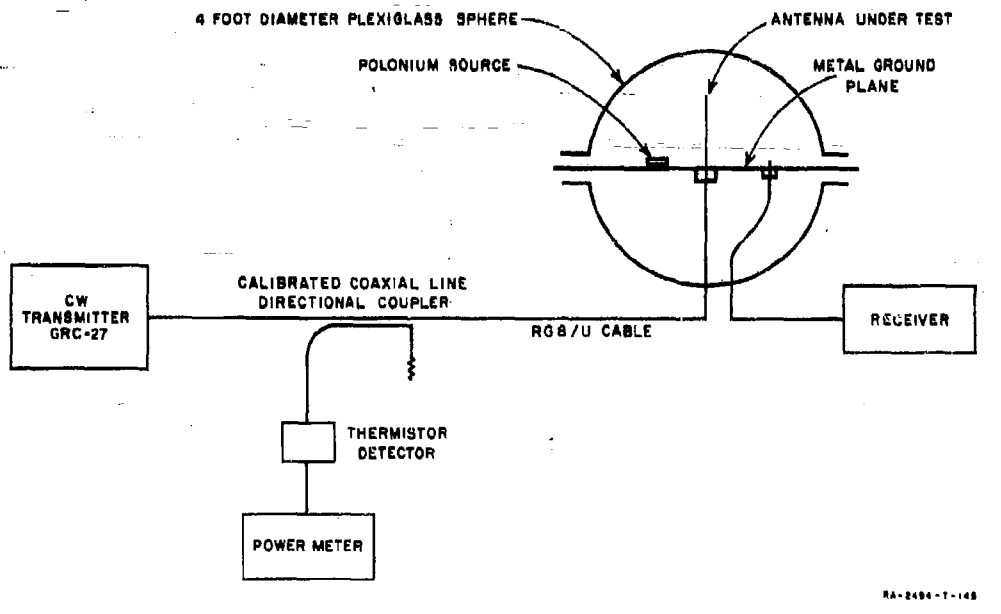

FIG. 18

BLOCK DIAGRAM OF MEASUREMENT SET-UP FOR CW BREAKDOWN STUDIES OF MONOPOLE ANTENNAS

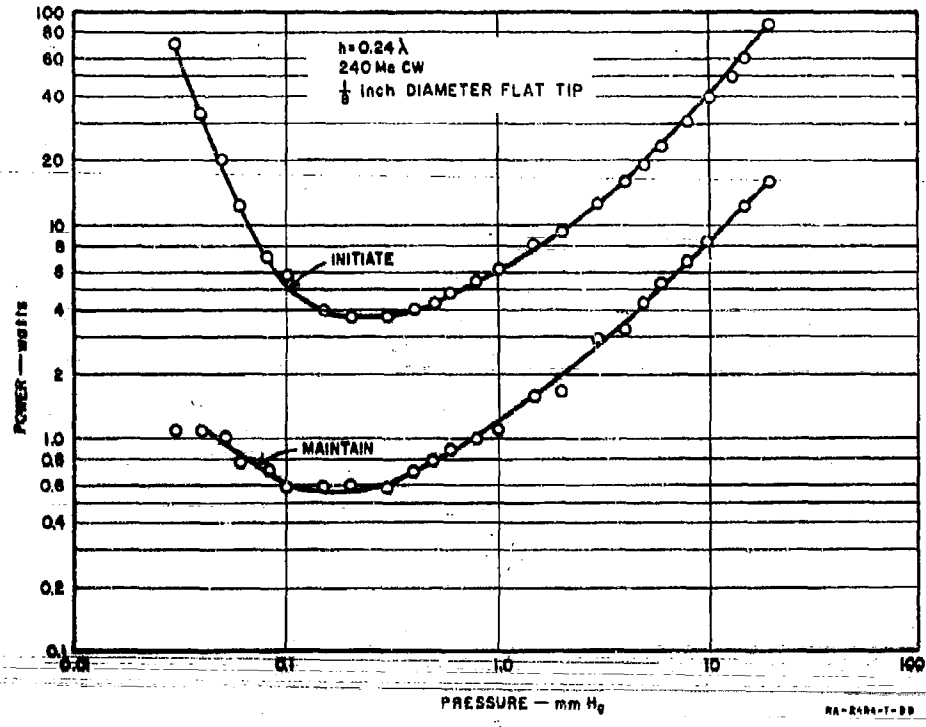

FIG. 19

CW POWER TO INITIATE AND MAINTAIN BREAKDOWN ON A MONOPOLE 0.24λ -LONG

Note that there is an appreciable difference between these two values as opposed to the pulsed breakdown case. This difference is attributed to the process of ambi-polar diffusion being important as a factor which decreases the electron losses after breakdown as compared to the free diffusion losses before breakdown.

Using a calculation discussed in Appendix A, the power was translated into terms of field at the surface of the monopole at the monopole tip. This value of field, combined with the pressure and the monopole radius, was put into the form of $(E_s/p)_n$ and pr_1. These results are plotted in Fig. 20 so that a comparison between the measured values and the values computed on the basis of coaxial line breakdown could be made. Also shown are the measured data for the coaxial line breakdown of a coaxial cavity with r_1 = 1/16-inch and r_2/r_1 = 48. The two pieces of measured data agree quite well, while the calculated data is in fair agreement with the measured monopole data. The agreement is satisfactory in view of the probable errors in the measured quantities, uncertainties in translating power to surface fields, and uncertainties in the calculated values.

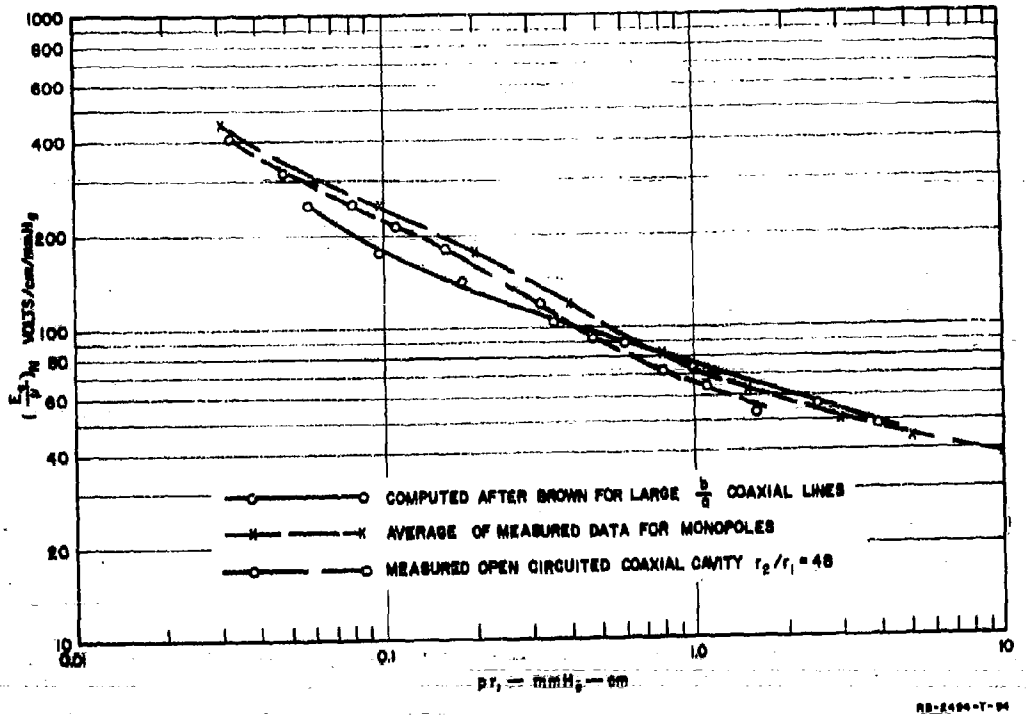

FIG. 20

COMPUTED VALUES OF $(E_g/p)_N$ AS A FUNCTION OF pr_1 FOR CW BREAKDOWN BETWEEN COAXIAL CYLINDERS WHEN $r_2/r_1 = \infty$, AND AVERAGE OF MEASURED VALUES FOR 0.24 λ-LONG MONOPOLE ANTENNAS

B. EFFECTS OF MONOPOLE DIAMETER AND HEIGHT ON CW BREAKDOWN

In order to verify that similarity relations would hold between monopoles with different diameters, measurements were made on monopoles of the same height but with diameters of 1/16, 1/8, and 1/4 inch. The results in terms of $(E_g/p)_n$ and pr_1 are given in Fig. 21. The agreement is quite good, showing that $E = F(r,p)$.

The results in terms of power are shown in Fig. 22. At pressures above the minimum, the thickest monopole has the largest power handling capability. However, at pressures below the minimum, the three curves merge, demonstrating that monopole thickness has little to do with power handling capability at low pressures. If maximum radiated power without breakdown at any pressure is of concern, then the thickest antenna will be the best to use. This behavior may be understood qualitatively by considering the radial electric field distribution for the various diameters.

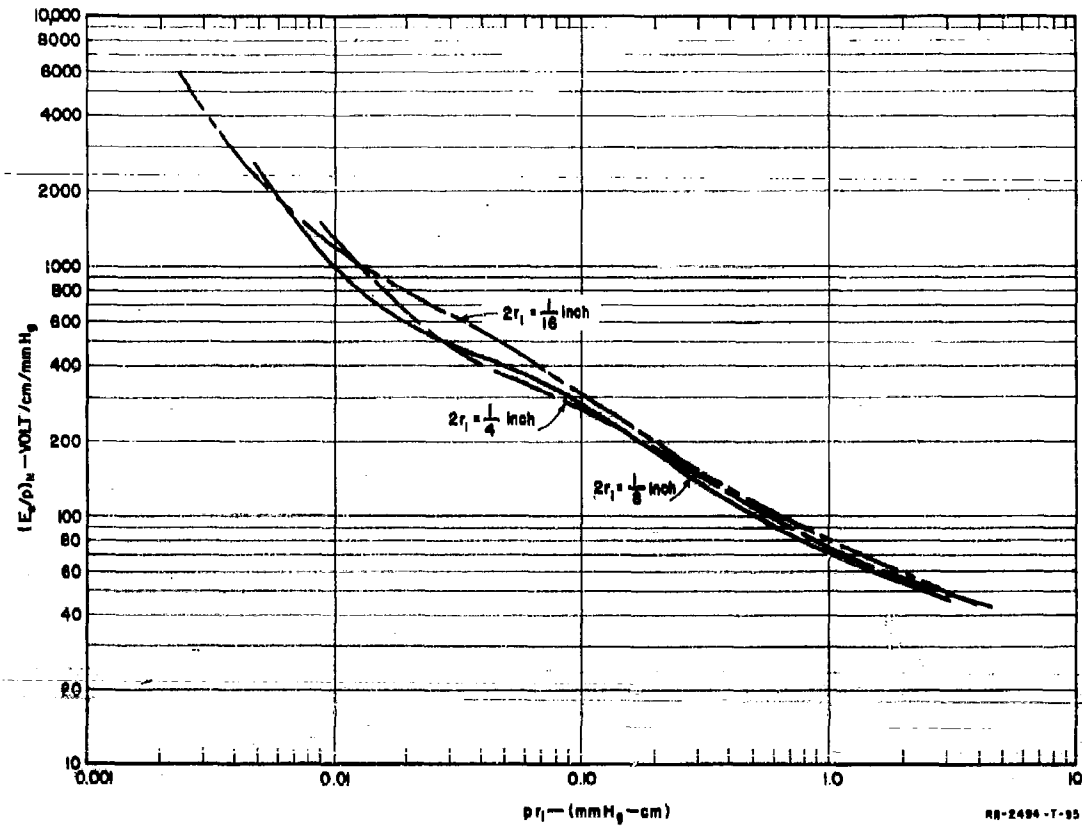

FIG. 21

MEASURED VALUES OF $(E_e/p)_N$ AS A FUNCTION OF pr, FOR THREE DIFFERENT MONOPOLE DIAMETERS

The impedances are approximately the same for different diameter monopoles over a large range of diameters. Therefore, the power radiated per input volt will be about the same for different diameter monopoles. The antenna with the greatest number of input volts without breakdown will radiate the most power.

For one-volt input at the feed terminals, the total charge at the monopole tip will be approximately the same for monopoles of different diameter. However, the maximum electric field at the monopole surface will be inversely proportional to the diameter. Therefore, the thickest monopole will have the lowest surface electric field per input volt. At high pressures, the radial extent of the region in which ionization occurs is small compared to the radius of the monopole, so that the field is relatively constant throughout this region. For this condition the

important parameter is the value of the electric field at the surface of the antenna. Therefore, the monopole of large radius requires more power to initiate breakdown than the thin monopole. At low pressure, both because of increased electron diffusion and reduced electron production per unit volume, the radial dimensions of the volume in which ionization occurs becomes substantially greater than the radius of the monopole. For this situation the radius of the antenna is of small importance and monopoles of different radii tend to require the same power for breakdown.

In order to justify the assumption that the axial distribution of electric field is of little significance for breakdown near the tip when the distribution is slowly varying (as previously defined), a series of measurements were made on monopoles of heights ranging from 0.08λ to 0.32λ. Brass rods $\frac{1}{8}$ inch in diameter were used for all the antennas, and all measurements were made at 240 Mc. The curves of power to initiate breakdown are shown in Fig. 23. They all exhibit similar characteristics, with the longest monopole capable of radiating the greatest amount of power without breakdown. Applying the results of King[14] for the charge/input volt at the tip of a quarter-wavelength monopole as described in Appendix A, and normalizing again to $(E_s/p)_n$ and pr_1, the curves of Fig. 24 were obtained. It is apparent that there is little change in the values of

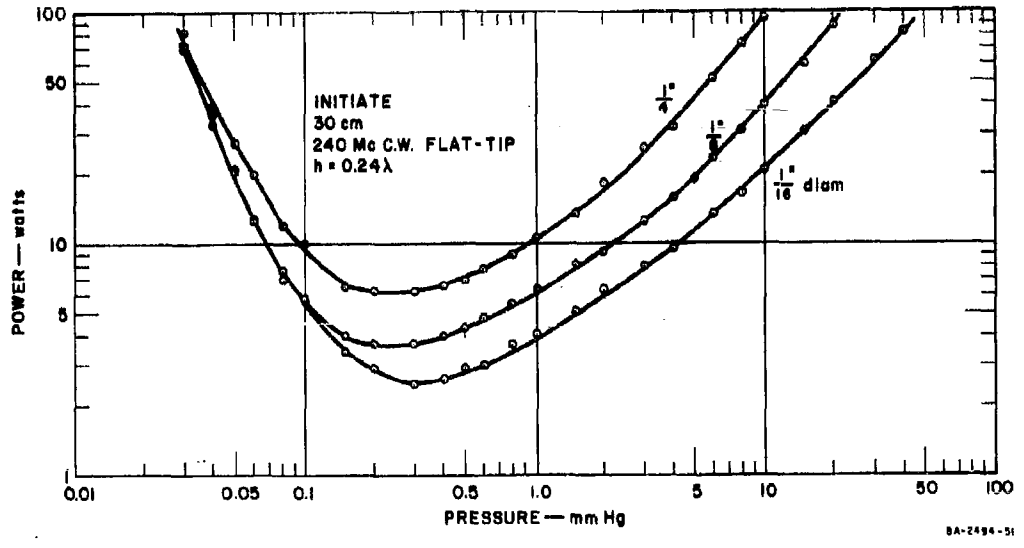

FIG. 22

MEASURED VALUES OF POWER TO INITIATE BREAKDOWN AS A FUNCTION OF PRESSURE FOR THREE DIFFERENT MONOPOLE DIAMETERS

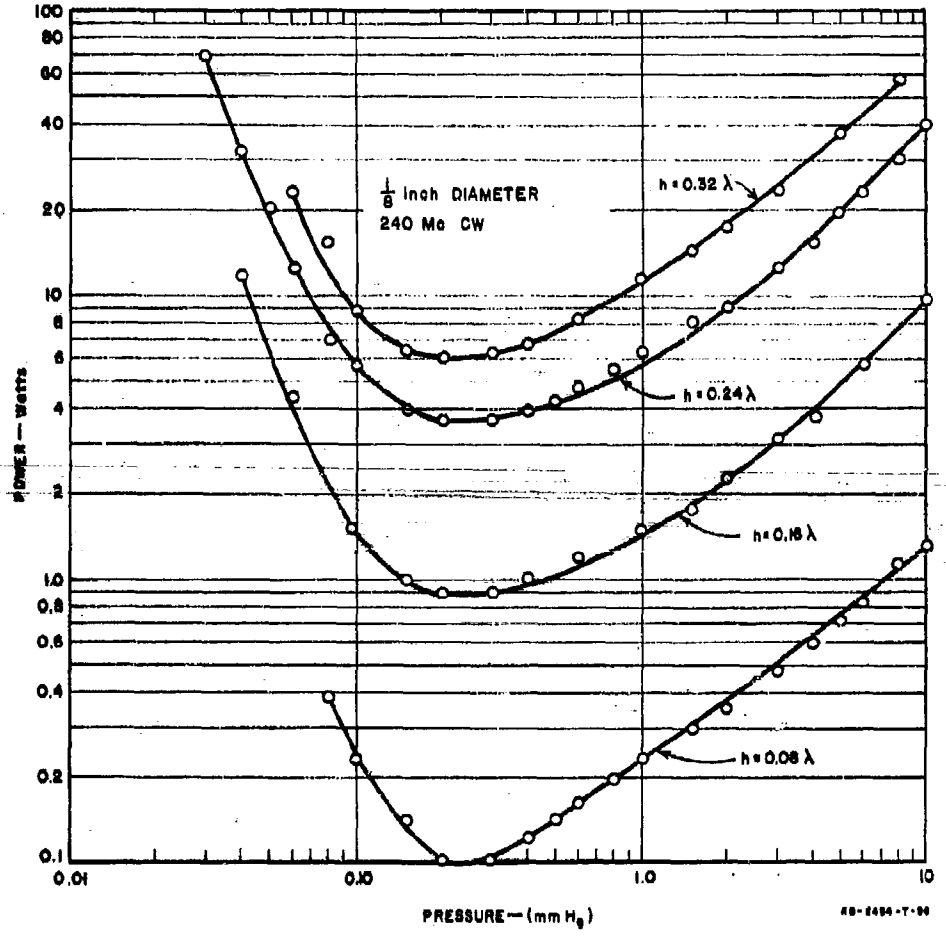

FIG. 23

MEASURED VALUES OF POWER TO INITIATE BREAKDOWN AS A FUNCTION OF PRESSURE FOR MONOPOLES 0.08λ, 0.16λ, 0.24λ, AND 0.32λ

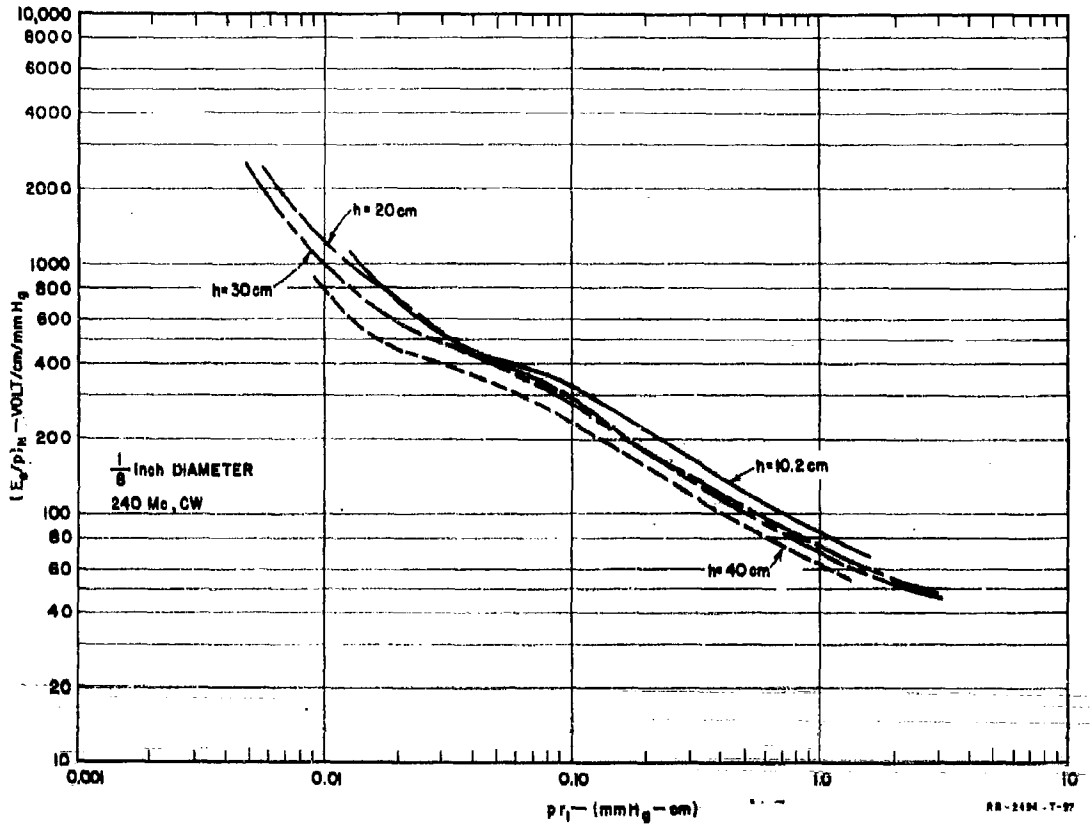

FIG. 24

NORMALIZED VALUES OF BREAKDOWN PARAMETERS FOR CW BREAKDOWN OF MONOPOLES, FOR MONOPOLE LENGTH OF 0.08λ TO 0.32λ

$(E_\theta/p)_n$ for different antenna heights. The spread of data is easily accounted for by uncertainties in the measured data and in the calculation of the field in terms of the power. Since the distribution along the antenna changes radically when the length is varied from 0.08λ to 0.32λ, it is concluded that for this range of conditions the axial distribution has only a negligible effect on breakdown

That frequency scaling was applicable to monopole antennas was demonstrated by measuring the breakdown power on a monopole 0.24λ at 399.9 Mc (the highest frequency high power CW source available). The antenna was ⅛ inch in diameter. The normalized results are shown in Fig. 25 along with the measured results for a 0.24λ, ⅛ inch diameter antenna at 240 Mc. The agreement is sufficiently good to confirm that frequency scaling is applicable.

The data shown in Fig. 21 as well as the data for various antenna diameters in Fig. 24 have been averaged to give in a single curve the approximate value of $(E_e/p)_n$ as a function of pr_1. This curve, plotted in Fig. 26, should be useful for estimating monopole breakdown over a wide range of conditions.

A study of breakdown at the feed point was made by using an antiresonant-length monopole 0.40 wavelength long. Measurements were again made at 240-Mc with ⅛-inch diameter brass rod. This antenna broke down at the feed point throughout the entire pressure range of the test. The measured results are shown in Fig. 27. The data in terms of $(E_e/p)_n$ and pr_1 are shown in Fig. 28. The data were plotted in this way so that a comparison with tip breakdown for the same diameter antennas could be made. The data show that appreciably higher values of $(E_e/p)_n$ are required for feed point breakdown as compared to tip breakdown for the same value of pr_1. This result is to be expected since the presence of the ground plane

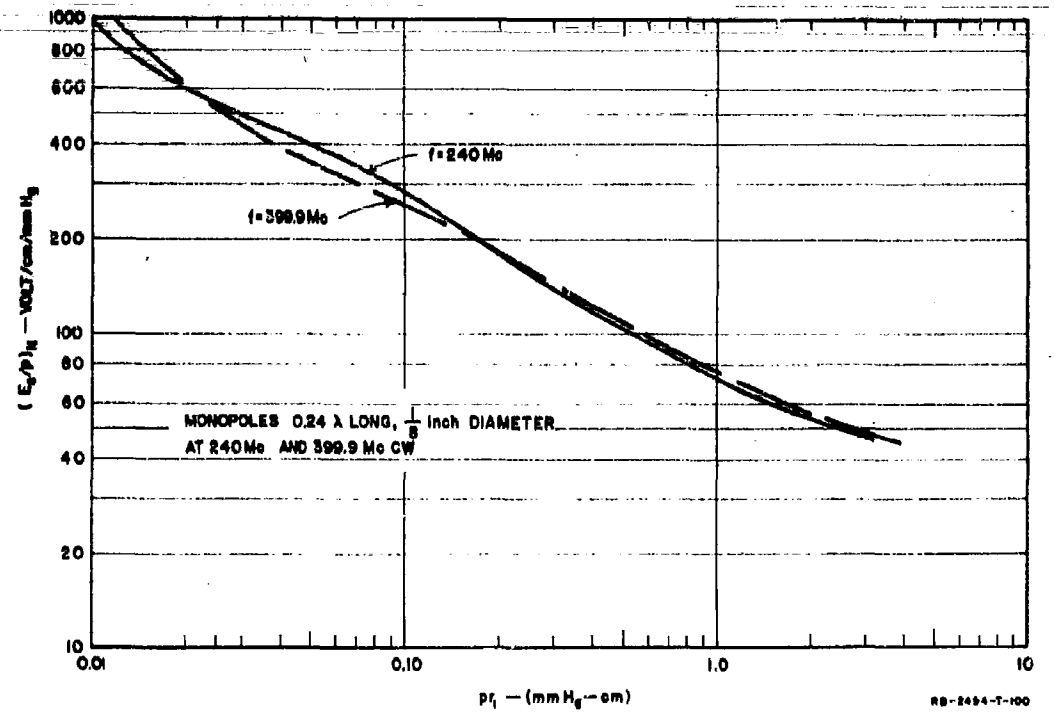

FIG. 25

NORMALIZED VALUE OF BREAKDOWN PARAMETERS FOR CW BREAKDOWN, FOR 0.24λ MONOPOLES AT 240 AND 399.9 Mc

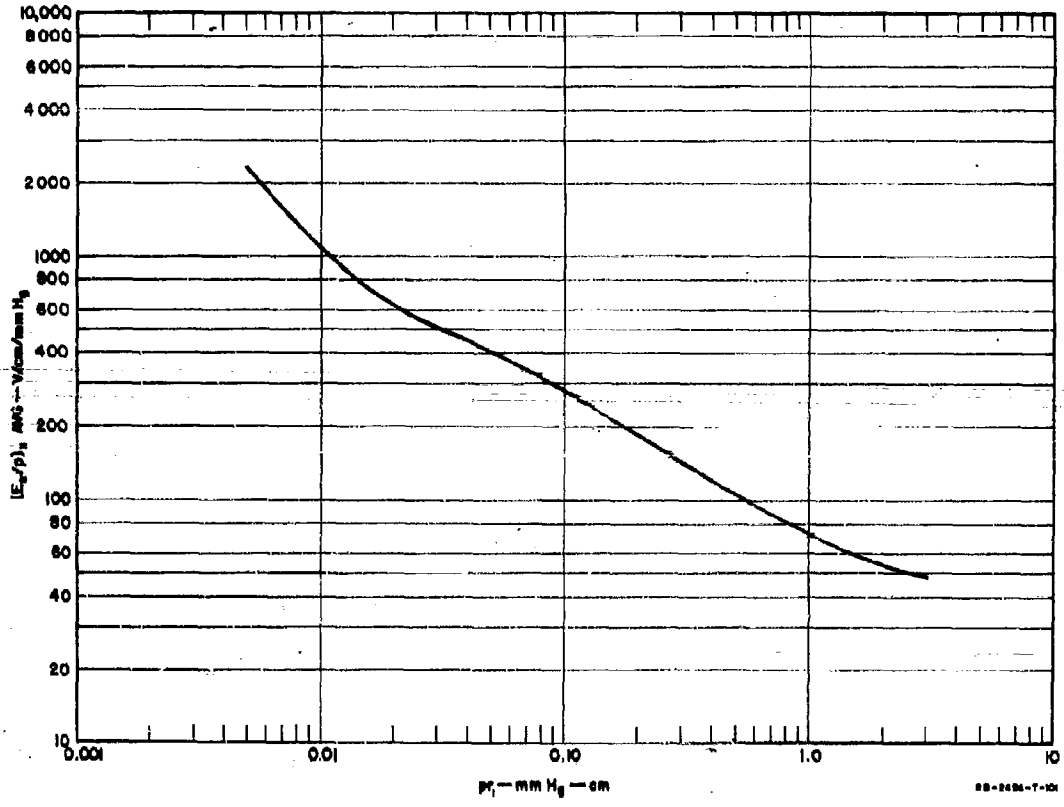

FIG. 26

AVERAGE VALUE OF NORMALIZED BREAKDOWN PARAMETERS FOR CW BREAKDOWN OF MONOPOLE ANTENNAS

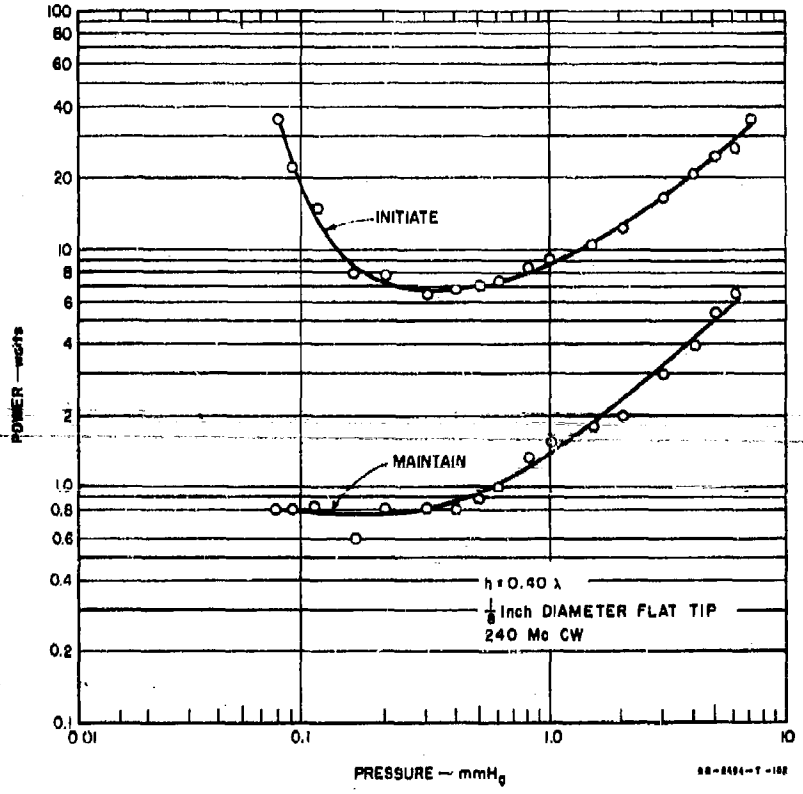

FIG. 27

CW POWER TO INITIATE AND MAINTAIN BREAKDOWN OF A 0.40λ-LONG MONOPOLE ANTENNA AS A FUNCTION OF PRESSURE

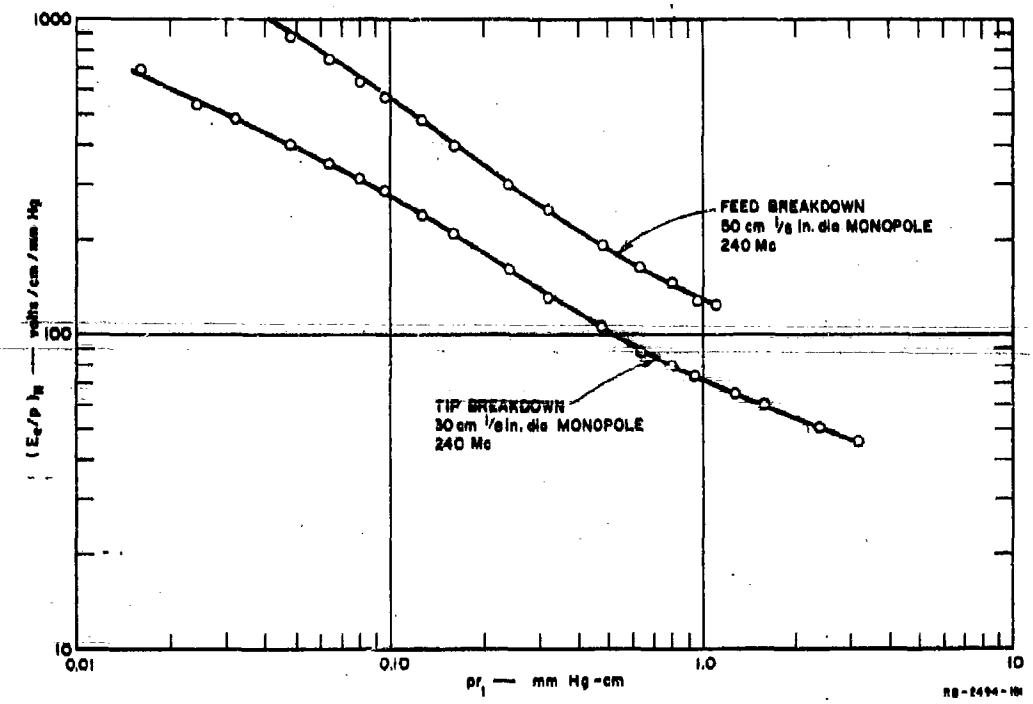

FIG. 28

$(E_e/p)_N$ AS A FUNCTION OF pr FOR FEED AND TIP BREAKDOWN

allows the loss of electrons by diffusion to the plane. No analytical solution has been attempted for this configuration.

The power required to initiate breakdown as a function of antenna height is plotted for pressures of 0.2 mm Hg—the pressure at which minimum power is required to initiate breakdown—in Fig. 29. The power to initiate breakdown for antennas that break down at the tip, increases monotonically with increasing antenna length even though the required value of E_e for antennas that break down at the tip is the same regardless of length. This distinction between the power to initiate breakdown and the value of E_e for breakdown must be kept in mind when one is concerned with antennas which are to radiate power. These two factors are related by the impedance and dimensions of the antenna structure. Thus, if one is interested in

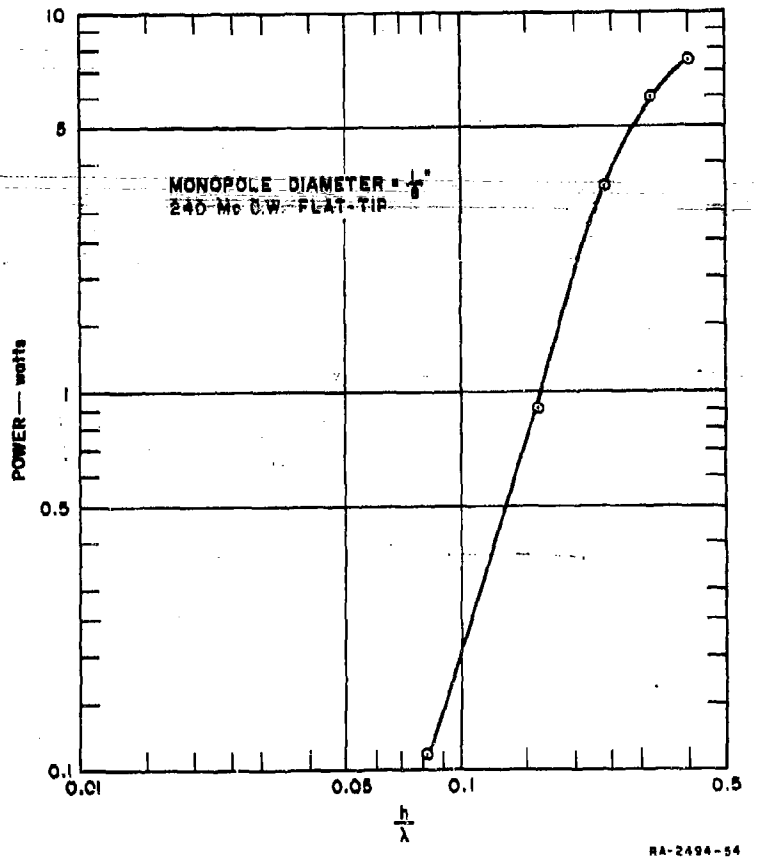

FIG. 29

CW POWER TO INITIATE BREAKDOWN ON A MONOPOLE ANTENNA AS A FUNCTION OF ANTENNA LENGTH

radiating the maximum power without breakdown, the highest obtainable value of E_e is not necessarily the parameter of interest. In maximizing E_e the impedance may be changed in such a way that the radiated power is decreased. Thus, though E_e is the same for tip breakdown of monopoles of height equal to 0.08λ, 0.16λ, 0.24λ and 0.32λ, the power to initiate breakdown is not the same because of the variation of impedance with length.

C. EFFECTS OF TIP SHAPE ON CW BREAKDOWN

In general, at high-altitudes and high radio frequencies, the effects of sharp edges on the breakdown fields become insignificant. This is due to the fact that at high radio frequencies many collisions of electrons with gas molecules are necessary before an electron can gain ionizing energy. Since the mean free path is larger than the radius of curvature of the edge no large increase in electron density can occur near the edge. That is, the electrons diffuse away from the localized high field region before an appreciable number of them can gain ionizing energy. That this is true was confirmed by comparing the power to initiate a monopole with a hemispherical tip and one with a flat tip. No difference was observable below about 10 mm Hg pressure.

A more systematic experiment was conducted in which the tip angle (see Fig. 30) was varied from 180 degrees to 15 degrees. The measured power to initiate breakdown as a function of pressure is shown in Fig. 30. There is some scatter of points, but it is clear that the tips with smaller angles broke down with less power than the tips with larger angles, at the higher pressures. As the pressure was reduced, the difference decreased until the curves merged at a pressure of about 0.7 mm Hg. There is some slight change in impedance when the tip angle is changed, but not enough to account for the changes in breakdown power observed. Even if there were a decrease due to impedance changes the variation with pressure would not be as shown—*i.e.*, the curves would not merge at low pressures.

D. PULSED BREAKDOWN OF MONOPOLE ANTENNAS

The behavior of a monopole antenna subjected to high pulsed power, was also investigated. The availability of a pulsed power source at *X*-band (9400 Mc) determined the frequency of operation. This choice would also allow a check of frequency scaling to be made over a range of 39 to 1 (9400/240). An *X*-band (0.4- by 0.9-inch inside dimensions) waveguide was

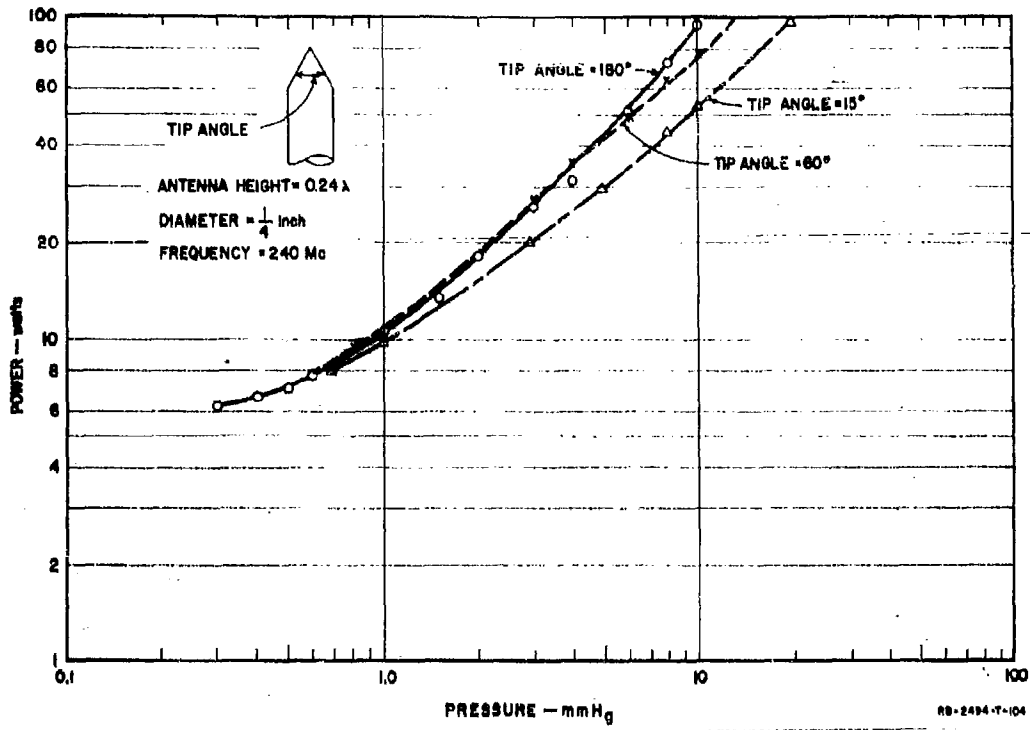

FIG. 30

CW POWER TO INITIATE BREAKDOWN ON A MONOPOLE ANTENNA 0.24 λ LONG AS A FUNCTION OF PRESSURE FOR DIFFERENT TIP ANGLES

fitted to feed a quarter-wavelength monopole as illustrated in Fig. 31. Provision was made for DC biasing to be applied to the monopole. The results of biasing will be discussed in a later chapter. The assembly was matched to a standard waveguide section by means of an inductive post. A wire 0.0115 inches in diameter served as the monopole (this corresponds to a diameter of 0.45 inches at 240 Mc). The measurement set-up was similar to that shown in Fig. 8 for tests of breakdown in rectangular waveguide. Breakdown was detected by any alteration in the reflected pulse. Even though a radioactive polonium source was used, breakdown levels at high pressures were erratic. Therefore, the power to initiate breakdown without waiting any length of time was recorded and compared to the power to initiate breakdown when the power was left on at a given level for sixty seconds. The difference between these two readings was as much as 12 db at 50 mm Hg pressure but decreased rapidly to about 1 db at pressures below 20 mm Hg. Measurements were made at pulse widths of 0.6, 1.04, and 2.25 microseconds with the largest difference in readings usually occurring

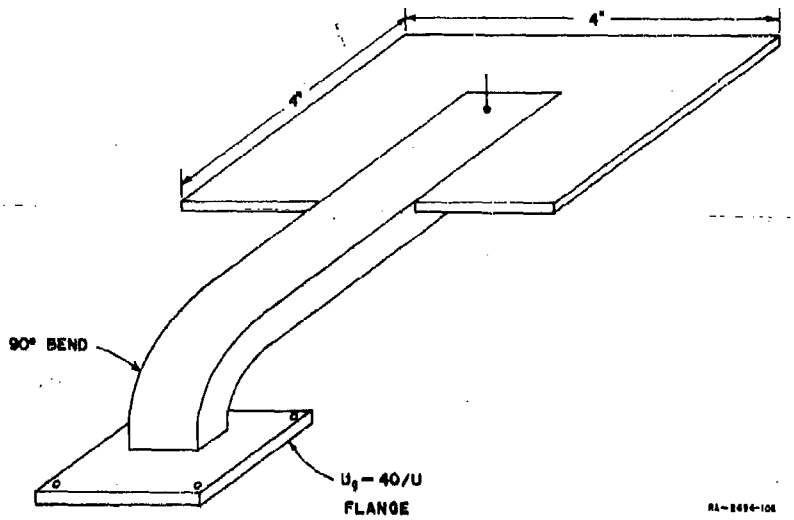

(a)

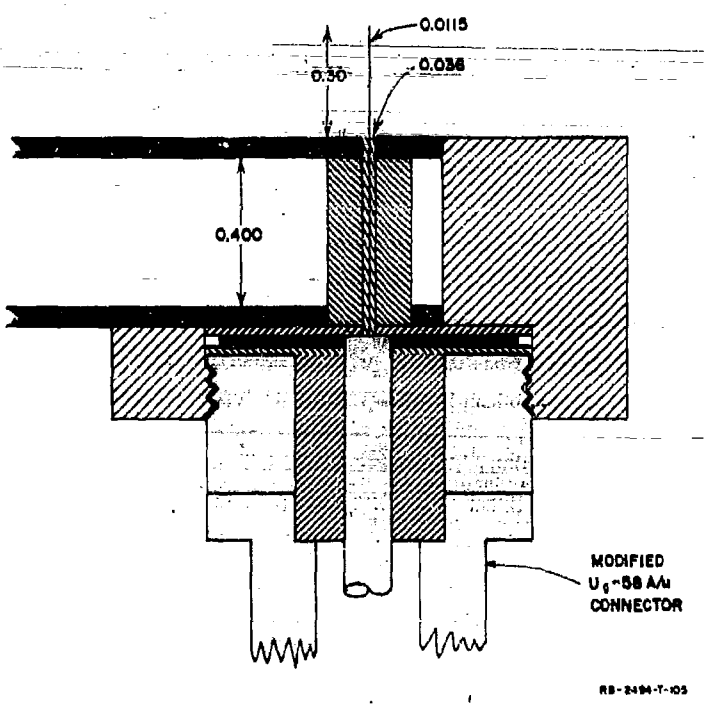

(b)

FIG. 31

CONFIGURATION USED FOR MEASURING PULSED MONOPOLE BREAKDOWN CHARACTERISTICS AT X-BAND

for the smallest pulse width. This effect may be due to a combination of short pulse widths, high pressure, rapid field variation with radial distance, and insufficient ionization from the radioactive source. Because of the high pressure and rapid field variation, the region over which a large electron density can build up is limited to a volume very close to the monopole. If the radioactive source is not sufficiently strong to produce enough electrons in this volume so that there is a high probability for breakdown while the pulse is on, test results will be erratic. The longer the pulse width the greater will be the probability for breakdown with a given source strength. Thus, there exists a smaller spread in the 2.25-microsecond data than in the 0.6-microsecond data. That is, the strength of the radioactive source necessary to ensure repeatable results is a function of pulse width, pressure, and field variation.

The measured results for the three pulse widths are given in Figs. 32 through 34. Note that the two curves for each pulse width tend to merge as the pressure is decreased.

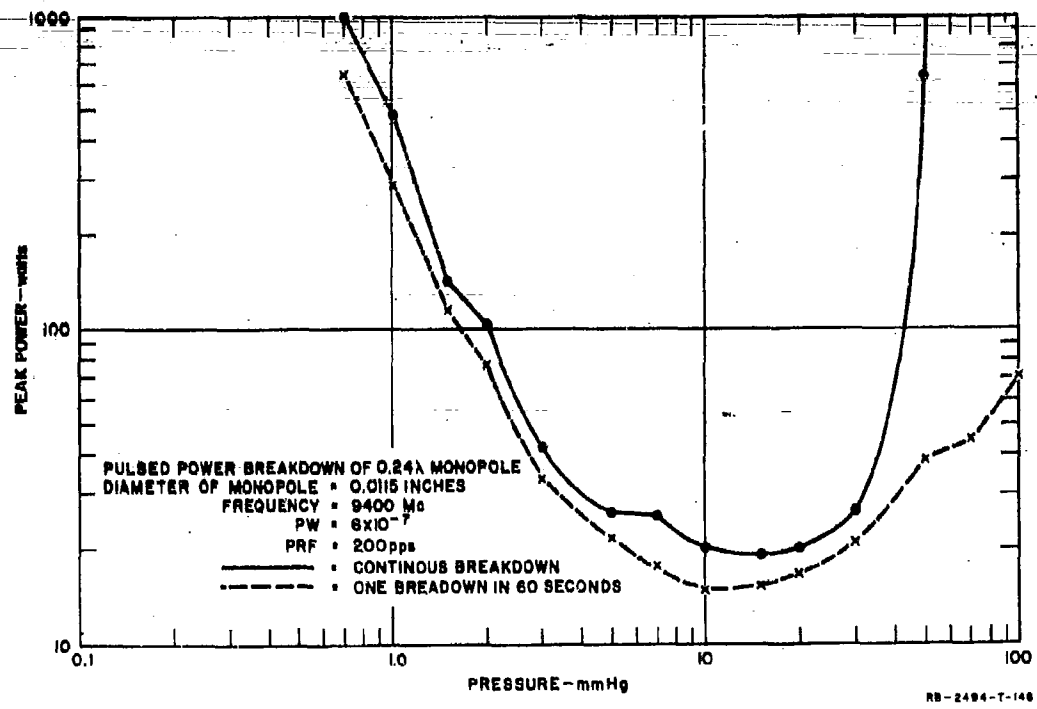

FIG. 32

PULSE POWER BREAKDOWN OF A 0.24λ-LONG MONOPOLE AT X-BAND WITH A PULSE WIDTH OF 0.60 MICROSECOND

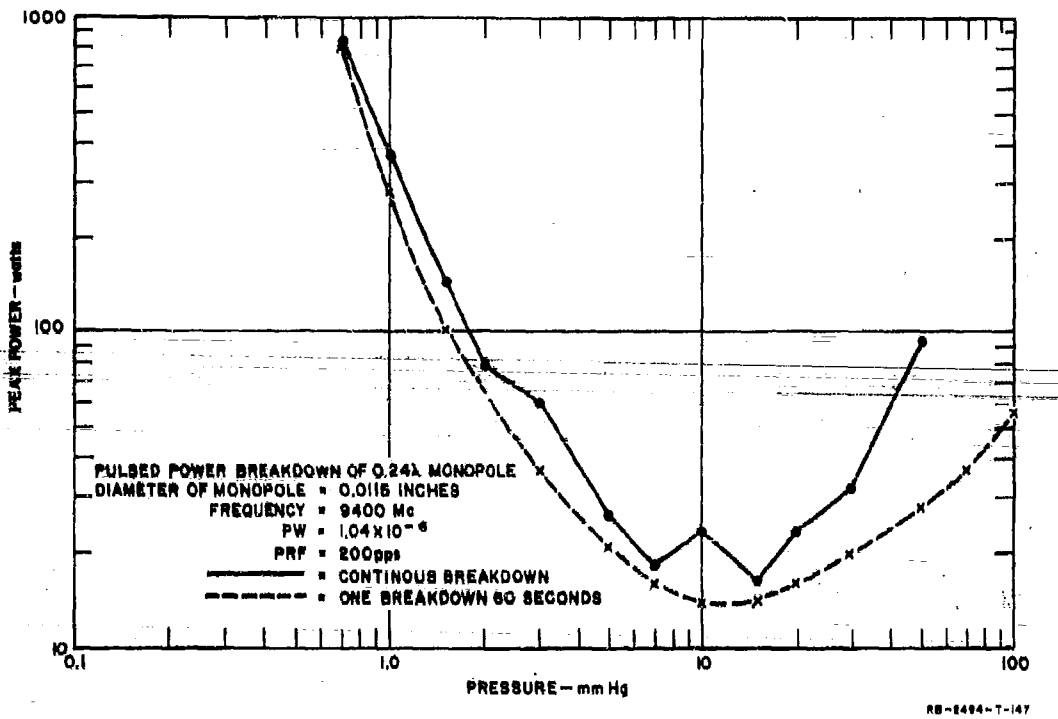

FIG. 33

PULSE POWER BREAKDOWN OF A 0.24λ-LONG MONOPOLE AT X-BAND WITH A PULSE WIDTH OF 1.04 MICROSECOND

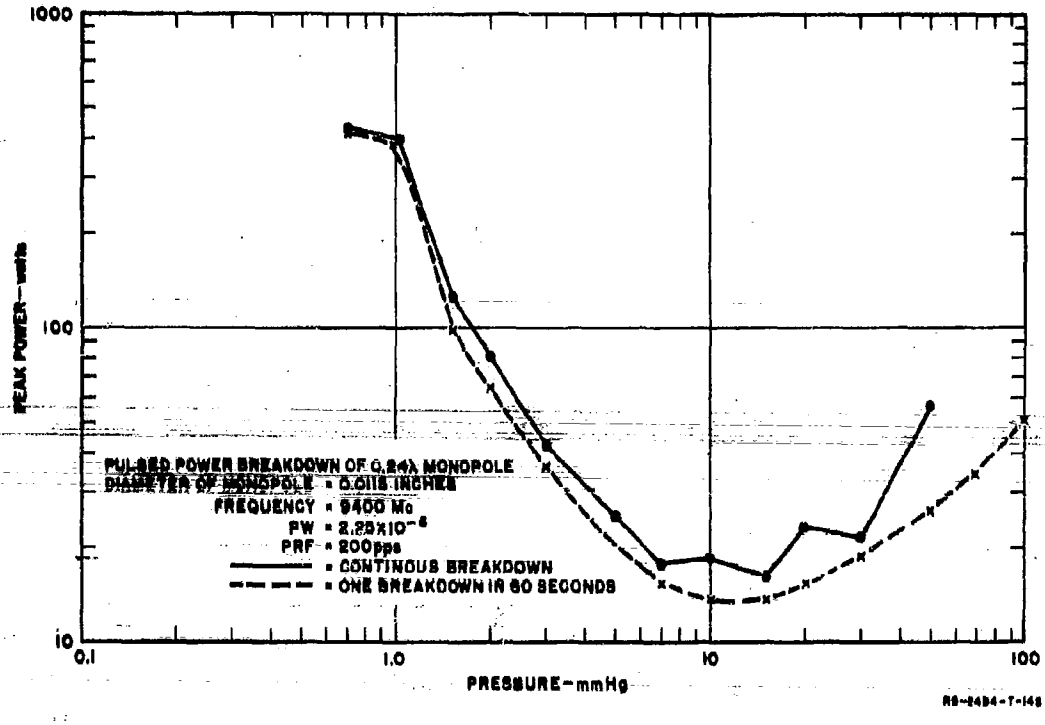

FIG. 34

PULSE POWER BREAKDOWN OF A 0.24λ-LONG MONOPOLE AT X-BAND WITH A PULSE WIDTH OF 2.25 MICROSECONDS

The data for at least one breakdown in sixty seconds were normalized to $(E_e/p)_n$, pr_1, and $p\tau$ and are plotted in Fig. 35. The striking thing about this figure is the small slope of the curves of $(E_e/p)_n$ as a function of $p\tau$ for different values of pr_1. Over the range of $p\tau$ measured, there is almost no change in $(E_e/p)_n$ required for breakdown for each value of pr_1. Further, since the measured data indicate almost no change in $(E_e/p)_n$ with $p\tau$ there should be little difference between CW and pulsed breakdown data. Therefore, the pulse data at X-band may be compared with the CW data at 240 Mc to determine how well scaling laws are working. Extending the pulse data curves to $p\tau = 10^{-3}$ mm Hg seconds, where the CW values are plotted, the curves continue as almost horizontal lines, indicating that scaling is applicable over a range of 39 to 1 in frequency.

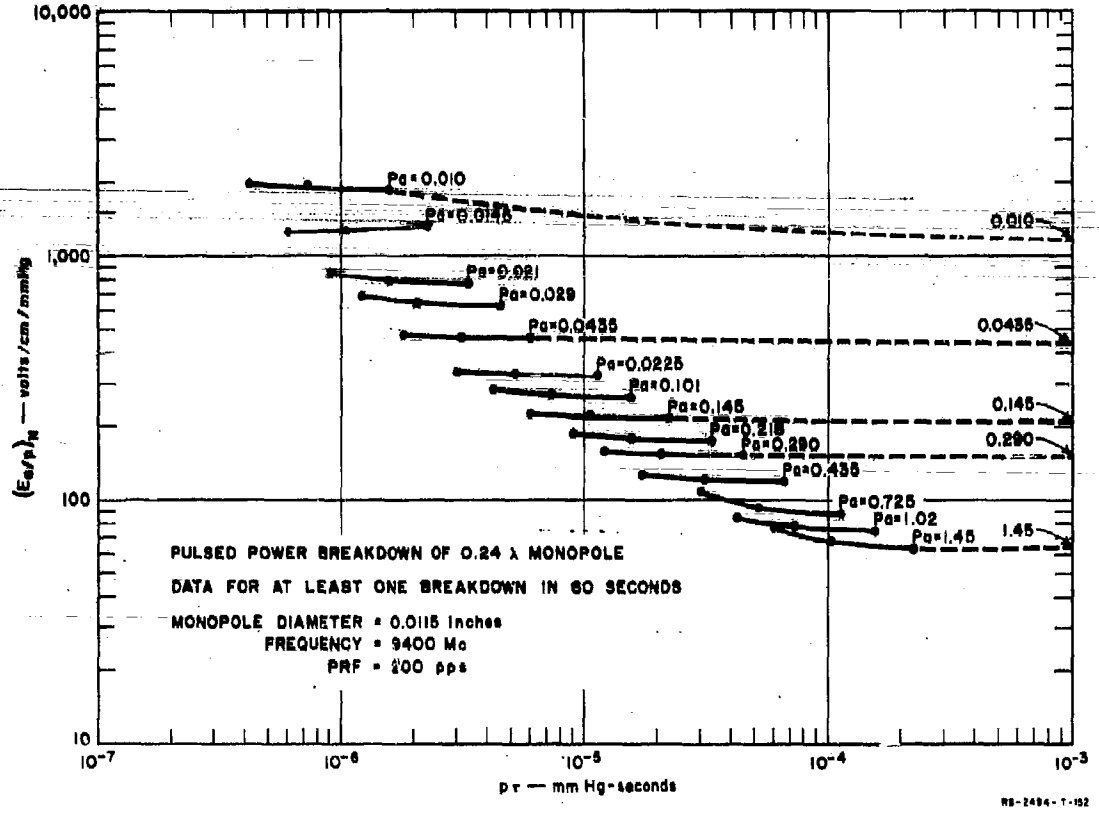

FIG. 35

NORMALIZED RESULTS OF BREAKDOWN MEASUREMENTS ON A 0.24λ-LONG MONOPOLE SUBJECTED TO X-BAND PULSE POWER

IV BREAKDOWN OF APERTURE ANTENNAS

A. BACKGROUND

The breakdown of aperture antennas requires the consideration of factors which are either not relevant or handled differently than either transmission line breakdown or monopole breakdown. In transmission line studies only a two dimensional field variation is considered, while in aperture breakdown the three dimensional field variation must be considered. In monopole antenna breakdown the process is easier to interpret because the field variation has the same form (r_1/r) for different values of monopole radii over the normally used range of radii. For aperture antennas this is not true. Very thin slot antennas have field variations that fall off at about r_1/r where r is measured from the aperture plane and r_1 is the equivalent radius of the complementary dipole but as the slot becomes wider the field variation changes so that r_1 does not change simply with the slot width.

B. CW BREAKDOWN OF OPEN SLOT ANTENNA

Measurements have been made by Worth[15] at 227 Mc on a cavity-fed slot antenna with the configuration chosen so that breakdown would occur in the aperture. A sketch of the antenna is shown in Fig. 36. The cavity was filled with wax to allow the waveguide mode to propagate. However, no dielectric was present in the space between the plates near the aperture. Since the highest fields existed between the plates near the aperture, breakdown occurred there. For the gap sizes used it seems likely that electrons formed in the gap diffused across the gap to the plates as well as in a direction normal to the aperture into the lower field regions. To the extent that the main electron loss was from diffusion to the plates, or attachment, there is little difference between breakdown of this antenna and breakdown in a rectangular waveguide. Since the ratio of $a/b > 8$, where a = aperture length, and b = aperture width, the transverse distribution in all cases considered should not be of importance and the antenna should appear similar to a parallel plate system. That this is so is demonstrated in Fig. 37 in which Worth's data have been normalized to $(E_e/p)_n$ and pb. Plotted in the same figure are the parallel plate breakdown data from Fig. 3. The curves are almost identical.

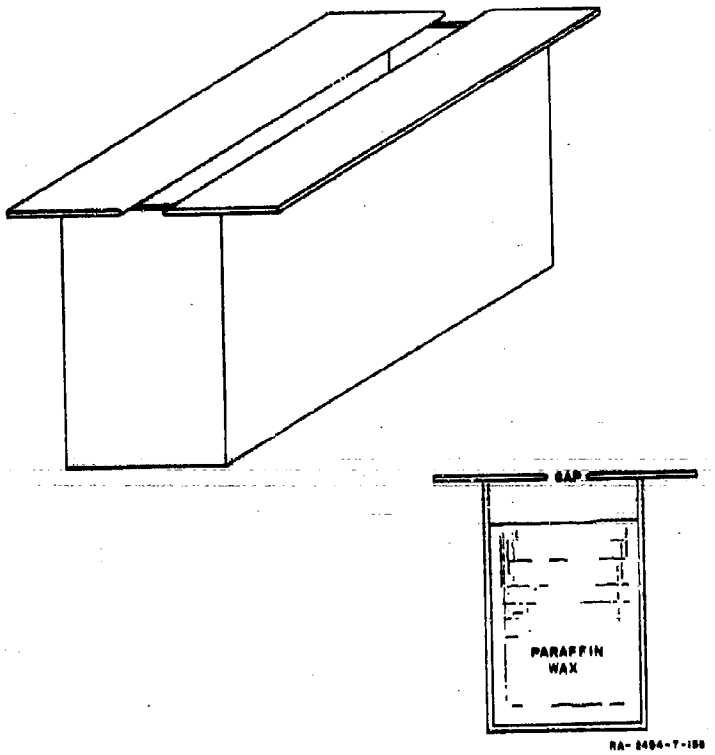

FIG. 36
SKETCH OF WORTH'S CAVITY-FED SLOT

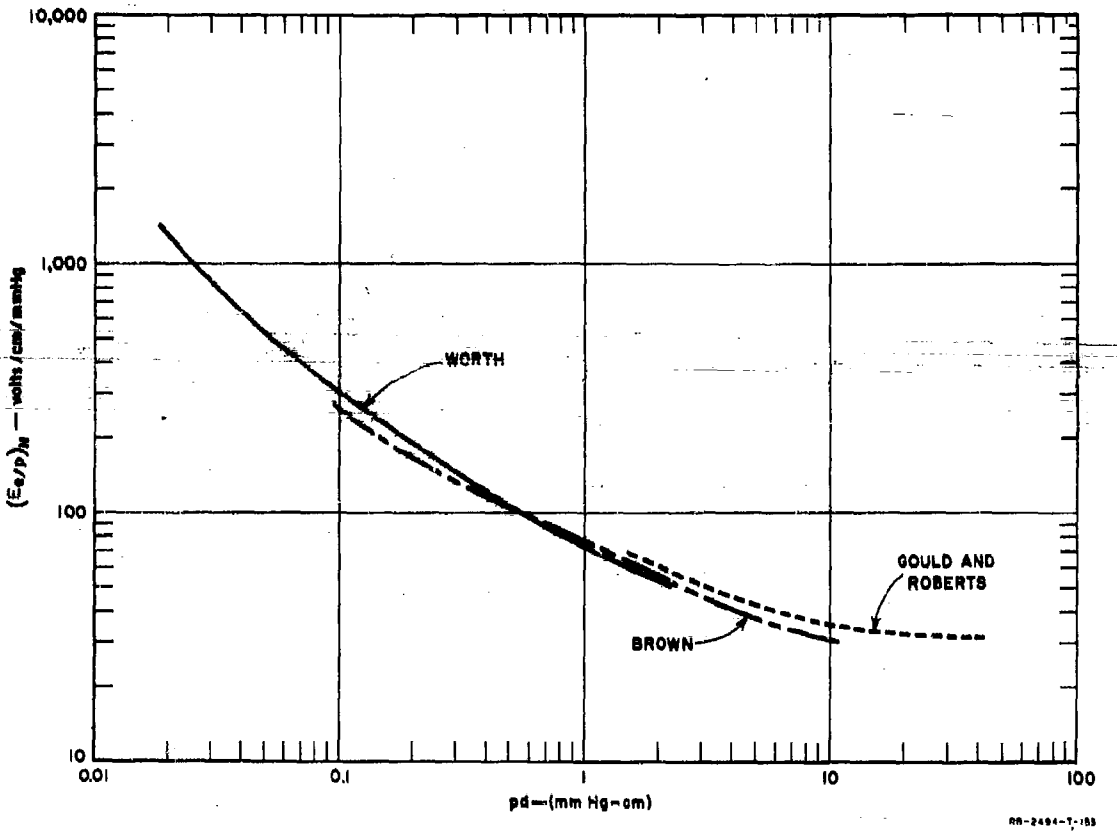

FIG. 37

NORMALIZED DATA ON WORTH'S SLOT COMPARED TO PARALLEL PLATE BREAKDOWN

C. CW BREAKDOWN OF COVERED SLOT ANTENNA

Interesting as the results of the previous section are, they are of little practical importance, since slot antennas that are flown on airplanes and missiles are covered by a dielectric cover. The reasons for the cover are numerous and usually include considerations of structural strength as well as mechanical protection of the aperture feed system. Further, without a cover over the antenna the feed line would be at the same pressure as the aperture. For many configurations the feed structure would then break down before the aperture broke down. In any event, aperture antennas with a dielectric covering the aperture are of great practical importance. Therefore, a series of measurement in dielectric covered slot antennas was carried out.

A slot antenna with an aperture 1 inch wide and 17 inches long was built to operate at 380 Mc. A sketch of the antenna is shown in Fig. 38. The cavity was filled with polyfoam to ensure that breakdown would occur in the aperture rather than inside the cavity. The power to initiate breakdown on this antenna as a function of pressure is shown in Fig. 39. The limited number of points is due to limitations of the power output of the GRC-27 transmitter. In order to obtain more data, plates were placed over the aperture so that the width was reduced to 0.5 inch. The data for this antenna are also shown in Fig. 39. The aperture impedance of the antennas was measured. With this information it was possible to compute the normalized aperture fields for breakdown as a function of pb shown in Fig. 40. The agreement in data between the 1.0- and 0.5-inch aperture is quite good over the range of overlap. Also plotted in Fig. 40 for comparison are Worth's data for open slot antennas. As can be seen from the figure, the main effect of the dielectric is to raise the values of $(E_e/p)_n$ required for breakdown by a factor of about 1.5 to 2. This result is to be expected since placing a dielectric in the aperture puts a surface to which electrons can diffuse at the point of maximum field, thus increasing the loss due to diffusion. The situation is complicated, however, since in the waveguide case the diffusion is to the walls while in the aperture case there is diffusion to the dielectric surface as well as into lower field regions normal to the aperture. Thus the significance of b in waveguide breakdown is in determining how far an electron must travel to diffuse out of the field. In aperture breakdown, b is significant in determining the rate of fall-off of the field outside the aperture.

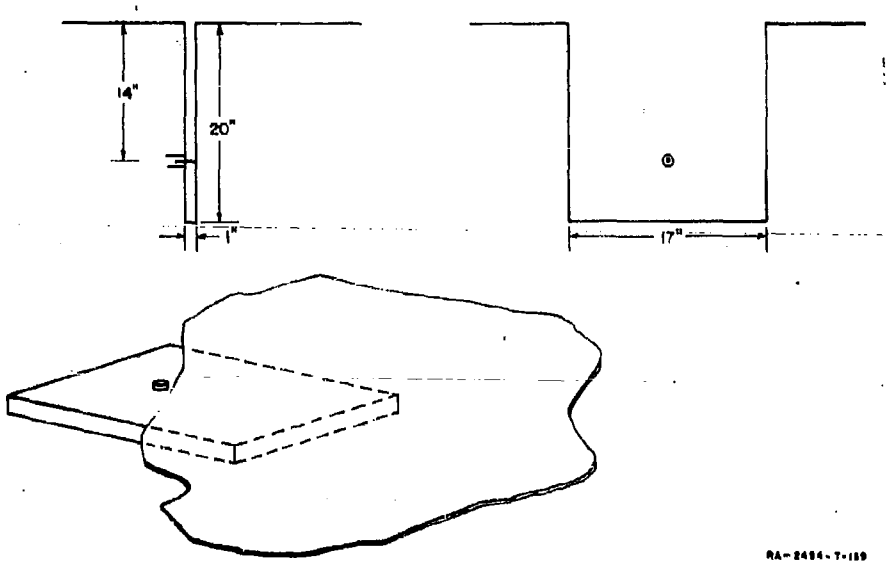

FIG. 38

SKETCH OF 1-BY-17-INCH SLOT ANTENNA

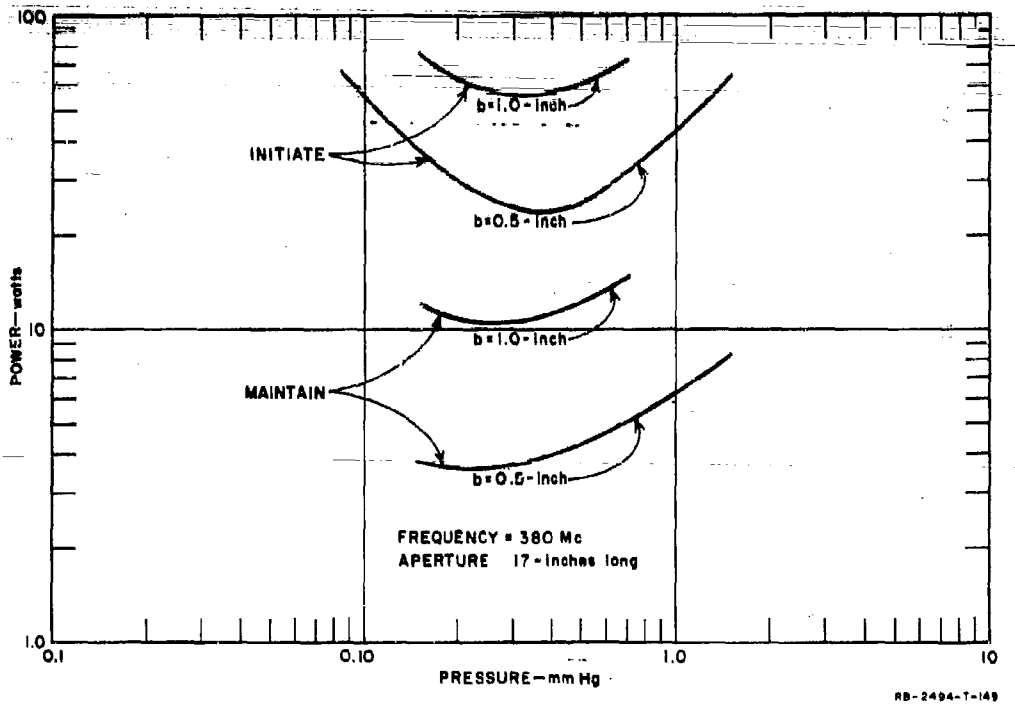

FIG. 39

POWER TO INITIATE AND MAINTAIN BREAKDOWN AS A FUNCTION OF PRESSURE FOR 1-BY-17-INCH AND 0.5-BY-17-INCH SLOT ANTENNAS

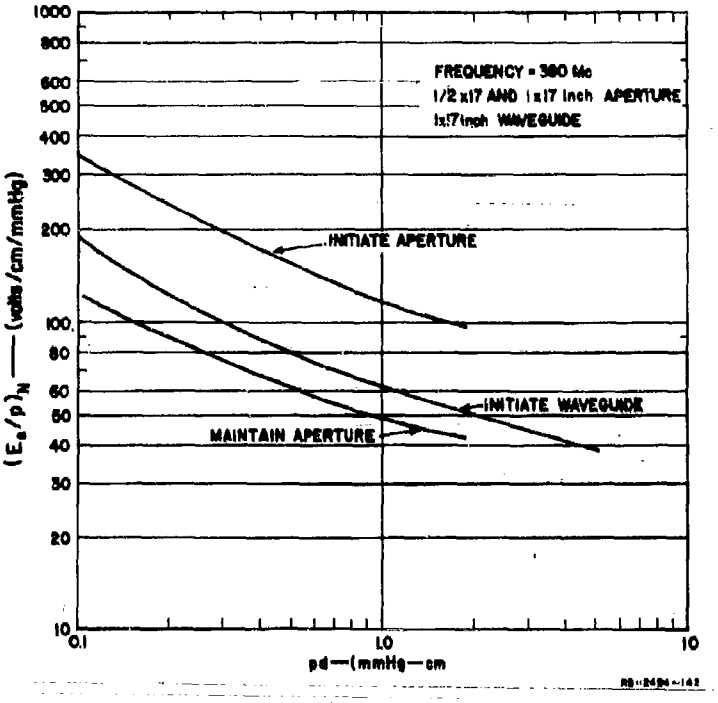

FIG. 40

NORMALIZED DATA ON CW BREAKDOWN OF SLOT ANTENNAS AND RECTANGULAR WAVEGUIDE

Because higher power CW sources were not available, further experiments with CW breakdown over a wider range of aperture size were not possible.

D. PULSED BREAKDOWN OF COVERED SLOT ANTENNA

Pulsed breakdown of aperture antennas was also investigated. Since measurements had already been made of breakdown inside standard *X*-band rectangular waveguide (see Sec. II-E) at *X*-band, a comparison between waveguide breakdown and aperture breakdown could be made by measuring the breakdown power of a 0.4- by 0.9-inch waveguide radiating into free space as shown in Fig. 41. The aperture was covered with a 0.010-inch-thick piece of teflon fibreglass. The power to initiate breakdown on this aperture for pulse width of 2.3, 1.0, and 0.55 microseconds as a function of pressure is shown in Fig. 41. The power to maintain breakdown was slightly below the initiate level for all pressures at which measurements were made. From these data the field in the aperture for breakdown was calculated and the results normalized to $(E_s/p)_n$, $p\tau$, and pb.

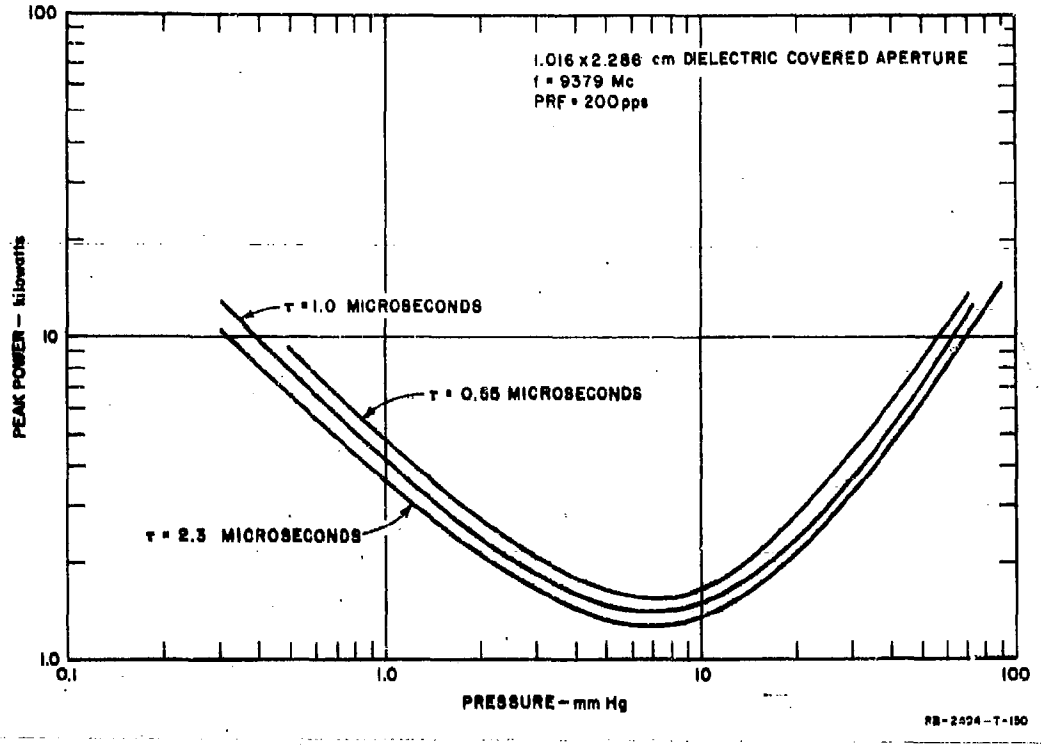

FIG. 41

POWER TO INITIATE PULSED BREAKDOWN OF X-BAND APERTURE FOR THREE PULSE WIDTHS

In Fig. 42 the normalized data for breakdown inside a waveguide are shown for several values of pb together with the data for aperture breakdown for the same values of pb. The waveguide and aperture require about the same values of $(E_e/p)_n$ for large values of pb (where the breakdown is attachment-controlled), but by the time $pb < 10$, the aperture requires increasingly larger values of $(E_e/p)_n$ for breakdown than does the waveguide.

Actually the width of a standard X-band waveguide used as a slot radiator is such that the near zone field fall off is no longer simply related to the aperture width. Therefore, the normalizations shown in Fig. 42 will not be accurate for widths other than 0.4 inch. The way in which the power and normalized field varies with slot width has been investigated to determine the range of parameters over which the normalizations are valid. Fig. 43 shows the power to initiate breakdown as a function of pressure for slot heights of 0.050, 0 100, and 0.400 inch. In all cases the aperture was covered with a dielectric cover. All measurements in Fig. 43 were made with a pulse width of 0.5 microseconds. Similar measurements were made with 1.0 and 2 3-microsecond pulse widths. These data have been normalized and are shown plotted in Fig. 44. The

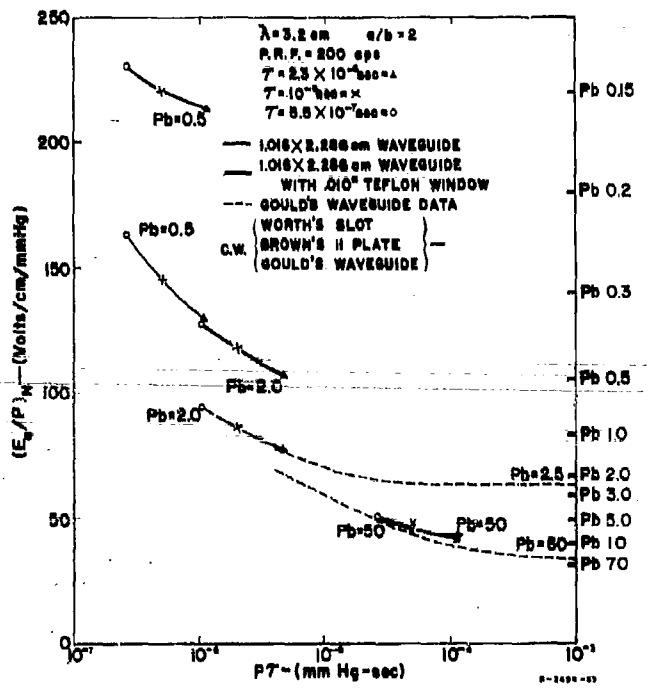

FIG. 42

NORMALIZED DATA FOR BREAKDOWN OF PULSED APERTURES AND WAVEGUIDES

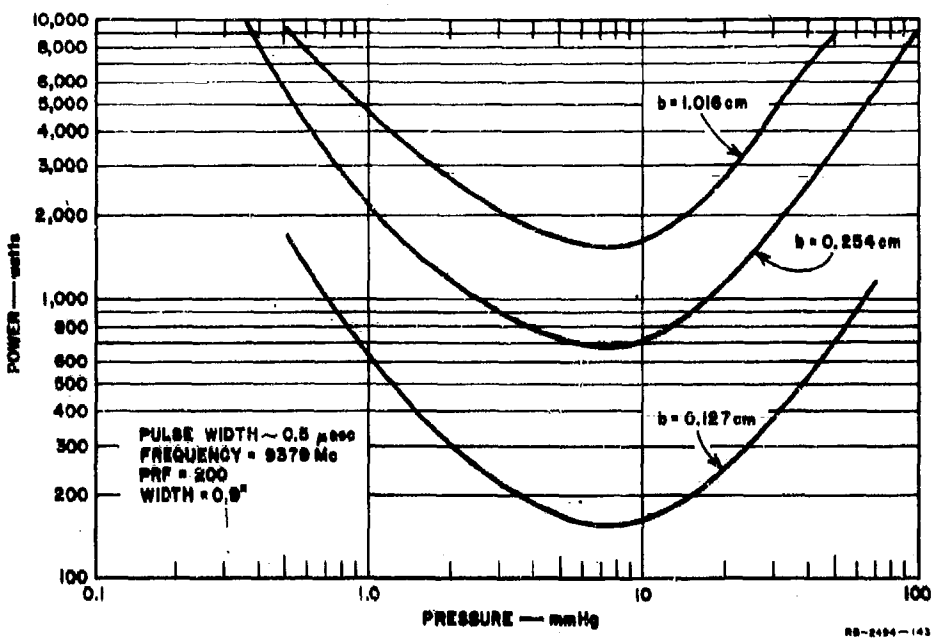

FIG. 43

POWER TO INITIATE PULSED BREAKDOWN FOR VARIOUS SLOT WIDTHS

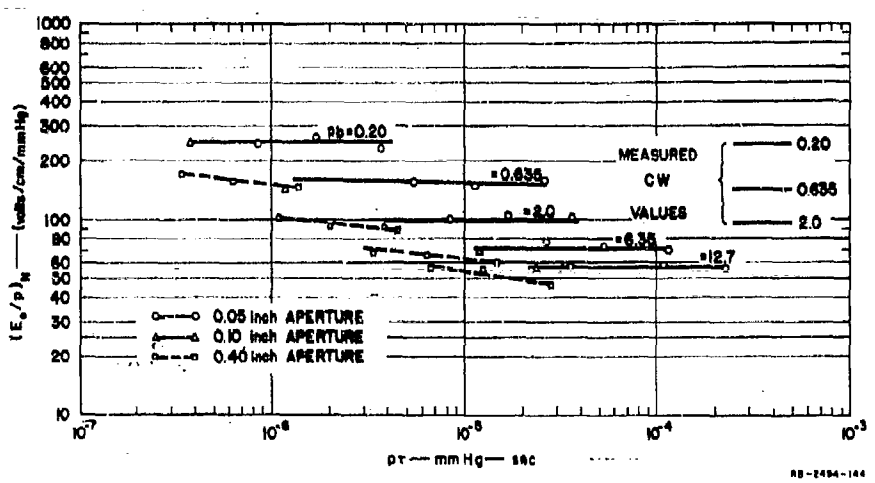

FIG. 44

NORMALIZED DATA FOR PULSED BREAKDOWN OF SLOT ANTENNAS

data for the 0.050- and 0.100-inch-width slots, when properly normalized, form a smooth curve. The values of E_e/p are the same for the same values of pb whether the width was 0.050 or 0.100 inch. However, the data for the 0.40 inch slot show a deviation from the narrower slot data, indicating that the normalization for this slot width is no longer significant and that the near-zone field fall-off is no longer simply related to the slot width.

On the extreme right hand side of Fig. 44 are plotted the CW values of E_e/p from Fig. 40. Note that the narrow slot pulse data are almost identical to the CW values. This is similar to the results obtained with monopoles for CW and pulse power. Over the range of $p\tau$ for which measurements were made, there is very little change in E_e/p for each value of pb.

Measurements have also been made on an E-plane sectoral horn with aperture dimensions of 9.2 by 2.84 cm and on a pyramidal horn 3 by 4.6 cm. Since the dominant factor with these horns is the rate of change of field fall-off, measurements were made of the near-zone field fall-off for these antennas as well as for several smaller antennas. The results are shown in Fig. 45. As would be expected, the larger the aperture the more slowly the field falls off. One can locate an effective center from which the fields are falling off at $1/r$ for each antenna over a range of r. However, the location of this center does not vary in any simple way with horn height for any but the smallest slots. Thus it is not surprising that a normalization involving simply the horn height is not satisfactory for determining the breakdown fields of all but the narrowest slots.

The measured values of the power as a function of pressure for the sectoral horn and the pyramidal horn are shown in Fig. 46. These data have been normalized and are plotted in Fig. 47 along with the data for the 0.40-inch slot. At a high value of pb (such as $pb = 45$) the region in which ionization is formed is essentially one of uniform field. Therefore the data for the different aperture sizes may be normalized to form a smooth curve as in Fig. 47. The varying rates of fall-off for different apertures are not significant for large pb. However for smaller pb ($pb = 5$) the particular type of field fall-off becomes significant. Since the fall-off is not simply related to b, except for very small values of b, the value of $(E_e/p)_n$ is no longer simply related to pb. Therefore, the curves for a constant value of pb obtained for different values of b (aperture heights) are different. As would be expected, the more uniform the near field region the lower the value of $(E_e/p)_n$ required for breakdown.

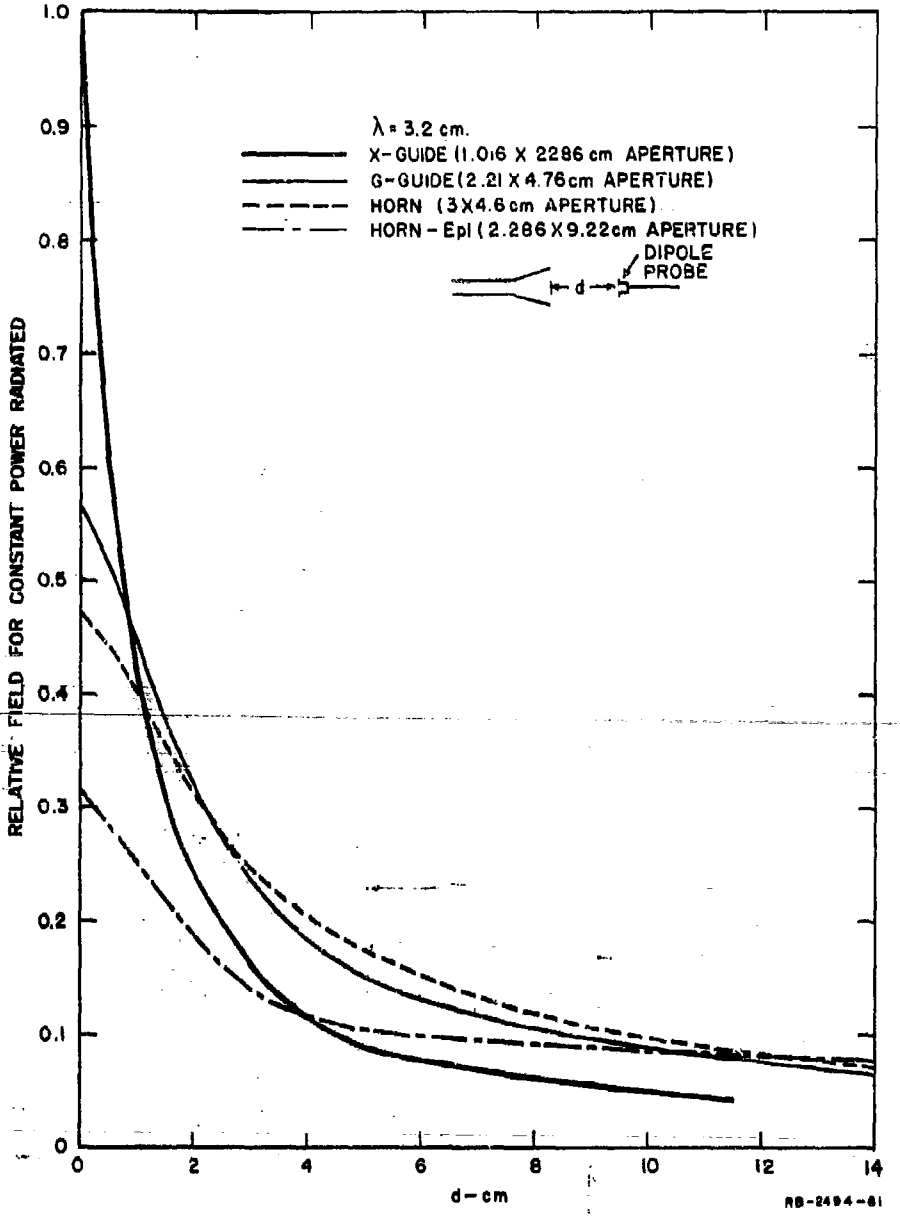

FIG. 45

FIELD FALL-OFF FOR DIFFERENT ANTENNAS

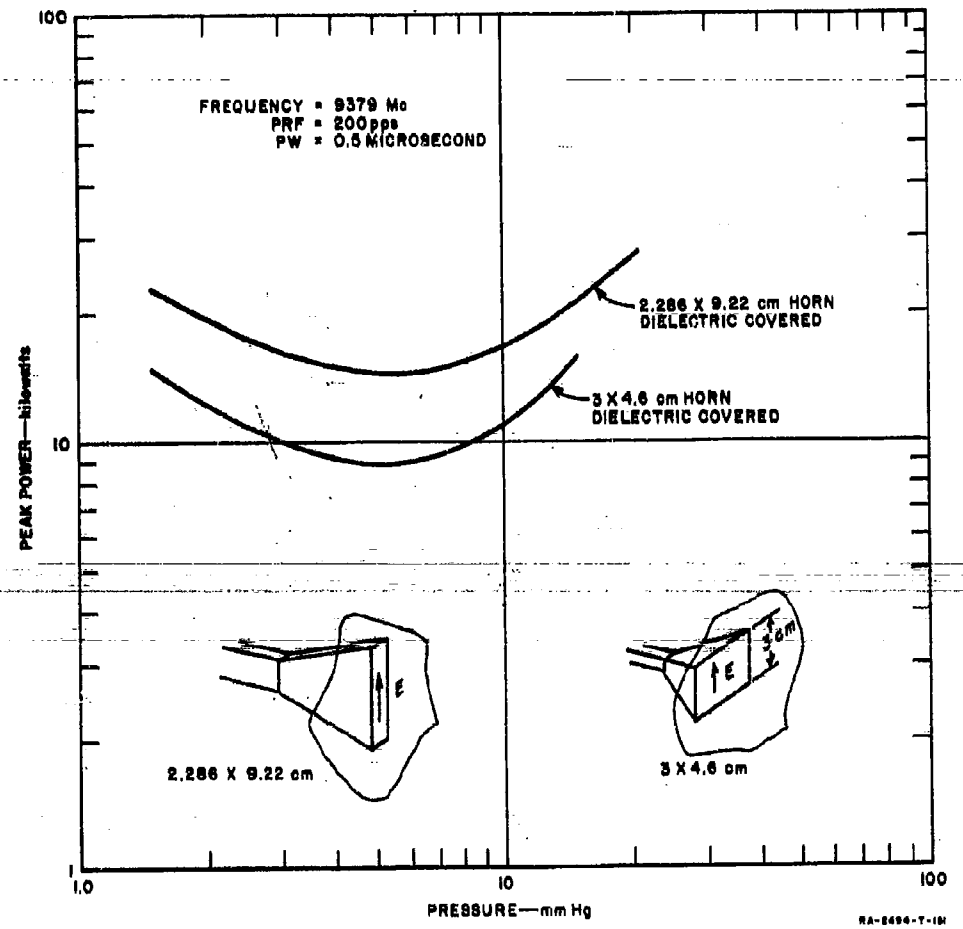

FIG. 46

POWER TO INITIATE PULSED BREAKDOWN OF A SECTORAL AND PYRAMIDAL HORN

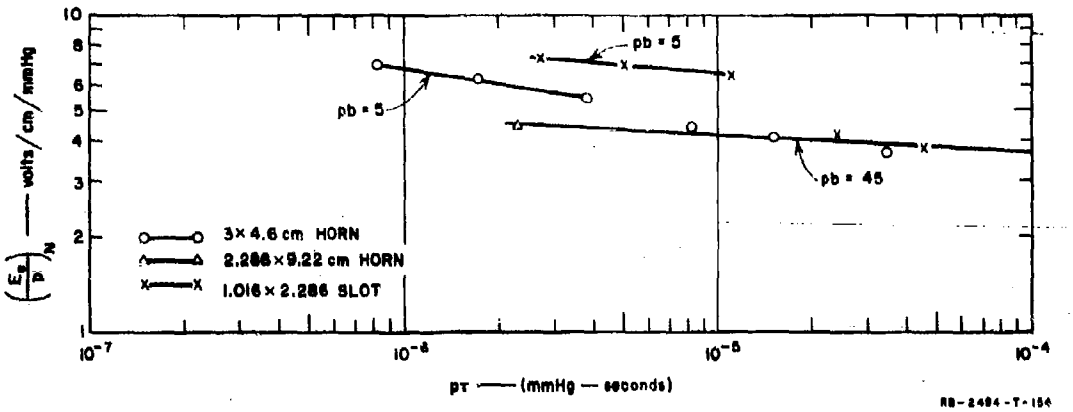

FIG. 47

NORMALIZED DATA FOR PULSED BREAKDOWN OF DIFFERENT HEIGHT ANTENNAS

It would be expected that when pb gets very large the values of E_s/p would tend toward the attachment-controlled values. While for CW breakdown the attachment-controlled value of E_s/p was a single value (about 30), for pulsed breakdown the attachment-controlled value of E_s/p is a function of pressure and pulse width. For large values of $p\tau$ the pulse and CW attachment-controlled breakdown levels are the same, but for small values of $p\tau$ the pulsed power attachment-controlled levels will be higher than the CW levels. Since a general solution for any type of horn would be very complicated, a conservative estimate of the breakdown field strength for the antenna designer to use would be the data shown in Fig. 5 for very large pb.

V ANTENNA OPERATION ON A WEAKLY IONIZED MEDIUM

A. BACKGROUND

When a nose cone is re-entering the earth's atmosphere a plasma sheath is formed about the nose cone. Signal drop-out has been reported for telemetry signals received from vehicles during this re-entry phase. While strong attenuation due to the plasma was to be expected, it was felt that probably voltage breakdown was also occurring.

The environment associated with a re-entry vehicle is very complicated and the conditions away from the stagnation region are not well understood. Clearly it is not feasible to scale the actual environmental condition; however, it was felt that knowledge of the behavior of antennas in the presence of plasmas with electron densities of the same orders of magnitude as the actual densities would aid in antenna design for a re-entry vehicle.

B. ANTENNA OPERATION IN THE PRESENCE OF A DC DISCHARGE

Figure 48 illustrates the DC discharge used to create the plasma over the aperture of a 0.53λ slot antenna (17-inch slot at 380 Mc) mounted on a conducting ground plane with a thin dielectric cover insulator. The cathode is formed by an aluminum block ¼ by 3/16 by 1 inch, elevated over the insulated ground plane, while the anode is formed by a ½- by 2-inch section of ground plane formed by removing the dielectric insulator. The DC glow discharge was placed so that negative glow area of the discharge was located over the aperture. In the negative glow area, the electron concentration may be as high as 10^{11} electrons per cc and the net charge density is nearly zero.[16] The negative glow area is a typical example of plasma and has been studied by other investigators with a Langmuir probe method. Measurement of the density by the Langmuir probe was attempted; but, because of the unbounded nature of the DC discharge, this was not successful. As soon as the probe was made positive with respect to the anode, the discharge would transfer over to the probe.

An estimate of the electron density produced by the discharge was made using the solution for a plane wave incident on an infinite plasma. With the antenna reasonably well matched (reflection coefficient = 0.09)

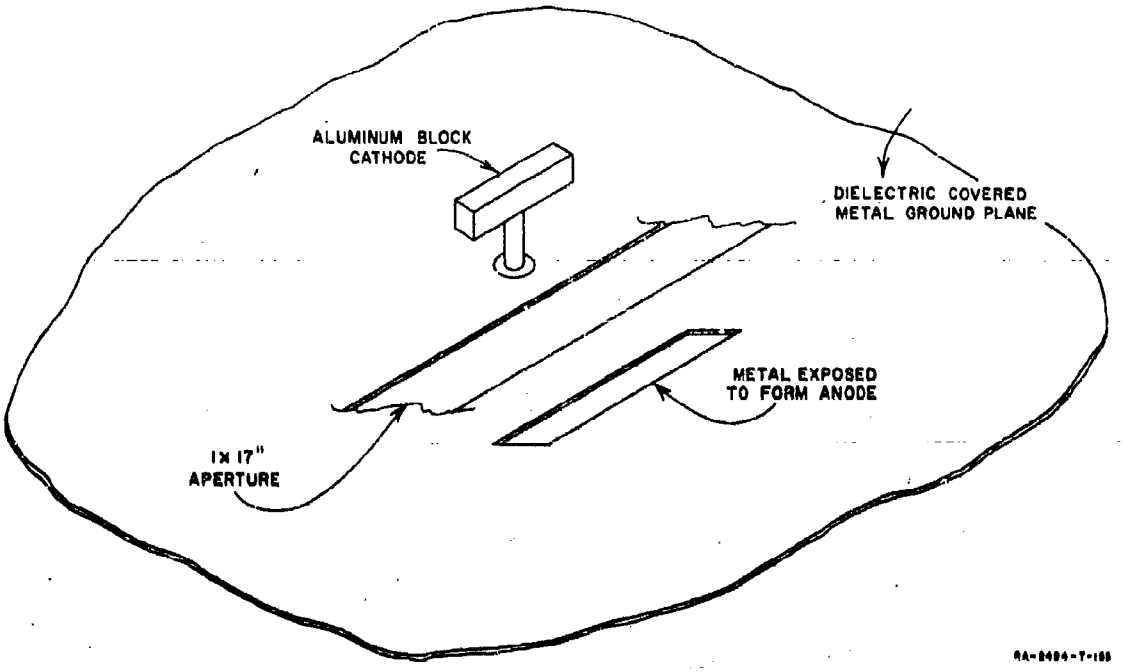

FIG. 48

CONFIGURATION USED IN PRODUCING A DC PLASMA

prior to the introduction of the plasma, the reflection from the plasma may be determined. The collision frequency is obtained from the pressure measurement since $\nu_c = 5.3 \times 10^9 p$ for air, where p is the pressure in mm Hg. A knowledge of the magnitude of the reflection coefficient, the RF frequency, and the collision frequency is then sufficient to determine the plasma density.

Figure 49 is a plot of the transmitted and absorbed power as well as the VSWR of the antenna in the presence of the plasma. The ratio of the collision to RF angular frequency is 0.45 Up to an input power of 4.5 watts to the antenna, the VSWR of the antenna remains constant at 1.15; the transmitted power, as measured by an external antenna increases linearly with the incident power and there is no absorbtion of energy by the plasma. From the change in the reflection coefficient from the condition of no plasma to with a plasma, it is estimated that the plasma frequency ($fp = 8{,}900\sqrt{N}$, where N is the density in electrons per cc) is less than one-half the RF angular frequency After the occurrence of voltage breakdown at 4.5 watts, the transmitted power remains almost constant while the absorbed power increases directly with incident power.

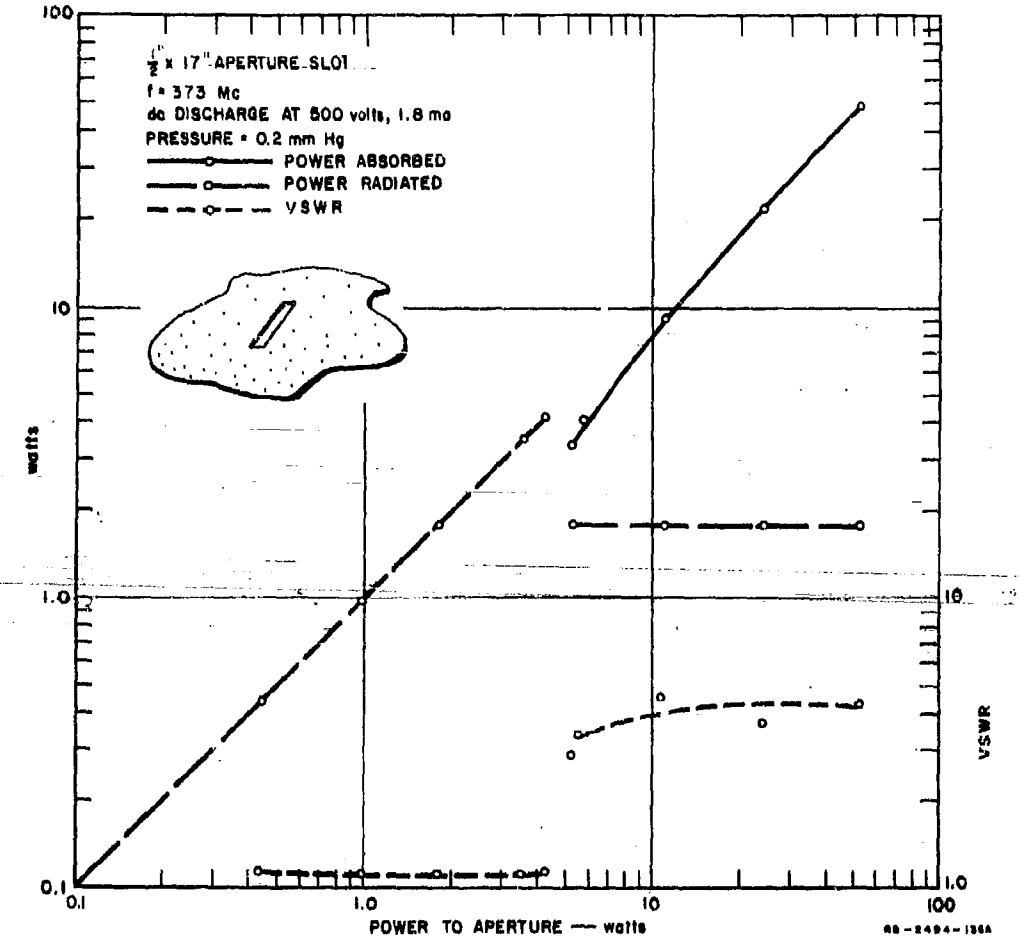

FIG. 49

PROPAGATION CHARACTERISTICS OF A 373-Mc SLOT ANTENNA IN THE PRESENCE OF A DC PLASMA PRESSURE = 0.2 mm Hg, 500 VOLTS DC

Since the VSWR of the antenna remains essentially constant after breakdown, this indicates that the plasma density, as well as the attenuation constant, remains constant as the power to the aperture is increased. The increased total attenuation as the power is increased is due primarily to the increase in the size of the plasma, rather than the change in its electrical characteristic.

Figure 50 shows the result obtained when the plasma frequency is approximately equal to the RF frequency at the same pressure. The characteristic after RF breakdown is almost identical to Fig. 49. Before

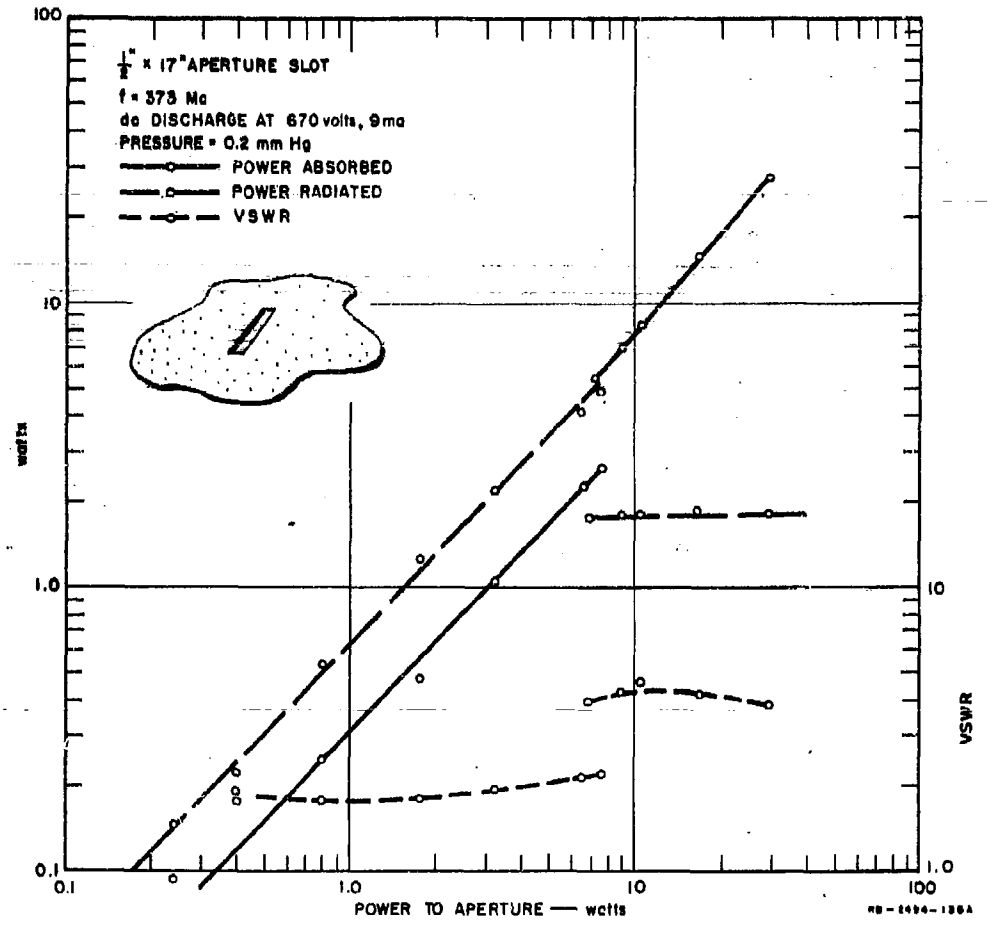

FIG. 50

PROPAGATION CHARACTERISTICS OF A 373-Mc SLOT ANTENNA IN THE PRESENCE OF A DC PLASMA PRESSURE = 0.2 mm Hg, 670 VOLTS DC

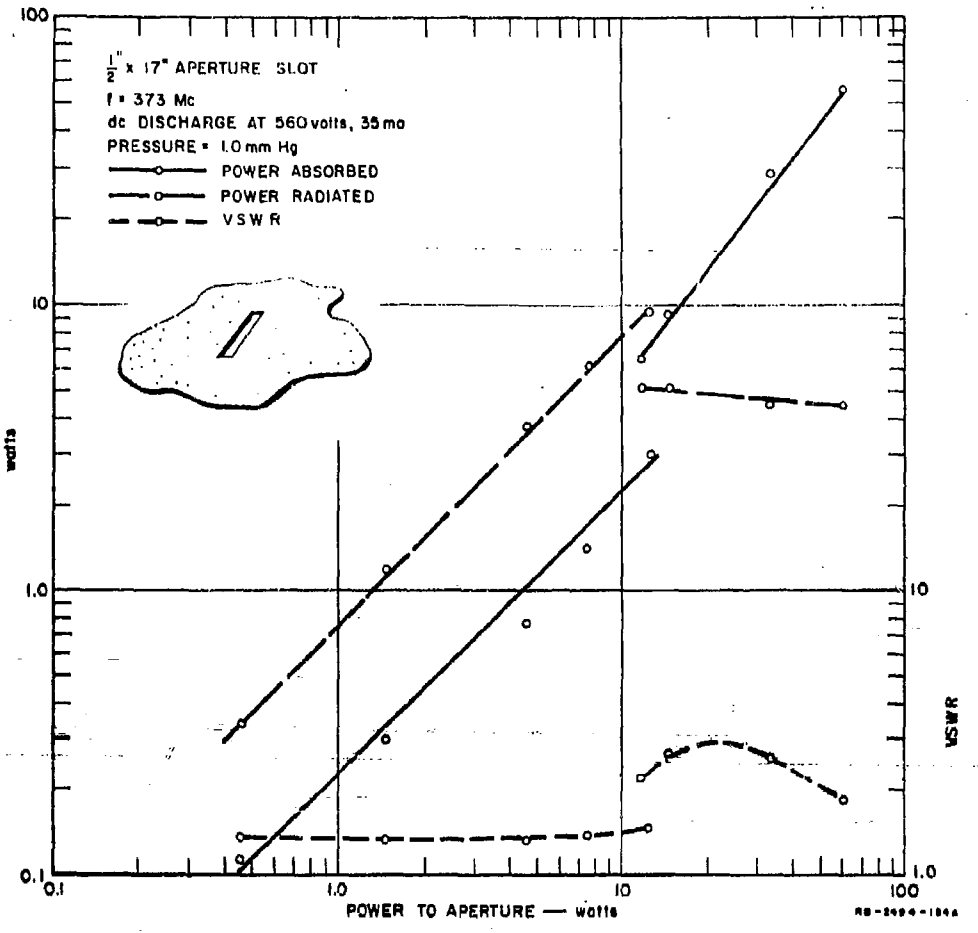

FIG. 51

PROPAGATION CHARACTERISTICS OF A 373-Mc SLOT ANTENNA IN THE PRESENCE OF A DC PLASMA PRESSURE = 1.0 mm Hg, 560 VOLTS DC

RF breakdown, attenuation is present and the RF conductivity appears to be constant, independent of the applied RF field

In the absence of a plasma, this antenna required about 40 watts for breakdown as compared to 7 watts with a plasma.

Figure 51 shows similar results obtained at 1 mm pressure ($\nu_c/\omega = 2.27$). In the absence of a plasma, 47 watts was required to initiate breakdown at this pressure as compared to 10 watts in the presence of the plasma.

One interesting result of this study is that the power handling capability of the slot in the presence of the ionized medium appears to

be about the same as the power required to maintain breakdown. This would be true if the RF field distribution is approximately the same, since ambipolar diffusion is the main loss mechanism for both cases. If this were to be found to be generally true, the design of antennas for operation in an ionized medium would be considerably simplified. Further work is required on the effect of ambient electron density, energy, and distribution on the breakdown phenomenon.

Despite the differences between the actual environment and our simulation of it, the results clearly indicate that antennas designed for operation in a non-ionized medium will break down in an ionized medium with power levels lower by about one order of magnitude. In order to avoid the attenuation due to re-entry ionization, telemetry equipment operating at frequencies above the expected plasma frequency is being developed. Unless antennas are designed for operation in an ionized medium, the occurrence of voltage breakdown may negate any gain expected from going to a higher frequency.

VI METHODS FOR INCREASING THE POWER HANDLING CAPABILITY OF ANTENNAS

A. BACKGROUND

There are two fundamental methods by which the power-handling capability of an antenna may be increased. One method depends upon the use of mechanisms to increase the electron-loss rates, thus increasing the ionization rates required to produce breakdown. Since the ionization rates are monotonically increasing functions of electric field, the higher the ionization rate required for breakdown the higher will be the field strength required for breakdown. The other method depends upon the use of mechanisms that will reduce the ionization rate without reducing the loss rate. Examples of both methods are discussed below.

B. INCREASING THE LOSS RATE

One means of increasing the electron loss rate is to apply a DC sweeping field to the region about an antenna. Since the RF field about an antenna is not uniform but has a maximum in some region and decreases in areas away from this region, the application of DC fields that will sweep electrons out of the high field region and into the lower field regions will act to effectively increase the electron loss rate. Alternatively, if the field about the antenna is relatively uniform but there are surfaces to which electrons may be attracted and so removed from the high field region, the application of DC fields to accomplish this will be useful. Brown[2] has worked out the relation for the application of DC fields in the case of uniform parallel plates and has shown that the effect is equivalent to a decrease in the diffusion length. The relation he derived is

$$\frac{1}{\Lambda_{DC}^2} = \frac{1}{\Lambda^2} + \left(\frac{E_{DC}}{2D/\mu}\right)$$

where

E_{DC} is the applied DC field, D is the diffusion coefficient of electrons, and μ is the electron mobility.

From this relation it appears that the effective diffusion length may be made as small as desired by the application of increasing amounts of DC voltage. A limitation, however, is imposed by the onset of DC voltage breakdown. Before this limit is reached, an appreciable increase in power handling capability may be achieved.

Measurements have been made of the breakdown power of a number of antennas both with and without DC fields. These measurements are described below.

1. Monopole Breakdown with DC Fields

The monopole antenna is ideal for the application of DC fields. DC fields may be easily applied between the monopole and its ground plane. The RF field around the monopole decreases rapidly with the radial distance from the antenna. Thus, if the application of DC fields can sweep electrons out of the region close to the monopole surface, appreciable increases in power handling capability can be achieved. Electrons close to the monopole surface may be removed from this region by making the monopole either negative or positive. If the monopole is positive, electrons will be attracted to it and so removed from the region of interest. However, this arrangement is undesirable since it may produce secondary emission at the monopole surface if large DC fields are used. Further, it draws electrons into the high RF field region where they may produce ionization before they are collected at the monopole surface. A better scheme is to make the monopole negative. This will repel electrons from the monopole surface out into the low RF field regions where the field is too low to produce appreciable ionization.

Measurements have been made at 240 Mc for the power to break down a quarter-wavelength monopole as the DC voltage was varied from minus 150 volts to plus 450 volts. A minus sign means that the monopole was negative with respect to the ground plane. The monopole diameter was $\frac{1}{8}$-inch and the antenna was made of brass. Measurements were made at pressures above, below, and at the pressure for minimum power handling capability. The results are shown in Fig. 52. With no DC voltage this antenna could only handle about 4 watts of power without voltage breakdown. With the application of about minus 150 volts this figure was increased an order of magnitude to 40 watts. The measurements were not carried to further negative voltages because of a limitation of available RF power. Application of positive DC voltages also increases the power handling capability

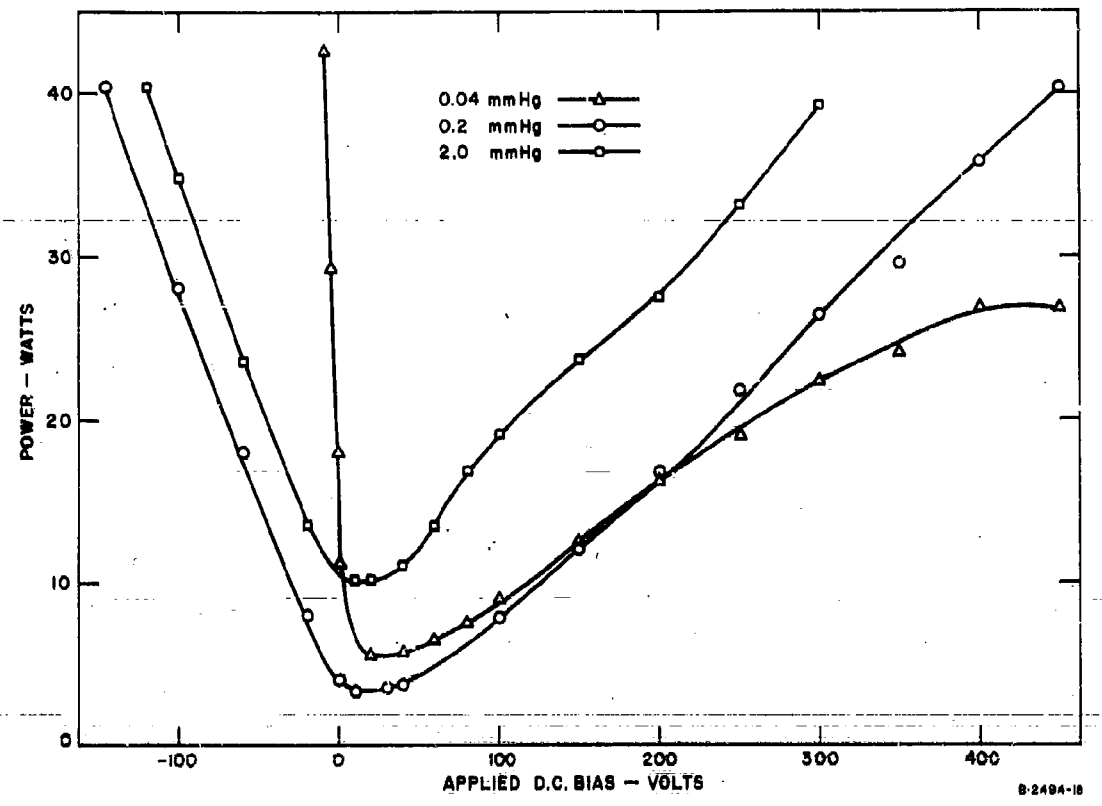

FIG. 52

CW POWER TO INITIATE VOLTAGE BREAKDOWN AS A FUNCTION OF APPLIED DC BIASING VOLTAGE FOR A 0.24-WAVELENGTH MONOPOLE

of this antenna, but the DC voltages necessary were larger than with negative biasing. This is reasonable in view of the previous discussion.

Very little DC current is drawn by the application of the DC voltage, so that a high voltage, low current battery is adequate to supply the required DC power.

Measurements made at 9400 Mc on a quarter-wavelength monopole, 11.5 mils in diameter, confirmed that biasing worked as well on pulsed power as it did with CW power. The results of this measurement are shown in Fig. 53.

It should be pointed out that DC voltages will not be effective with an antenna embedded in a dielectric. A charge will build up on the dielectric so that the DC voltage will appear across the dielectric rather

than in the region where electrons are being formed. This is also true for operation in an ionized medium. The total DC voltage appears across the dipole and the ionized sheath, and there is no sweeping action. A large DC current may flow due to the finite conductivity of the plasma, causing a drainage of the DC power supply.

2. Aperture Breakdown with DC Fields

The application of DC voltages to slot radiators has been tried also. For large slot widths the near-zone field fall-off normal to the slot surface is relatively slow and the DC voltage is not very effective. Further, the DC voltage is not so easily applied as in the case of monopoles. An *X*-band waveguide aperture with a dielectric cover was used for tests on the effectiveness of DC voltages on the power handling capability of slot antennas. Standard size *X*-band waveguide was used so that the near-zone field fall-off was relatively slow. Various arrangements were made

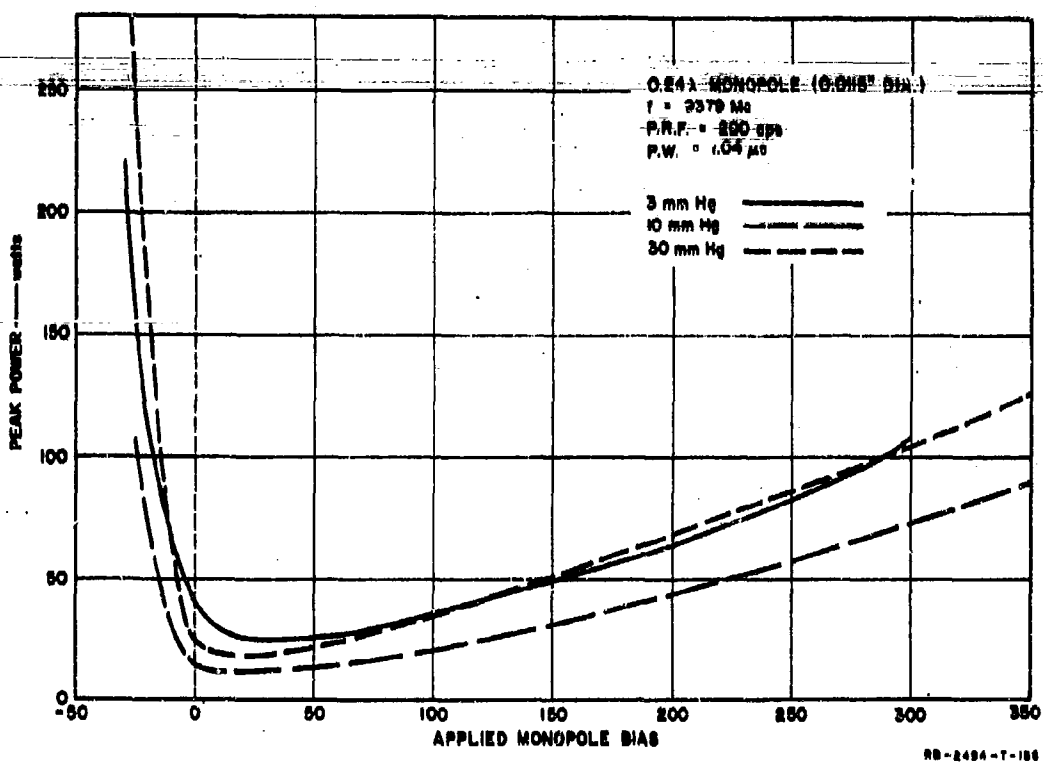

FIG. 53

PULSED POWER TO INITIATE VOLTAGE BREAKDOWN AS A FUNCTION OF APPLIED DC BIASING VOLTAGE FOR A 0.24-WAVELENGTH MONOPOLE

to produce a DC field in the aperture. In a typical arrangement, DC voltage was applied between the ground plane and a wire run across the aperture perpendicular to the RF electric field vector so that there would be a minimum disturbance of the RF field. Only about a 3-db increase in power handling capability was obtained before DC breakdown occurred.

Similar measurements were made at 380 Mc on a 0.5- by 17-inch slot aperture with the results shown in Fig. 54. In this case there was not sufficient RF power available to fully determine the increase in power handling capability with DC fields. Measured increases of a factor of two were recorded, but it seems, from the curves, as though larger increases may be obtainable before DC breakdown occurs. This is reasonable when it is remembered that this slot is much narrower, electrically, than the standard size *X*-band slot mentioned above. Thus the field fall-off is much more rapid in the 380-Mc slot, and the DC field is more effective.

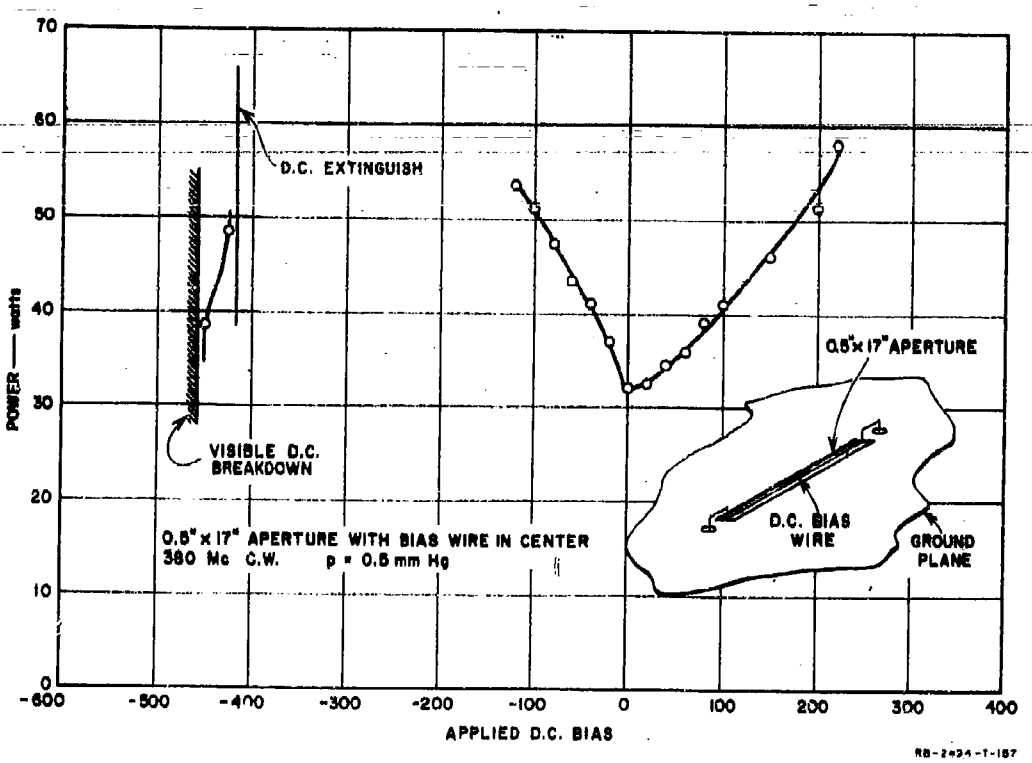

FIG. 54

CW POWER TO INITIATE VOLTAGE BREAKDOWN AS A FUNCTION OF APPLIED DC BIASING VOLTAGE FOR A 380-Mc SLOT ANTENNA

C. DECREASING THE IONIZATION RATE

The lower the RF electric field strength is made, the lower is the ionization rate. Therefore, any method that will enable the near-zone electric field strength to be decreased while radiating the same amount of power will increase the power handling capability of the antenna. In the case of monopole antennas, simply increasing the diameter will decrease the surface field strength and thus raise the breakdown power for certain conditions (see the discussion of the effect of diameter on breakdown power in Sec. III).

Choosing antenna configurations that will minimize the maximum field strength will optimize the breakdown power levels. For example, if a short monopole antenna is called for, a much greater amount of power can be radiated from a top-loaded folded monopole than from a vertical stub. As shown in Fig. 29, a vertical stub 0.10 wavelengths long can only handle 0.20 watt of power. A top-loaded folded monopole of the same height as illustrated in Fig. 55 has been designed and tested. This antenna can handle 8.5 watts of power.

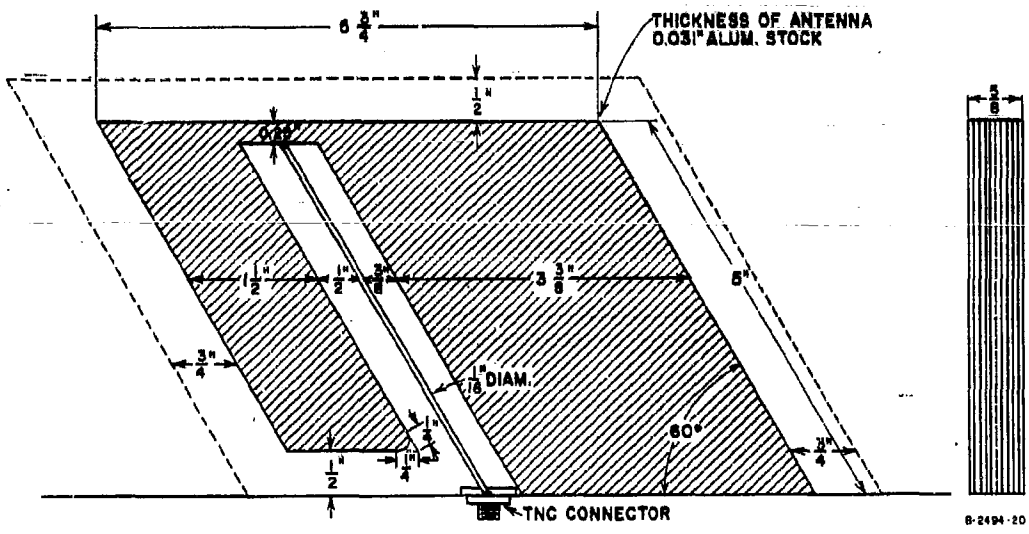

FIG. 55

SKETCH OF TOP-LOADED FOLDED MONOPOLE 0.10 WAVELENGTHS HIGH

A method not always available as a possible solution because of aerodynamic considerations is the use of a pressurized radome over the antenna structure. By using a radome of sufficient size, large increases in power handling capability are possible.

Caution must be exercised in considering means of increasing the power handling capability of antennas that one does not focus on means of increasing the *field strength* required for breakdown. Increasing the *field strength* required for breakdown may not always be desirable, since it is the *maximum radiated power* that is desired and not maximum near-zone electric field. As an illustration, consider the case of an open-waveguide slot with no dielectric cover. When the slot width is large, the field strength for breakdown can be increased by decreasing the slot width since the loss of electrons to the walls is increased as the walls are brought closer together. However, the drop in radiation resistance as the slot width is decreased is faster than the increase in the breakdown field strength, so that the power handling capability decreases even though the breakdown field strength is increased. When the slot width is very narrow, the radiation resistance is essentially independent of slot width. Then, the aperture field strength per watt radiated is inversely proportional to the slot width. Although the losses to the walls may increase and the field fall-off is sharper, the increase in field strength per watt radiated more than offsets these factors, so that the narrowest slot radiates the least power without breakdown. The situation is analagous to the effect of diameter on monopole breakdown. The thinnest antenna required the least power for breakdown at the pressure for minimum power. At lower pressures the antennas required about the same power for breakdown.

VII CONCLUSION

It has been shown that the electron loss mechanisms which are important in determining breakdown on transmission line components are the same as those which are important in determining antenna breakdown fields. Electron attachment and diffusion are the dominant loss mechanisms, while ionization by collision is the dominant source of electron production. At pressures for which the collision frequency is much greater than the angular radio frequency the dominant loss mechanism is generally attachment. For pressures at which the collision frequency is much less than the radian radio frequency, diffusion is generally the dominant loss mechanism. The particular geometry of the antenna will determine the pressure at which the transition from attachment-controlled to diffusion-controlled breakdown occurs.

A qualitative discussion of the manner in which the various loss mechanisms enter into the breakdown process for different pressure ranges for the breakdown of parallel plate, rectangular waveguide, coaxial line, monopole antenna, and aperture antennas has been presented. By expressing the breakdown condition in terms of $(E_e/p)_n$ as a function of the pressure times some characteristic dimension (parallel plate spacing, monopole radius, slot width), quantitative results useful for a wide range of parameters have been obtained. In the case of monopoles, a single curve showing the variation of $(E_e/p)_n$ as a function of pr describes the measured results within about 20 percent for measurements at 240 and 400 Mc, for variations in monopole diameter of a factor of 4, and for monopole lengths from 0.08 to 0.32 wavelengths. Pulsed breakdown measurements on monopole antennas at 9400 Mc show very little change in the value of $(E_e/p)_n$ for different pulse widths over the range of pressures at which measurements were made. In fact, the CW and pulse levels are almost identical, showing that frequency scaling is good over a 40-to-1 range.

For narrow slot antennas a single curve of $(E_e/p)_n$ as a function of pd is sufficient to describe the breakdown condition. For aperture antennas that cannot be classified as narrow slots there is no simple relation between the value of $(E_e/p)_n$ and pd. This is because the field fall-off near the aperture is not a simple function of the aperture height.

For very large apertures, the field fall-off may be so small within the region where ionization occurs, that this factor may be considered uniform. Under these conditions the breakdown would be attachment-controlled. The values of $(E_e/p)_N$ for attachment-controlled breakdown would represent a lower limit for aperture breakdown.

The effect of an ionized medium near the antenna on the breakdown level has been investigated by means of a DC discharge to simulate the plasma. The results show that appreciable decreases in the power-handling capability of antennas may occur when an antenna is operating in an ionized medium. Since the energy of the electrons used in this experiment was much greater than would be the case for electrons during re-entry the results are not strictly applicable to operation under these conditions. Additional work is needed in this area to determine the effect of ionized media under different conditions of energy and density. The results presented here illustrate that such effects can be important in limiting the power-handling capability of antennas that must work in such environments. Consideration should also be given to any special design procedures that the antenna designer would use when the environment which his antenna is to operate in includes an ionized medium.

Consideration has been given to different means of increasing the power-handling capability of antennas. Methods of increasing the electron loss rates and decreasing the ionization rates in the vicinity of the antennas have been considered. The effectiveness has been demonstrated of DC electric fields in increasing the electron loss rates in the vicinity of antennas that have RF field distributions which decrease rapidly with distance from the antenna, and quantitative data have been presented.

APPENDIX A

DETERMINATION OF THE ELECTRIC FIELD AT THE TIP OF A MONOPOLE

APPENDIX A

DETERMINATION OF THE ELECTRIC FIELD AT THE TIP OF A MONOPOLE

Since sharp edges have little effect on high-altitude, high-frequency breakdown, this discussion will be concerned with calculating the field at the end of a monopole, regardless of the particular shape of the tip. If the monopole lies along the Z-axis, the continuity of current relation may be expressed as:

$$\frac{\partial I(z)}{\partial z} = -j\omega q \qquad \text{(A-1)}$$

where $I(z)$ is the current distribution along the monopole and q is the charge distribution along the monopole.

We may write $I(z)$ as the product of the current at the input terminals, $I(0)$, and a distribution function $f(z)$. Thus

$$I(z) = I(0)\,\frac{f(z)}{f(0)} \qquad \text{(A-2)}$$

We may then express Eq. (A-1) as

$$\frac{I(0)}{f(0)}\,\frac{\partial f(z)}{\partial z} = -j\omega q \qquad \text{(A-3)}$$

For very thin monopoles ($\Omega \to \infty$) $f(z)$ is given by $\sin \beta(h - z)$ and is slightly modified for thicker monopoles. β is $2\pi/\lambda$, and h is the monopole height. Since the precise distribution for a given value of Ω is a complex function, the results of King[14] for $\beta h = \lambda/4$ and $\Omega = 10$ will be used to determine $\partial f(z)/\partial z$, while the value of $f(0)$ is determined from the assumption of a sinusoidal current. The value of $f(0)$ will not be in error by a large amount, but $\partial f(z)/\partial z$ could be in error by an appreciable amount if the actual current distribution were not used (as was done by King). Thus, at the tip

$$\frac{\partial f(z)}{\partial z} = C_1 \text{ for a given } \Omega \text{ and any length.} \qquad \text{(A-4)}$$

From Eq. (A-2), $f(0)$ is found to be

$$f(0) = \sin \beta h \quad . \qquad \text{(A-5)}$$

Substituting these values into Eq. (A-3) we obtain

$$\frac{I(0)}{\sin \beta h} C_1 = -j\omega q \quad . \qquad \text{(A-6)}$$

King gives the value of $q_t/V(0)$ for $\beta h = \lambda/4$ and $\Omega = 10$. Therefore, rearranging Eq. (A-6) we may solve for C_1/ω. We introduce the input impedance Z(0) to get an expression in terms of the input voltage, $V(0)$. Thus

$$\frac{C_1}{\omega} = \frac{q}{V(0)} Z(0) \sin \beta h \quad . \qquad \text{(A-7)}$$

Using King's values we obtain

$$\frac{C_1}{\omega} = 5.05 \times 10^{-9} \quad . \qquad \text{(A-8)}$$

Rearranging Eq. (A-6) for the charge at the tip and using the value given in Eq. (A-8) for C_1/ω we find that

$$q_t = 5.05 \times 10^{-9} \frac{I_0}{\sin \beta h} \quad . \qquad \text{(A-9)}$$

Eq. (A-9) should be a fairly accurate expression for the charge at the tip for a wide range of Ω and any length monopole that is not close to anti-resonance. At anti-resonance the value of $f(0)$ varies rapidly with Ω and the approximation given in Eq. (A-9) would no longer be valid.

The field produced by q_t is given by

$$E_t = \frac{q_t}{2\pi\epsilon a} \quad . \tag{A-10}$$

Substituting Eq. (A-9) into Eq. (A-10) we find the field of the tip is

$$E_t = \frac{9iI(0)}{a \sin \beta h} \quad V/\text{cm} \quad \text{if } a \text{ is in cm.} \tag{A-11}$$

For example, the field at the tip of an $\frac{1}{8}$-inch diameter monopole is

$$E_t = \frac{570I(0)}{\sin \beta h} \quad V/\text{cm} \quad . \tag{A-12}$$

As a separate check on these results we may use King's results for small dipoles. For $\Omega = 10$

$$q_t = \frac{1.32\ I(0)}{\omega h} \quad . \tag{A-13}$$

This may be expressed as

$$q_t = \frac{4.4 \times 10^{-9}\ I(0)}{\beta h} \tag{A-14}$$

This may be compared directly with Eq. (A-9) since the electric field is proportional to the charge. For small dipoles $\sin \beta h \approx \beta h$. Thus for the same feed currents, the electric field calculated from Eq. (A-9) differs by only about 10 percent from the field calculated from Eq. (A-14).

APPENDIX B

CALCULATION OF THE ELECTRIC FIELD IN A NARROW SLOT ANTENNA UP TO $\lambda/2$ LONG

APPENDIX B

CALCULATION OF THE ELECTRIC FIELD IN A NARROW SLOT ANTENNA UP TO $\lambda/2$ LONG

If the impedance of a dipole of total length $2h$ is given by Z_d, then by Babinet's principle the impedance of a slot antenna radiating into free space on both sides of a ground plane is given by

$$Z_s = \frac{35476}{Z_d}$$

This presumes that the current distribution along the dipole is the same as the distribution of electric field in the slot. Thus, the transformation from center fed dipoles will be true for slots fed in the TE_{10} mode only if the aperture is less than $\lambda/2$.

Once the slot impedance is known, the electric field may be found as follows: The power radiated by the slot is given by

$$P = \frac{V^2}{|Z_s|^2} R_S$$

where R_S is the slot resistance and V is the voltage across the slot. The electric field is related to the slot voltage by

$$V = E_S b$$

where b = slot width. Therefore

$$E_S = \frac{|Z_S|}{b} \sqrt{\frac{P}{R_S}}$$

For a slot antenna radiating into only one side of the ground plane the slot impedance is doubled so that

$$Z_S = \frac{70,952}{Z_d} .$$

As an example, consider a resonant slot 0.475λ long and 0.01λ wide. This corresponds to a dipole 0.475λ long and 0.005λ in diameter. The dipole impedance is a pure resistance equal to 67 ohms. Therefore, the complimentary slot impedance for a cavity fed slot is

$$Z_S = \frac{70,952}{67} = 1060\ \Omega$$

and

$$E_S = \frac{32.6}{b} \sqrt{P} .$$

APPENDIX C

CALCULATION OF THE FIELD IN THE APERTURE OF A LARGE HORN ANTENNA

APPENDIX C

CALCULATION OF THE FIELD IN THE APERTURE OF A LARGE HORN ANTENNA

The total power radiated is given by the integral over the aperture of the power density in the aperture. Thus,

$$P = \int \frac{E^2}{Z_0}\, dA \qquad \text{for large horns.}$$

For a typical horn distribution, the electric field is uniform in one direction and sinusoidal in the other. Therefore,

$$P = 1.33 \times 10^{-3}\, E^2\, A$$

and

$$E = 27.5 \sqrt{\frac{P}{A}}$$

APPENDIX D

CALCULATION OF E_{max} IN A WAVEGUIDE THAT IS NOT MATCHED

APPENDIX D

CALCULATION OF E_{max} IN A WAVEGUIDE THAT IS NOT MATCHED

The incident power in a waveguide excited in the TE_{10} mode is

$$P_{inc} = 1.33 \times 10^{-3}\ ab \frac{\lambda}{\lambda_g} E_{inc}^2$$

where

a is the width of the guide

b is the height of the guide

λ is the free space wavelength

λ_g is the guide wavelength

E_{inc} is the incident field strength.

The real power flowing down the guide is the difference between the incident and reflected power in the guide. Therefore

$$P_{inc} = \frac{P_{real}}{1 - \Gamma^2}$$

where Γ is the voltage reflection coefficient.

Rearranging terms we obtain

$$E_{inc}^2 = \frac{P_{real}}{(1 - \Gamma^2)} \frac{1}{1.33 \times 10^{-3}\ ab \frac{\lambda}{\lambda_g}}$$

or

$$E_{inc} = \sqrt{\frac{P_{real}}{(1 - \Gamma^2)\ 1.33 \times 10^{-3}\ ab \frac{\lambda}{\lambda_g}}}$$

The maximum electric field in the guide may be expressed in terms of the reflection coefficient and the incident field

$$E_{max} = (1 + \Gamma)\, E_{inc}$$

Therefore

$$E_{max} = \sqrt{\frac{1 + \Gamma}{1 - \Gamma} \; \frac{P_{real}}{1.33 \times 10^{-3}\; ab\; \frac{\lambda}{\lambda g}}}$$

or

$$E_{max} = 27.5(VSWR)^{1/2} \sqrt{\frac{P_{real}}{ab\; \frac{\lambda}{\lambda g}}} \quad V/cm \quad \text{if } a \text{ and } b \text{ are in cm}$$

ACKNOWLEDGMENT

The authors would like to acknowledge the assistance of Mr. Willard Wadsworth in the performance of the experimental work. The authors are also deeply indebted to Mr. Jack Chown for many helpful discussions concerning the contents of this report.

REFERENCES

1. J. Chown, W. Scharfman, T. Morita, "Voltage Breakdown Characteristics of Microwave Antennas," *Proc. IRE* **47**, 8, pp. 1331. 1337 (August 1959).

2. S. C. Brown, "High Frequency Gas Discharge-Breakdown," *Proc. IRE* **39**, 12, pp. 1493-1501 (December 1951).

3. L. Gould and L. W. Roberts, "Breakdown of Air at Microwave Frequencies," J. Appl. Phys., **27**, 10, pp. 1162-1170 (October 1956).

4. H. Margenau, "Theory of High Frequency Discharges, IV Note on the Similarity Principle," *Phys. Rev.* **73**, 4, p. 826 (February 15, 1958).

5. W. P. Allis, D. J. Rose, "The Transition from Free to Ambipolar Diffusion," *Phys. Rev.* **93**, 1, pp. 84-93 (January 1, 1954).

6. A. D. MacDonald, "High-Frequency Breakdown in Air at High Altitudes," *Proc. IRE* **47**, 3, p. 436 (March 1959).

7. M. A. Herlin and S. C. Brown, "Microwave Breakdown of a Gas in a Cylindrical Cavity of Arbitrary Length," *Phys. Rev.* **74**, 11. p. 1650 (December 1, 1948).

8. J. A. Pim, *Proc. IEE* (London) Vol. 96, Part III, p. 117 (1949).

9. M. A. Herlin and S. C. Brown, "Breakdown of a Gas at Microwave Frequencies," *Phys. Rev.* **74** 3, p. 291 (August 1, 1948).

10. C. C. Allen and P. P. Keenan, "Low Pressure, Microwave Breakdown of Antennas Radomes, and Associated Radar Components," General Engineering Laboratory Report 57GL235, (General Electric Co., Schenectady, New York (July 29, 1957).

11. L. Gould, *Handbook On Breakdown of Air in Waveguide Systems*, (Microwave Associates Inc., Burlington, Massachusetts, April 1956).

12. M. A. Herlin and S. C. Brown, "Electrical Breakdown of a Gas Between Coaxial Cylinders at Microwave Frequencies," *Phys. Rev.* **74**, 8, p. 910 (October 15, 1948).

13. R. A. Paska, "VHF Breakdown of Air at Low Pressures," Report 944, Ballistic Research Laboratories, Aberdeen Proving Ground, Maryland (August 1955).

14. R. W. P. King, *The Theory of Linear Antennas*. Chapter II, (Harvard University Press, Cambridge, Massachusetts, 1956).

15. F. Worth, "A Study of Voltage Breakdown In The Cavity-Fed Slot Antenna," MSD Report 2030, Lockheed Aircraft Corporation, Missile Systems Division, Palo Alto, California (January, 1957).

16. James D. Cobine, *Gaseous Conductors, Theory and Engineering Applications*, pp. 212-226 (Dover Publications Inc., New York, N.Y., 1958).

TECHNICAL REPORTS IN THIS SERIES

Reports Issued on Contract AF 19(122)-78

1. "Electric Dipoles in the Presence of Elliptic and Circular Cylinders," by W. S. Lucke, September 1949.
2. "Asymmetrically Fed Antennas," by C. T. Tai, November 1949.
3. "Double Fed and Coupled Antennas," by C. T. Tai, February 1949.
4. "Equivalent Radii of Thin Cylindrical Antennas with Arbitrary Cross Sections," by Carson Flammer, March 1950.
5. "Use of Complementary Slots in Aircraft Antenna Impedance Measurements," by J. T. Bolljahn, February 1950.
6. "Wing-Cap and Tail-Cap Aircraft Antennas," by J. V. N. Granger, March 1950.
7. "Investigation of Current Distribution on Asymmetrically-Fed Antennas by Means of Complementary Slots," by R. M. Hatch, Jr., February 1950.
8. "Electromagnetic Resonance Phenomena in Aircraft Structures," by A. S. Dunbar, May 1950.
9. "The Effect of a Grounded Slab on the Radiation from a Line Source," by C. T. Tai, June 1950.
10. "A Method for the Calculation of Progressive-Phase Antennas for Shaped Beams," by A. S. Dunbar, June 1950.
11. "Admittance of an Open-Ended Coaxial Line in an Infinite Grounded Plane," by W. S. Lucke, June 1950.
12. "A Variational Solution to the Problem of Cylindrical Antennas," by C. T. Tai, August 1950.
13. "Uniform Progressive-Phase Antennas Having Asymmetrical Amplitude Distributions," by A. S. Dunbar, September 1950.
14. "Small Dipole-Type Antennas," by J. T. Bolljahn, September 1950.
15. "Tables of Modified Cosine Integrals," January 1951.
16. "Prolate Spheroidal Wave Functions," by Carson Flammer, February 1951.
17. "An Antenna Evaluation Method," by W. S. Lucke, April 1951.
18. "Radar Response from Thin Wires," by C. T. Tai, March 1951.
19. "The Measurement of Low-Frequency Aircraft Antenna Properties Using Electrostatic Methods," by J. T. Bolljahn, September 1951.

20. (Dropped).

21. "A Method for the Calculation of Progressive-Phase Antennas for Shaped Beams," Part II, by A. S. Dunbar, May 1951.

22. "The Prolate Spheroidal Monopole Antenna," by Carson Flammer, August 1957, issued on Contract AF 19(604)-1295.

23. "Variational Solution for the Problem of the Asymmetric Dipole," by I. Reese, August 1951.

24. "Quasi-Static Solution for Diffraction of a Plane Electromagnetic Wave by a Small Oblate Spheroid," by C. T. Tai, September 1952 [Issued on Contract AF 19(604)-266].

25. "Transmission Through a Rectangular Aperture in an Infinite Screen," by W. S. Lucke, September 1951.

Reports Issued on Contract AF 19(604) 266

26. "Improvements in Instrumentation for the Investigation of Aircraft Antenna Radiation Patterns by Means of Scale Models," by R. M. Hatch, Jr., August 1952.

27. "The Vector Wave Solution of the Diffraction of Electromagnetic Waves by Circular Disks and Apertures," by Carson Flammer, September 1952.

28. "An Investigation of the Distribution of Current on Collinear Parasitic Antenna Elements," by R. M. Hatch, Jr., August 1952.

29. "On the Theory of Diffraction of Electromagnetic Waves by a Sphere," by C. T. Tai, October 1952.

30. "High-Frequency Airborne Direction Finding," by P. S. Carter, Jr., December 1952.

31. "An Electrolytic Tank Method for Low-Frequency Loop Antennas Studies," by R. F. Reese, July 1953.

32. "Radiation from a Uniform Circular Loop Antenna in the Presence of a Sphere," by C. T. Tai, December 1952.

33. "A Computer for Use with Antenna Model Ranges," by C. E. Fisher, February 1953.

34. "Tail-Cap Antenna Radiation Pattern Studies," by J. H. Bryan, January 1953.

35. "U-H-F Tail-Cap Antenna Pattern Characteristics and Their Control," by A. R. Ellis, March 1955 [issued on Contract AF 19(604)-1296].

36. "Mutual Admittance of Slots in Cylinders," by W. S. Lucke, February 1953.

37. "Radio Interference from Corona Discharges," by R. L. Tanner, April 1953.

38. "Effects of Airframe Configuration on Low-Frequency Antenna Characteristics," by C. M. Hoblitzell, April 1953.

39. "The Effects of Thin Resistive Coatings on Low-Frequency Aircraft Antenna Performance," by C. W. Steele [issued on Contract AF 19(604)-1296] January 1956.

40. "Analysis of the Overstation Behavior of Airborne ADF Systems," by H. H. Ward, June 1954.

41. "Some Electromagnetic Problems Involving a Sphere," by C. T. Tai, April 1953.

42. "Radiation Pattern Measurements of Stub and Slot Antennas on Spheres and Cylinders," by J. Bain, April 1953.

43. "Current Distribution on Wing-Cap and Tail-Cap Antennas," by Irene C. Carswell, May 1954.

44. "A Study of Radiating Structures for Perpendicularly-Polarized Flush Radar Antennas," by Edward M. T. Jones and Seymour B. Cohn, July 1953.

45. "Radiation from Current Elements and Apertures in the Presence of a Perfectly Conducting Half-Plane Sheet," by C. T. Tai, July 1954.

46. "A Glossary of Dyadic Green's Functions," by C. T. Tai, July 1954.

47. "Horizontally Polarized Long-Slot Array," by R. C. Honey, August 1954.

Reports Issued on Contract AF 19(604)-1296

48. "Microwave Radiation from Large Finite Bodies," by Seymour B. Cohn and Tetsu Morita, January 1955.

49. "Radiation from Electric and Magnetic Dipoles in the Presence of a Conducting Circular Disk," by Carson Flammer, February 1955.

50. "A Study of Some Inherent Errors in the Three-Dimensional Raydist System," by Irene Carswell, March 1955.

51. "Operating Characteristics of Flush-Mounted Bombing Antennas," by E. M. T. Jones, November 1955.

52. "Properties of the Asymmetric Dipole," by Irene Carswell, December 1955.

53. "Notch Coupling to the Electromagnetic Resonances of a Delta-Wing Aircraft," by William L. Jones, December 1955.

54. "A Flush-Mounted Horizontally Polarized Directional Antenna," by R. C. Honey, January 1956.

55. "Radiation from a Flush-Mounted Scanning Antenna on the Nose Section of a Supersonic Aircraft," by J. K. Shimizu and T. Morita, December 1955.

56. "An Economical Logarithmic Recording System," by Lloyd A. Robinson, June 1956.

57. "Variational Formulae for Domain Functionals in Electromagnetic Theory," by Carson Flammer, March 1957.

58. "Systems Considerations for High Speed Missile Seeker Antennas," by Donald L. Margerum and E. Thomas Brandon, May 1957. Confidential.

59. "High-Strength Dielectric Materials for Very Fast Aircraft," by Henry J. Sang, March 1957.

60. "Impedance Matching Limitations with Application to the Broadband Antenna Problem," by Arthur Yassiliadis, January 1957.

61. "Shunt-Fed and Notch-Fed H-F Aircraft Antennas," by Robert L. Tanner, July 1957.

62. "A Study of Precipitation-Static Noise Generation in Aircraft Canopy Antennas," by Joseph E. Nanevicz, September 1957.

63. "Electromagnetic Wave Propagation in a Medium with Variable Dielectric Constant $1 + kr^{-1}$," by Carson Flammer, January 1958.

Reports Issued on Contract AF 19(604)-3458

64. "The Back-Scattering Cross Sections of Missile Trails," by Carson Flammer, June 1958.

65. "Ray-Tracing and Diffraction in a Medium with Variable Permittivity and Attenuation," by James A Cochran, October 1958.

66. "Feasibility Study of Aircraft Antennas for Forward-Scatter and Meteor-Burst Communication," by J. F. Cline, July 1959.

67. "A Study of Possibilities for Improving Space Utilization and Performance of Rhombic Antennas," by Angel Martin-Caloto, July 1959.

68. "Aerodynamic Characteristics of Trailing-Wire Antennas at Supersonic Speeds," by F. B. Harris, Jr., March 1960.

69. "Voltage Breakdown of Antennas at High Altitudes," by W. E. Scharfman and T. Morita, April 1960.

STANFORD
RESEARCH
INSTITUTE

MENLO PARK, CALIFORNIA

REGIONAL OFFICES AND LABORATORIES

SOUTHERN CALIFORNIA LABORATORIES
820 Mission Street
South Pasadena, California

PACIFIC NORTHWEST OFFICE
421 S. W. 6th Avenue
Portland, Oregon

WASHINGTON OFFICE
711 14th Street N. W.
Washington, D. C.

EUROPEAN OFFICE
Pelikanstrasse 37
Zurich, Switzerland

HAWAII OFFICE
195 South King Street
Honolulu, Hawaii

NEW YORK OFFICE
60 East 42nd Street
New York 17, New York